CHEMICAL REVIEWS

REVIEW

pubs.acs.org/CR

Carbon Dioxide Capture in Metal−Organic Frameworks

Kenji Sumida,† David L. Rogow,† Jarad A. Mason, Thomas M. McDonald, Eric D. Bloch, Zoey R. Herm, Tae-Hyun Bae, and Jeffrey R. Long*

Department of Chemistry, University of California, Berkeley, California 94720-1460, United States

CONTENTS

1. INTRODUCTION

The sharply rising level of atmospheric carbon dioxide resulting from anthropogenic emissions is one of the greatest environmental concerns facing our civilization today. These emissions, which stem predominantly from the combustion of coal, oil, and natural gas (ca. 80% of CO_2 emissions worldwide),[1] are projected to continue to increase in the future due to economic growth and industrial development, particularly in developing nations.[2] Although the transition of the existing infrastructure from carbon-based sources to cleaner alternatives would be ideal in this regard, such a change requires considerable modifications to the current energy framework, and many of the proposed technologies are not yet sufficiently developed to facilitate large-scale industrial implementation. Thus, carbon capture and sequestration (CCS) technologies that efficiently capture CO_2 from existing emission sources will play a vital role until more significant modifications to the energy infrastructure can be realized.

Special Issue: 2012 Metal-Organic Frameworks

Received: August 19, 2011
Published: December 28, 2011

One scenario under which CO_2 capture technologies could be rapidly implemented is at stationary point sources, such as coal- and natural gas-fired power plants. In the United States, 41% of the total CO_2 emissions can be attributed to electricity generation[3] (ca. 60% worldwide),[2] and hence the installation of effective capture systems to existing plant configurations could offer a large reduction in emissions. The captured CO_2 would then be subjected to permanent sequestration, where the CO_2 is injected into underground geological formations, such as depleted oil reservoirs or salt water aquifers. Here, similar technologies are already established in the context of processes such as enhanced oil recovery (EOR), and several trial CO_2 sequestration sites are in construction.[4] Note that the reuse of the captured CO_2 as a reactant in chemical transformations presents an alternative sequestration pathway, although it would not be a viable long-term strategy owing to the tremendous scale of worldwide CO_2 emissions (ca. 30 Gt per year)[5] resulting in the market for any commodities prepared therefrom being rapidly saturated. A potentially more promising scenario that could utilize a considerable fraction of the captured CO_2 would be its conversion into a fuel for transportation, provided efficient methods for carrying out the conversion via a renewable energy source can be developed.[6,7] Nevertheless, regardless of the sequestration pathway, CCS systems must capture the CO_2 from flue gas in an efficient, reversible fashion, and as will be discussed, the discovery of new materials exhibiting the right properties for performing CO_2 capture is an area requiring urgent development.

In this regard, the most significant challenge for CO_2 capture at present is the large energy penalty associated with the capture process. With current technologies, approximately 70% of the cost of CCS is associated with the selective capture of CO_2 from the power plant flue gas,[8] a value that must certainly be reduced if such an approach for CO_2 mitigation is to become viable. The high cost primarily arises from the large energy input required for regeneration of the capture material. Indeed, CO_2 capture from a post-combustion flue gas using the most highly developed current technologies involving aqueous alkanolamine solutions carries an energy penalty of roughly 30% of the output of the power plant, most of which is associated with the liberation of the captured CO_2 from the capture medium.[8] Thus, minimization of the energy input for regeneration, through fine-tuning of the thermodynamics of the interaction between CO_2 and the adsorbent, for example, is one of the most crucial considerations in improving the energy efficiency of CO_2 capture.

Metal−organic frameworks are a new class of materials that could serve as an ideal platform for the development of next-generation CO_2 capture materials owing to their large capacity for the adsorption of gases and their structural and chemical tunability.[10,17,92−98] The ability to rationally select the framework components is expected to allow the affinity of the internal pore surface toward CO_2 to be precisely controlled, facilitating materials properties that are optimized for the specific type of CO_2 capture to be performed (post-combustion capture, pre-combustion capture, or oxy-fuel combustion) and potentially even for the specific power plant in which the capture system is to be installed. For this reason, significant effort has been made in recent years in improving the gas separation performance of metal−organic frameworks, and some studies evaluating the prospects of deploying these materials in real-world CO_2 capture systems have begun to emerge.[9−16] Here, we review the progress that has been made in this area, with an emphasis on comparing the performance of metal−organic frameworks to existing technologies, as well as highlighting the most crucial areas in which improvements in properties are urgently required. Note that, as a result of the rapid progress being made, we will limit the scope to CO_2 capture from power plants. Other scenarios of CO_2 capture, such as natural gas processing (CO_2/CH_4 separation), capture from transportation emissions, or direct air capture, are also highly important areas of research, and we direct the interested reader to a number of reviews that address a broader scope of gas separations for more detail.[10,11,15,17−19]

This review is intended to provide the reader with a comprehensive overview of the considerations associated with CO_2 capture from power plants using metal−organic frameworks and is arranged in the following manner. The remainder of section 1 provides an overview of the CO_2 problem, a description of the current technologies utilized for CO_2 capture from power plant flue gas streams, and an introduction to metal−organic framework chemistry. Section 2 summarizes the various performance parameters to be evaluated in order to determine the performance of metal−organic frameworks for CO_2 capture applications and outlines a number of key characterization methods that are used for gaining a detailed correlation between the structural and chemical features of a metal−organic framework and its adsorption properties. The potential utility of metal−organic frameworks under the three main scenarios for CO_2 capture from power plants, namely, post-combustion capture (section 3), pre-combustion capture (section 4), and oxy-fuel combustion (section 5) are then discussed. The emerging area of CO_2 capture by membrane technologies, where the varying diffusion properties of the flue gas components are harnessed to effect gas separation, is presented in section 6. Finally, the outlook for utilizing metal−organic frameworks for CO_2 capture is discussed in section 7, noting areas in which further work is urgently required in order to realize next-generation metal−organic frameworks that will be suitable for deployment within real-world systems.

1.1. Carbon Dioxide Emission from Anthropogenic Sources

The escalating level of atmospheric CO_2 has been well-documented in recent times due to its implication in global warming, generating widespread environmental concerns toward the continued use of carbon-based fuels. The concentration of CO_2 in the atmosphere at the present time is greater than at any other time in modern history, exceeding 390 ppm in 2011.[20] To put this value into perspective, through analysis of ocean sediments for seawater pH and calcium, magnesium and carbonate mineralogy, and ice core data, it has been concluded that the atmospheric concentration has not approached such a level over the past 400 000 years.[21,22] Indeed, over that period, prior to the extremely rapid increases observed over the past few decades, the atmospheric CO_2 level has varied only gradually within the range 100−300 ppm. Thus, it is clear that global industrial development over the past century has created anthropogenic sources of CO_2 leading to a rapid increase in the atmospheric concentration of CO_2 to levels well above those to be expected from natural fluctuations.

As shown in Figure 1, the combustion of fossil fuels represents over half of the global greenhouse gas emissions.[2] Global CO_2 emissions have increased by approximately 80% over the period 1970−2004 (from 21 to 38 Gt/year), and these emission levels are projected to increase further over the next several decades owing to rises in energy demands associated with a growing

dx.doi.org/10.1021/cr2003272 |Chem. Rev. 2012, 112, 724–781

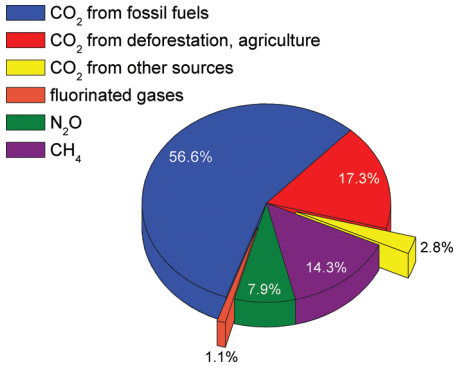

Figure 1. Global greenhouse gas emission sources in 2004 of which approximately 77% are represented by CO_2 emissions.[2]

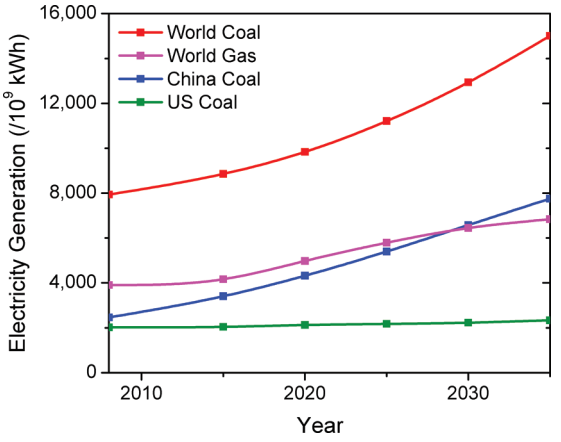

Figure 2. Projected electricity generation levels for coal and gas from 2007 to 2035.[28]

global population and economic and industrial development. The International Panel on Climate Change (IPCC) was formed in 1988 to assess the effects of greenhouse gas emissions on the global climate and predict possible future outcomes and to suggest remediation strategies.[23] Based on the possible scenarios presented in the most recent IPCC climate report in 2007, the average global temperatures are expected to rise by between 1.8 and 6.4 °C by the end of the 21st century. Furthermore, current mitigation approaches are centered around the implementation of CO_2 emissions pricing structures on the energy generation sector and a transition toward low- and non-carbon fuel sources. Among the strategies outlined, CO_2 capture from fossil fuel-fired power plant emissions was deemed paramount to avoiding exacerbating climate change, since adaptation to low-carbon and alternative energy technologies, while urgent, will require many more years of research, development, and implementation.

1.2. CO_2 Capture at Stationary Point Sources

Here, we review the main strategies that have been considered to date for CO_2 capture from power plants. The CO_2 emissions resulting from the combustion of coal for electricity generation represent 30−40% of the total anthropogenic CO_2 contributions.[24,25] In the United States, 43% of electricity production is derived from coal as of July 2011.[26] In 2004, coal was responsible for 82.3% of the CO_2 emissions originating from the electricity generation sector in the U.S.[25] Coal-based power generation is expected to play an increasingly significant role in the future owing to the large reserves (>100 years) available for extraction,[27] as well as the escalating global energy demands. For example, in China, which surpassed the United States as the largest emitter of greenhouse gases in 2006, the use of coal for electricity generation is projected to increase at a rate of 3.5% per year from 2.3 trillion kW·h in 2007 to 7.8 trillion kW·h in 2035.[28,29] A similar trend is predicted at the global scale, where electricity generation from coal and gas is expected to increase from 11.8 trillion kW·h in 2007 to 21.9 trillion kW·h in 2035 (see Figure 2).[28]

Although the tremendous scale of coal and gas combustion for electricity generation is of significant concern, it also presents one of the most promising scenarios under which CO_2 emissions could be dramatically reduced. Indeed, the installation of CO_2 capture systems within coal- or gas-fired power plants that selectively remove the CO_2 component of the flue gas would significantly reduce the global annual emissions, as well as lessen the environmental impact of an energy framework that will have an increased reliance on carbon-based fuels in the short to medium term until more environmentally sustainable energy sources can be deployed. The goal of the US Department of Energy/National Energy Technology Laboratory effort, which is being carried out as part of the Existing Plants, Emissions, and Capture Program, is to develop advanced CO_2 capture and compression technologies for both existing and new coal-fired power plants that when combined can achieve capture of 90% of the CO_2 produced at less than a 35% increase in the cost of electricity.[2]

Currently, the greatest challenge for the implementation of CO_2 capture within power plants is the discovery of new materials that display suitable physical and chemical properties to be utilized within real-world systems that reduce the large energy requirements to perform the capture step. The composition of a typical post-combustion flue gas is shown in Table 1. Owing to the relatively low concentration of CO_2 (15−16%) and the large quantities of N_2 (73−77%) originating from the air in which the coal is combusted, a high selectivity toward CO_2 is crucial, such that only pure CO_2 is captured and subjected to sequestration. Current technologies involving aqueous amine absorbents capture the CO_2 from the gas mixture with a high selectivity (see section 1.4.1 for further detail), but carry an energy penalty of approximately 30% of the power produced at the power plant.[30] Here, the energy penalty originates primarily from the need to heat the large quantities of water in which the amine is dissolved, as well as the energy required to break the C−N bond that is formed in the interaction between CO_2 and the amine functionality. Thus, from the aspects of cost and environmental impacts of coal consumption, there is an urgent need to explore new materials that offer a lower energy penalty, ideally close to the thermodynamic minimum of approximately 10−20%.[8]

In the context of coal- or gas-fired power plants, there are three main scenarios under which new materials could serve to reduce the energy requirements of capture, as illustrated in Figure 3. In post-combustion capture (section 3), CO_2 is removed from the flue gas that results after combustion of the fuel in air (see Table 1). This is predominantly a CO_2/N_2 gas separation owing to the high content of N_2 in the air used for combustion and has been the most explored strategy to date since a post-combustion CO_2 capture system could be readily retrofitted to existing power plants. Alternatively, pre-combustion capture (section 4) can be performed following gasification of the coal prior to combustion,

dx.doi.org/10.1021/cr2003272 |Chem. Rev. 2012, 112, 724–781

Table 1. Typical Postcombusion Flue Gas Composition for a Coal-Fired Power Plant[31]

molecule	concentration (by volume)
N_2	73−77%
CO_2	15−16%
H_2O	5−7%
O_2	3−4%
SO_2	800 ppm
SO_3	10 ppm
NO_x	500 ppm
HCl	100 ppm
CO	20 ppm
hydrocarbons	10 ppm
Hg	1 ppb

producing a high-pressure flue gas flue gas containing H_2 and CO_2. This carries the advantage of being an easier separation than the CO_2/N_2 separation required for post-combustion CO_2 capture. Once the CO_2 is removed from the gas mixture, the H_2 is then used for electricity generation, resulting in only H_2O as the byproduct. Another possible method of reducing CO_2 emissions would be to perform oxy-fuel combustion (section 5), in which pure O_2 is utilized for the combustion of coal or natural gas. In this case, an O_2/N_2 separation from air is performed, and the O_2 is diluted with CO_2 prior to combustion, leading to a flue gas that is a mixture of CO_2 and H_2O, which can be efficiently separated using existing technologies. Here, we note that each of the three processes requires a different gas separation, and there is a need for an entirely different set of materials properties for each separation due to the different physical properties of the gases, as listed in Table 2. This serves to highlight the importance of materials optimization, which will be essential in the development of next-generation separation materials.

1.3. Options for CO_2 Sequestration

While the objective of this review is to discuss progress made in the area of the capture of CO_2 from power plant emissions, we now briefly consider the aspect of CO_2 storage (sequestration) of the enormous quantities of CO_2 that would be obtained as a result of a successful capture framework. Although approximately 70% of the cost of CCS is derived from the capture step (a figure that is projected to decrease following future materials optimization), there are significant practical considerations associated with the other steps within a CCS system. For example, given that the quantities of CO_2 that would be captured are too large for reuse by any chemical industry, the sustainable storage of CO_2 is paramount of the successful development of the CCS. Currently, the most feasible scenario is one in which the CO_2 removed from the power plant flue gas is, following compression, injected into an underground containment environment that facilitates CO_2 storage without leakage and limited impact on the surrounding environment. The geological formations considered most suitable for long-term sequestration of CO_2 are depleted oil and natural gas wells, shale, coal, and saline formations.[34] Saline or brine-containing aquifers provide an environment where CO_2 is able to react with mineral salts to form carbonates.[35] In fact, injection of CO_2 gas into oil and natural gas deposits can enhance the extraction of these fossil fuels by pressurization of the well in enhanced oil recovery (EOR) processes.[36] In this case, the CO_2 is usually recovered along with the oil or natural gas, then separated

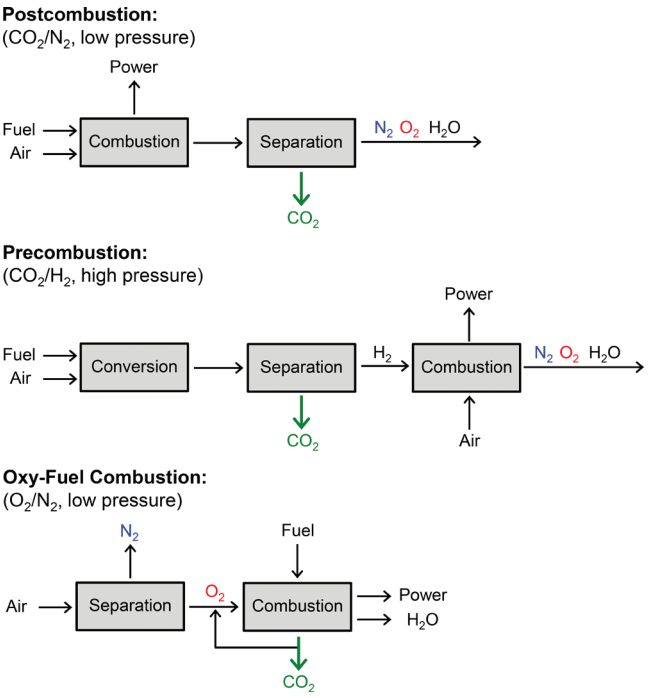

Figure 3. Basic schemes showing the types of CO_2 capture relevant to the present review. The processes for post-combustion capture, pre-combustion capture, and oxy-fuel combustion, which are described in further detail in sections 3, 4, and 5, respectively. The main separation required for each type of process is indicated next to each of the headings in parentheses.

and injected back into the well. A number of CCS demonstration projects are in the planning, implementation and operation stages around the world.[37] The smallest example is a coal seam in Kaniow, Poland, where 760 t of CO_2 was injected between 2004 and 2005. The largest project is the Erdos project in Inner Mongolia, China, where 3.6 million metric tons of CO_2 per year is captured from a coal-to-liquid fuel plant and used for EOR.

Storage in ocean water at depths of between 1000 and 3000 m, where CO_2 is in the liquid form, is another option for sequestration of CO_2. Potentially, up to 1 trillion tons of CO_2 could be stored in deep ocean saline water as a result of injecting concentrated CO_2 into deep water or creating CO_2 pools on the ocean floor.[38] Much of the CO_2 could be stored on the ocean floor in the form of solid gas hydrates.[39] It is well-known that enormous deposits of methane hydrates exist on the ocean floor. The ice-like solid complexes of water and CO_2 formed under high pressure and cold temperatures may be an achievable form of storage that would be stable for long periods of time.

1.4. Current CO_2 Capture Materials

The need for materials that can be used within CO_2 capture systems for installation in coal- and gas-fired power plants has prompted the study of several classes of materials to date. The development of such materials requires the consideration of numerous performance parameters, which must be finely tuned depending on the type of CO_2 capture and the specific configuration of the power plant. Optimization of these parameters should allow the energy penalty and cost of CO_2 capture to be lowered, enabling widespread implementation under the various scenarios mentioned in section 1.2.

The most crucial performance parameter for any CO_2 capture material is its selectivity toward CO_2. A high selectivity is

dx.doi.org/10.1021/cr2003272 |Chem. Rev. 2012, 112, 724–781

Table 2. Physical Parameters of Gases Relevant to Carbon Dioxide Capture Processes[10,32,33]

molecule	kinetic diameter (Å)	polarizability (10^{-25} cm^{-3})	dipole moment (10^{-19} esu^{-1} cm^{-1})	quadrupole moment (10^{-27} esu^{-1} cm^{-1})
H_2	2.89	8.04	0	6.62
N_2	3.64	17.4	0	15.2
O_2	3.46	15.8	0	3.9
CO	3.76	19.5	1.10	25.0
NO	3.49	17.0	1.59	
H_2O	2.65	14.5	18.5	
H_2S	3.60	37.8	9.78	
CO_2	3.30	29.1	0	43.0
NO_2		30.2	0	

essential, such that the CO_2 component of the flue gas is completely removed for subsequent sequestration. However, the affinity of the material toward CO_2 is also a major consideration for optimizing the energy penalty of capture. Indeed, if the interaction is too strong, this leads to a high energy requirement for desorption of the captured CO_2. On the other hand weak interactions, while lowering the regeneration cost, would afford low selectivities for CO_2 over the other components of the flue gas. Furthermore, the material should exhibit a high stability under the conditions of capture and regeneration, such that it can be deployed for the lifetime of the power plant. Owing to the large quantities of CO_2 that need to be removed from the flue gas, the materials should take up CO_2 at a high density, such that the volume of the adsorbent bed can be minimized.

In the following sections, we describe the main existing CO_2 capture technologies in the context of these performance considerations, namely, aqueous alkanolamine solutions and porous solids, such as zeolites and activated carbons. As we shall see, none of the materials fulfill all of the criteria mentioned above, which highlights the urgent need for new materials to emerge that improve upon the characteristics of these materials. In this regard, metal−organic frameworks represent an opportunity to create next-generation materials that are optimized for real-world applications in CO_2 capture. However, the other types of materials also carry a number of advantages, and further optimization of these materials could also potentially allow development of suitable candidates that satisfy many of the performance criteria.

1.4.1. Aqueous Alkanolamine Absorbents. Aqueous alkanolamine solutions have been extensively studied to date for CO_2 capture and are still considered the state-of-the-art despite being known for many decades.[30] Here, the amine functionalities participate in a nucleophilic attack of the carbon atom of CO_2 to form a C−N bond, and depending on the amine, this results in the formation of a carbamate or bicarbonate species, as shown in Scheme 1.[40] The affinity of these molecules for CO_2 can be tuned to some extent by altering the substitution of the amine, although the strong orbital interactions usually require a high energy input for cleavage of this bond, and subsequent release of CO_2. Indeed, the mechanism of CO_2 adsorption in the case of alkanolamines falls into the chemisorptive regime, where the enthalpy of absorption lies the range of −50 to −100 kJ/mol at 298 K and low CO_2 loadings.[41]

Monoethanolamine (MEA, Scheme 1, upper) is perhaps the most well-studied alkanolamine for CO_2 capture applications and is usually dissolved in water at a concentration of approximately

Scheme 1. Reaction of CO_2 with Monoethanolamine (MEA) To Give a Carbamate Product (Upper), and the Corresponding Reaction with Triethanolamine (TEA) Resulting in a Bicarbonate Species (Lower)

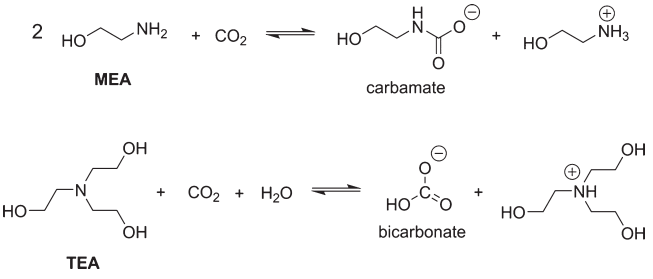

20−30 wt %. Here, the reaction of 2 equiv of MEA with CO_2 results in the formation of an anionic carbamate species and a corresponding ammonium cation. The total working capacity of a 30 wt % MEA solution is between 2.1 and 5.5 wt %, depending upon the specific configuration of the scrubbing process.[42,43] In some cases, MEA is used in mixtures with secondary or tertiary alkanolamines, such as diethanolamine (DEA) and triethanolamine (TEA).[30] In the case of TEA, the steric bulk about the nitrogen center of the tertiary amine results in the formation of a bicarbonate species rather than a carbamate species. Note that the stoichiometry of the reactions also has a significant impact on the maximum loading capacity for CO_2, since the primary amines interact with CO_2 in a 2:1 ratio, while the secondary and tertiary amines react in a ratio of 1:1. With regard to the enthalpy associated with the two reactions shown in Scheme 1, the bicarbonate species is comparatively less stable relative to the carbamate compound, resulting in a more readily reversible CO_2 absorption reaction for the tertiary alkanolamine. Thus, the energy required to reverse the amine−CO_2 interaction generally decreases in the order of 1° > 2° > 3° amines, although the total regeneration energy within an actual capture system would depend on other factors, such as the concentration of the amine.

Several other industrially relevant alkanolamines, including 2-amino-2-methyl-1-propanol (AMP) and *N*-methyldiethanolamine (MDEA), have also been investigated for use in CO_2 absorbent solutions. Recently, some new amine-type solvents, piperazine[44] and imidazolium-based ionic liquids,[45] have gained much interest and have been shown to exhibit enhanced absorption properties in addition to a higher chemical and thermal stability compared with conventional amine solutions. For example, a 4:1 mixture of MEA amd MDEA used within a pilot plant exhibited a reduction in the overall energy requirement for CO_2 capture compared with a system employing just MEA as the amine species in solution.[46]

Aqueous alkanolamine solutions have several significant limitations as adsorbents for large-scale CO_2 capture. First, the solutions are relatively unstable toward heating, which limits the regeneration temperatures available for full regeneration of the capture material. Decomposition of the amine results in a decrease in absorbent performance over time, diminishing the lifetime of the solutions. The amine solutions are also corrosive toward the vessels in which they are contained, although this is usually prevented by the addition of corrosion inhibitors or by limiting the concentration of the alkanolamine species to below 40 wt %. Note that the latter is a key disadvantage for the use of alkanolamines, since a lower concentration results in a larger

dx.doi.org/10.1021/cr2003272 |*Chem. Rev.* 2012, 112, 724–781

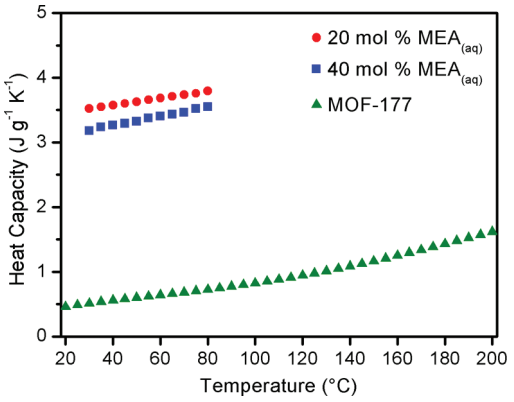

Figure 4. Heat capacities recorded for alkanolamine solutions[47] and a representative metal−organic framework, MOF-177.[48] The heat capacity of the solid adsorbent is significantly lower, which is expected to result in a lower energy penalty for CO_2 capture.

volume of water that must be heated in order to regenerate the material. In fact, the high heat capacity of water ($C_p = 4.18\ J\ K^{-1}\ g^{-1}$) represents the main contribution to the regeneration energy costs.[30] Indeed, as shown in Figure 4, the heat capacity of both 20 and 40 mol % MEA solutions are close to the heat capacity of pure water,[47] and this is the main reason that solid porous adsorbents, which can have much lower heat capacities, are thought to present a promising strategy for reducing the regeneration energy penalty.

1.4.2. Solid Porous Adsorbent Materials. The lower heat capacity of solid porous adsorbents has led to their investigation as new materials for CO_2 capture. In particular, zeolites,[49] which are porous aluminosilicate materials that possess a high chemical and thermal stability, have been studied especially in the context of upgrading of natural gas and CO_2 capture from post-combustion flue gas.[50−54] For example, zeolite 13X, which has a relatively high surface area (SA_{BET} = 726 m^2/g) and micropore volume (0.25 cm^3/g), has been shown to display promising capacities for CO_2 at room temperature (16.4 wt % at 0.8 bar and 298 K).[55,56] The large variety of structures[57,58] that have been reported to date presents an opportunity for the study of the effect of composition, or certain structural or chemical features, on the adsorption performance. For example, it has been observed that the Si/Al ratio of the material can have a significant impact on the CO_2 adsorption within zeolite LTA, which in turn has crucial implications toward the adsorption selectivity and regeneration costs associated with the capture process.[59]

In comparison with post-combustion CO_2 capture employing the alkanolamine solutions discussed above, small-scale pilot plants using zeolites have demonstrated more rapid adsorption of CO_2 and lower energy penalty for the process.[60] However, many of the zeolites studied to date become readily saturated with the water vapor present in the flue gas stream, and the CO_2 adsorption capacity is consequently reduced over time.[61,62] Furthermore, the large enthalpy of adsorption of CO_2 leads to relatively high CO_2 desorption temperatures (ca. 135 °C).[63] This point highlights the importance of materials optimization for controlling the affinity of the pore surfaces toward CO_2, and while improved synthetic procedures that provide a greater degree of control over the properties of the resulting zeolite have emerged, it still remains challenging to precisely tune the materials to the extent possible for metal−organic frameworks. Nevertheless, the robust nature of zeolites coupled with their low cost and well-developed structural chemistry makes these materials an attractive target for use in CO_2 capture applications.

One feature of zeolites that may enhance their selectivity toward CO_2 is the presence of charge-balancing metal cations within the pores. As will be discussed in the following sections, highly charged species on the surfaces of porous solids can afford high affinities for CO_2 over other components of flue gas owing to the propensity for CO_2 to be polarized to a higher extent compared with gases such as N_2 or H_2. For this reason, alkali and alkaline earth metal cation-exchanged chabazite-type zeolites were investigated as CO_2 capture adsorbents.[65] Indeed, it was found that the presence of exposed cations within the pores led to a higher affinity at low CO_2 coverages, with the zero-coverage isosteric heat of adsorption falling in the range of −30 to −42 kJ/mol. The effect of such sites will be discussed in full detail when metal−organic frameworks with exposed metal cation sites are considered in section 3.

Activated carbons have also attracted much interest as CO_2 adsorbents. These materials are amorphous porous forms of carbon that can be prepared by pyrolysis of various carbon-containing resins, fly ash, or biomass.[9] The relatively uniform electric potential on the surfaces of activated carbons leads to a lower enthalpy of adsorption for CO_2, and hence lower capacities for CO_2 compared with zeolites at lower pressures. However, their significantly higher surface areas lead to greater adsorption capacities at high pressures, which has resulted in activated carbons being considered for a variety of high-pressure gas separation applications. In the context of CO_2 capture, the high-pressure flue gas produced in pre-combustion CO_2 capture has been a major target application for these materials. Indeed, one study has shown that the upper limit for the CO_2 adsorption capacity within activated carbon materials is approximately 10−11 wt % under post-combustion CO_2 capture conditions, while it reaches 60−70 wt % under pre-combustion CO_2 capture conditions.[66] A very recent study has also demonstrated that careful selection of the material precursors and the reaction conditions employed can lead to carbon-based adsorbents that have a volumetric CO_2 adsorption capacity that is greater than some of the highest surface area metal−organic frameworks at high pressure.[67] One further advantage of activated carbons over zeolites is that their hydrophobic nature results in a reduced effect of the presence of water, and they consequently do not suffer from decomposition or decreased capacities under hydrated conditions.[68] Moreover, consistent with the lower heat of adsorption for CO_2, activated carbons require a lower temperature for regeneration compared with zeolites.[68]

Combining the high affinity of amines and the advantages of using a porous solid adsorbent holds tremendous promise for the development of new materials that exhibit properties that are appropriate for CO_2 capture applications. New materials in which amines, alkanolamines, or alkylamines are grafted to the interior surfaces of activated carbons and zeolites are currently being surveyed experimentally.[64,69−71]

In one study, zeolite 13X was impregnanted with MEA at loadings ranging from 0.5 to 25 wt % by immersing the solid in methanol solutions of MEA.[64] It was shown that an intermediate loading of 18.7 wt % was optimal for the selective adsorption of CO_2 over N_2, although the surface area decreased dramatically from 616 to 9 m^2/g as a result of the amine molecules filling the pores of the zeolite. High-temperature (120 °C) adsorption studies found that the capacity for CO_2 had increased from 4 to 14 mL/g, while at temperatures below 75 °C, the capacity was decreased.

dx.doi.org/10.1021/cr2003272 |Chem. Rev. 2012, 112, 724–781

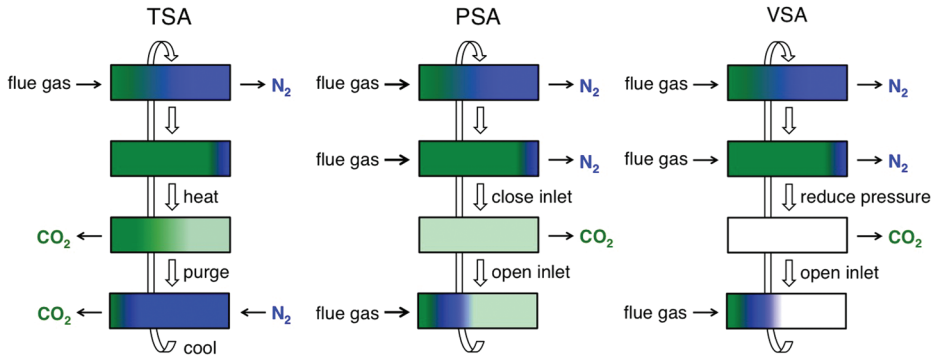

Figure 5. Schematic diagrams of idealized temperature swing adsorption (TSA), pressure swing adsorption (PSA), and vacuum swing adsorption (VSA) processes for regenerating solid adsorbent in a fixed-bed column.

It was also demonstrated that the capacity decreased only slightly when the gas feed stream was saturated with moisture, compared with unmodified zeolite 13X. Carbamate species were identified in the infrared spectrum of the material at 120 °C, suggesting that the amines within the pores indeed do interact with CO_2 in a chemisorptive fashion similar to that observed in the alkanolamine solutions.

More recently, activated carbons and zeolite 13X were loaded with MEA and TEA by solution processing.[71] Here, it was found that both materials exhibited selectivity for CO_2 over CH_4 (an important separation for natural gas sweetening) and N_2 (post-combustion CO_2 capture), although the CO_2 capacity was decreased compared with the bare material owing to the lower surface area accessible to the gas molecules following installation of the amines. However, it was found that CO_2 adsorption capacity increased with temperature from 298 to 348 K, which was attributed to an enhanced propensity for formation of carbonate species at the higher temperature.

In addition to zeolites and carbon-based materials, other classes of porous materials are emerging as potential adsorbents in CO_2 capture applications, including covalent-organic frameworks[72−77] and amine-grafted silicas.[78−80] In addition, microporous organic polymers[81,82] have been shown to be of possible utility in gas separations relevant to CO_2 capture.[83,84] Here, the high mechanical processability of polymers (which is one of the significant advantages they hold over conventional crystalline porous materials) can be used to fabricate the material into the desired form, such as membranes. Furthermore, although the inherent selectivity of polymers is often limited, the fabrication of composite materials, where porous crystalline materials that are highly selective toward CO_2 are embedded within the polymer phase, may afford new materials with enhanced properties. Nevertheless, significant work still needs to be performed to identify the most promising class of materials for CO_2 capture, although the rich and highly diverse nature of the materials discovered recently holds tremendous promise for the discovery of next-generation materials that are optimized for this application.

1.4.2.1. Temperature and Pressure Swing Adsorption. In any CO_2 capture process, the adsorbent must be regenerated after each adsorption cycle. Regeneration of a solid adsorbent is typically accomplished by temperature swing adsorption (TSA), pressure swing adsorption (PSA), vacuum swing adsorption (VSA), or some combination of these processes. In all cases, the solid adsorbent will likely be packed into a large fixed-bed column, and the adsorbate would be desorbed from the material by increasing the temperature (for TSA) or reducing the pressure (for PSA and VSA) of the bed.

Due to the possibility of using low-grade heat from the power plant as a source of energy for regeneration, TSA is particularly promising for many CO_2 capture processes.[85,86] In a TSA cycle (Figure 5, left), the saturated adsorbent is heated from ambient pressure to the optimal desorption temperature of the material. As the temperature is increased, gas molecules desorb from the adsorbent surface, and the increased gas pressure drives the desorbed gases from the column. Once equilibrium is reached at the maximum desorption temperature and no more adsorbed gas elutes from the column, a purge is used to push off any desorbed gases that fill the void spaces of the bed until the purity of eluted gas falls below a desired level. Finally, the bed is cooled and prepared for the next adsorption cycle.

For a PSA (Figure 5, center) or VSA (Figure 5, right) regeneration process, the column pressure is lowered after adsorption in order to desorb the captured gas. For PSA, the inlet gas is pressurized via compression, and flowed through the column until saturation. Once the inlet valve is closed, the column pressure decreases toward ambient pressure. The pressure drop desorbs significant quantities of adsorbates from the surface, which elute from the column. Similarly, VSA lowers the pressure of the column to subatmospheric pressure after adsorption at a higher pressure. The vacuum applied to the column removes the adsorbates from the pores. Since post-combustion flue gas is released near ambient pressure, compressing or applying a vacuum to such a large volume of gas is expected to be difficult, and therefore, TSA might represent the most viable process. For pre-combustion capture, the gas stream is inherently pressurized after the conversion reactions, and a PSA cycle is expected to be most appropriate. Indeed, selected metal−organic frameworks have recently been evaluated in detail for use in post-combustion CO_2 capture via TSA and a pre-combustion CO_2 capture via PSA.[48,87]

The possibility of optimizing the parameters in each of these regeneration cycles (i.e., desorption temperature and pressure of inlet/outlet gas stream) and of combining multiple processes presents the option of tailoring the regeneration process to match the properties of a given adsorbent.[88,89] Above all, regeneration strategies must be designed to minimize the total cost of capturing CO_2, and as such, there will be a trade-off between maximizing the working capacity (the amount of CO_2 that can be captured in a given adsorption cycle) and minimizing the energy required for regeneration.[86,90,91] While detailed analysis of the energy and economic optimization issues in

dx.doi.org/10.1021/cr2003272 |*Chem. Rev.* 2012, 112, 724–781

CO_2 capture is beyond the scope of this review, such efforts will be crucial in directing the optimization of real-world CO_2 capture processes.

1.5. Metal−Organic Frameworks

Metal−organic frameworks are a new class of porous solids that have attracted much recent attention owing to their potential applications in a variety of areas, including gas storage, molecular separations, heterogeneous catalysis, and drug delivery.[10,17,92−98] These structures consist of metal-based nodes (single ions or clusters) bridged by organic linking groups to form a one-, two-, or three-dimensional coordination network. From an applications point of view, their extraordinary surface areas,[99] finely tunable pore surface properties,[100−103] and potential scalability to industrial scale[104] have made these materials an attractive target for further study. Although a number of excellent reviews already exist on the synthetic and structural aspects of metal−organic frameworks,[92,93,105,106] we briefly describe a number of key aspects of these materials to aid the reader in grasping the promises and challenges of utilizing metal−organic frameworks for CO_2 capture.

1.5.1. Synthesis and Structural Features. The synthesis of metal−organic frameworks is conventionally achieved by employing a so-called modular synthesis, wherein metal ions and organic ligands are combined to afford a crystalline, porous network. A large variety of synthetic methods have been developed in recent years for the preparation of these materials, and the conditions that lead to the formation of the desired phases are widely variable. Indeed, the reported synthetic procedures encompass a wide range of temperatures, solvent compositions, reagent ratios, reagent concentrations, and reaction times, and the fine-tuning of all of these parameters is crucial in optimizing the synthesis of the materials. Microwave heating,[107] sonication-assisted synthesis,[108,109] or mechanochemical procedures[110,111] have also been employed to effect formation of the framework. More recently, the first example of electrosynthetic deposition of metal−organic frameworks has also been demonstrated.[112] In most of the resulting materials, the solvent used during synthesis occupies the void space within the pores but can be removed by application of vacuum or heat, resulting in a large pore volume and large surface area accessible to guest molecules. In the context of CO_2 capture, these surfaces can then be utilized to perform the gas separation.

One of the most well-studied metal−organic frameworks to date is the $Zn_4O(BDC)_3$ (MOF-5) compound depicted in Figure 6,[113−115] which consists of tetrahedral $[Zn_4O]^{6+}$ clusters bridged by ditopic BDC^{2-} ligands to form a cubic, three-dimensional network. Importantly, functionalized derivatives of the MOF-5 structure type can be prepared using other substituted linear dicarboxylate linkers, allowing the linker length or functional groups present on the aromatic backbone to be readily modified, while preserving the overall connectivity of the framework.[100,116] This family of materials, referred to as isoreticular metal−organic frameworks (IRMOFs), feature considerably different pore sizes and pore functionalities, suggesting that the properties of the materials can be finely tuned by employing the appropriate linker type. More recently, this concept has been extended to other families of materials, such as the $Zr_6O_4(OH)_4(BDC)_6$ (UiO-66),[117,118] $Al(OH)(BDC)$ (MIL-53),[119,120] and $Cu_2(BPTC)$ (NOTT-100)[121] structure types. In each case, the length and functionality of the ligands can be changed, while forming materials of the same network

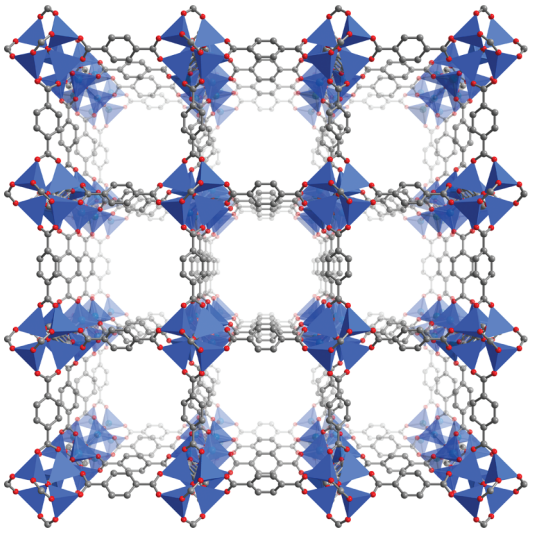

Figure 6. A portion of the crystal structure of $Zn_4O(BDC)_3$ (MOF-5). Blue tetrahedra represent ZnO_4 units, while gray and red spheres represent C and O atoms, respectively; H atoms are omitted for clarity.

connectivities. In the case of the MIL-53 structure type, there is also a dynamic (flexible) behavior, which is dependent on the constituents of the material. Note that the flexibility of metal−organic frameworks is an area that has also begun to be explored in the context of providing high selectivity,[122,123] although, as we discuss in section 3, the evaluation of their performance is more complex compared with rigid structures. Nevertheless, in the context of CO_2 capture, the ability to readily modify the surface chemistry of metal−organic frameworks is of particular interest for installing the desired chemical features (such as amines or polarizing groups) for enhancing the performance of the material.

An important route to installing the desired functionalities on the organic bridging unit is the postsynthetic modification of the surface functional groups following the initial formation of the crystalline structure.[102,103] One advantage of such an approach is that functional groups that might interfere with the formation of the framework owing to their propensity to bind metal ions (such as amines, alcohols, and aldehydes) can be installed with well-known organic transformations once the framework scaffold has been formed, eliminating the need to develop precise reaction conditions to form the material directly. Such a procedure has been demonstrated on compounds such as IRMOF-3,[124] DMOF-1-NH_2,[125,126] UiO-66-Br,[118] and MIL-101(Cr),[127] and the scope of reactions available is growing rapidly.

An alternative strategy of preparing metal−organic frameworks with functionalized surfaces is the generation of materials possessing exposed metal cation sites in the pores.[128−132] As will be discussed in section 3.2.3, such sites can facilitate highly selective interactions with certain gas molecules in separation applications and can also be of benefit for high-density gas storage applications, since they permit close approach of guest molecules to the pore surface. One of the most studied materials featuring such binding sites is $Cu_3(BTC)_2$ (HKUST-1), which exhibits a cubic, twisted boracite topology constructed from dinuclear Cu^{2+} paddlewheel units and triangular 1,3,5-benzenetricarboxylate linkers (see Figure 7).[133] The as-synthesized form of the framework contains bound solvent molecules on the axial coordination sites of each Cu^{2+} metal center, which can be

dx.doi.org/10.1021/cr2003272 |Chem. Rev. 2012, 112, 724–781

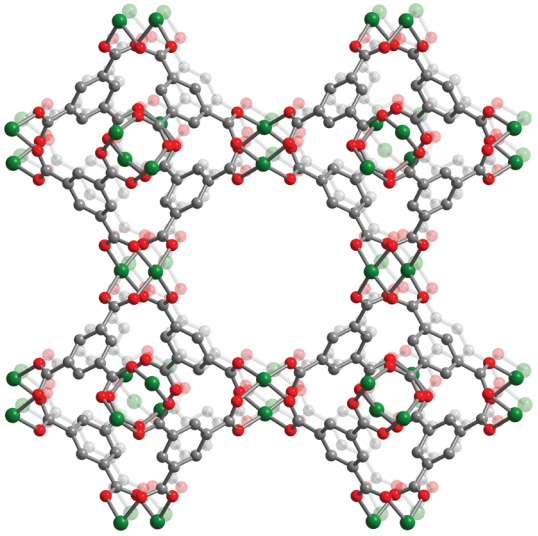

Figure 7. A portion of the crystal structure of $Cu_3(BTC)_2$ (HKUST-1).[133] Green, gray, and red spheres represent Cu, C, and O atoms, respectively; H atoms are omitted for clarity.

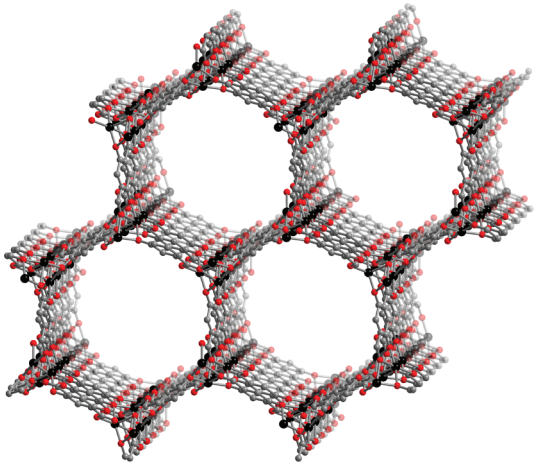

Figure 8. A portion of the crystal structure of M_2(dobdc) (M-MOF-74 or CPO-27-M). Black, gray, and red spheres represent M, C, and O atoms, respectively; H atoms are omitted for clarity.

subsequently removed *in vacuo* at elevated temperatures to create open binding sites for guest molecules. Indeed, these sites act as charge-dense point charges, which provide an opportunity for discrimination of certain components of gas mixtures based on their polarizability and dipole or quadrupole moment.

Interestingly, the HKUST-1 structure type can be prepared using a variety of metal ions (M = Cr, Fe, Zn, Mo).[134−137] In fact new members of several structure types, such as M_2(dobdc), M-BTT,[138−140] MIL-53,[119,141−147] and MIL-88,[148] have been prepared following their initial reports, highlighting that the metal is an additional variable worthy of consideration when tuning the properties of the material. In cases where the metal ions possess exposed coordination sites, the adsorptive properties can be dramatically tuned based on the charge density present at the metal coordination site.

In the context of CO_2 capture, the M_2(dobdc) (M = Mg, Mn, Fe, Co, Ni, Zn) series of metal−organic frameworks displayed in Figure 8 have recently been intensively studied.[100,130,149,150] These compounds exhibit a honeycomb-type network topology featuring hexagonal one-dimensional channels with a high density of exposed M^{2+} adsorption sites. As discussed in section 3, the specific metal that is employed has a dramatic effect on the adsorption capacity, binding strength, and material stability, highlighting the importance of materials optimization for specific applications. In the case of the Fe_2(dobdc), the ability for the exposed Fe^{2+} cations to engage in redox chemistry has allowed selective interactions with O_2 over N_2, which is of importance for oxy-fuel combustion (see section 4). Nevertheless, the systematic study of such a large family of isostructural compounds allows the effect of changing the metal ion to be identified, and more studies of this type would allow a greater understanding of the role of the metal ion in facilitating the adsorption properties of metal−organic frameworks.

Despite the apparent simplicity of the modular synthesis of metal−organic frameworks, one of the greatest challenges in preparing new materials lies in optimizing the reaction conditions that lead to the desired metal−organic framework in high yield and crystallinity. Slight changes in the reaction parameters employed, such as the reactant concentration, the presence of a cosolvent, solution pH, metal-to-ligand ratio, metal counteranion, reaction temperature, and reaction time, can have a considerable impact on the products that are obtained. Note that even in cases where just a single metal and ligand are combined, a large number of network connectivities may be possible, many of which are nonporous structures that are not of interest for gas storage and gas separation applications. These undesired phases can often coprecipitate with the porous phase of interest, giving rise to a mixture that is not readily separated owing to the insolubility of the components. Thus, the discovery of optimized conditions that afford the desired product can involve a large number of trial reactions in which the reaction parameters are systematically varied. Consequently, numerous studies involving the use of high-throughput technologies have appeared in recent years.[140,151−154]

1.5.2. Physical Properties. The chemical and thermal stability of metal−organic frameworks is generally lower than that of zeolites and other porous inorganic solids due to relatively weak coordination bonds that connect the metal and ligand components. Many are especially air- and moisture-sensitive following evacuation of the pores, leading to the need for careful handling under an inert atmosphere if the best performance characteristics are to be obtained. In the case of MOF-5, even slight exposure of the activated form of the material to the air results in rapid degradation of the crystallinity of the material and a concomitant loss of its surface area owing to the hydrolysis of the Zn−O bonds.[115,155] For applications such as post-combustion CO_2 capture, where significant quantities of water are present in the incoming gas stream, an increased chemical stability will be crucial if metal−organic frameworks are to be employed as separation materials. Several approaches for improving the stability of metal−organic frameworks (mainly through the use of components expected to yield stronger metal−ligand bonding) will be addressed in section 3.3.1.

The mechanical properties of metal−organic frameworks is an aspect that has not been thoroughly explored compared with organic polymers, though recent progress has been made in correlating the chemical structure to the observed characteristics.[156] For CO_2 capture applications, the materials should be sufficiently mechanically stable to allow a dense packing of the adsorbent bed without loss of the network structure. Even slight perturbations to the structural or chemical features under a high mechanical

dx.doi.org/10.1021/cr2003272 |*Chem. Rev.* 2012, 112, 724–781

pressure could have a considerable effect on the overall performance of the capture system. In terms of the magnitude of the structural changes that have been observed to date, it has been demonstrated for the metal−organic framework $Cu_3(BTC)_2$ that the application of large pressures (on the order of several GPa) can lower the total lattice volume of the material by as much as 10%.[157] It is not yet apparent how this compression would affect the adsorption properties of the material, but such effects would certainly be worthy of investigation when evaluating metal−organic frameworks within a real-world CO_2 capture system.

An additional bulk property that should be considered when assessing metal−organic frameworks for installation within a packed bed is its thermal conductivity. This parameter is crucial in determining the heating efficiency of the adsorbent bed and the duration of the regeneration cycle of a temperature swing adsorption-based capture process. Some analyses of this type have been performed in recent years, although owing to the limited scope of the studies, it is not yet established how much variation might exist in the thermal conductivity between compounds of different compositions and structure types. In a study of MOF-5,[158] the thermal conductivity was shown to decrease rapidly at the lowest temperatures (20−100 K), but remain relatively constant above 100 K. The thermal conductivity value of 0.32 $W \cdot m \cdot K$ is higher than that measured for zeolite NaX,[159] although the significant effect of particle size (larger particles exhibit higher thermal conductivities) presents a difficulty in comparing two materials. Nevertheless, the values observed for MOF-5 suggest that the thermal conductivity would not be a barrier for the implementation of metal−organic frameworks within an adsorbent bed.

One particular advantage of the use of a solid adsorbent such as a metal−organic framework would be the greatly reduced heat capacity compared with the aqueous alkanolamine solutions discussed in section 1.4.1. This is a particularly important parameter in temperature swing adsorption-based processes since it reflects the quantity of energy required for heating of the sorbent material to the desorption (regeneration) temperature. Indeed, as shown in Figure 4, the heat capacity of $Zn_4O(BTB)_2$ (MOF-177) over a temperature range of 25−200 °C was determined to be between 0.5 and 1.5 $J \cdot g^{-1} \cdot K^{-1}$, which lies considerably below the corresponding values recorded for 20 and 40 wt % aqueous MEA solutions.[47] Thus, if robust metal−organic frameworks exhibiting suitable gas separation performance can be prepared, there is tremendous promise in realizing CO_2 capture processes with greatly reduced energy requirements.

2. CO_2 ADSORPTION IN METAL−ORGANIC FRAMEWORKS

In this section, we address a number of aspects related to the adsorption of CO_2 within metal−organic frameworks that are important considerations when evaluating new materials for CO_2 capture applications, such as the adsorption capacity and enthalpy of adsorption. Single-component gas adsorption isotherm data can further be used to estimate the adsorption selectivity for CO_2 over other gases, which is a crucial parameter that determines the purity of the captured CO_2. Detailed knowledge of the binding environment of CO_2 within the pores of the framework can give vital information regarding the structural and chemical features contributing to the observed material performance, and *in situ* vibrational spectroscopy and crystallographic methods have recently emerged as invaluable tools for probing the adsorption phenomena. In this section, we present the most significant results that have been reported in this regard.

2.1. Capacity for CO_2

The adsorptive capacity is a critical parameter for consideration when evaluating metal−organic frameworks for CO_2 capture. The *gravimetric* CO_2 uptake, which refers to the quantity of CO_2 adsorbed within a unit mass of the material, dictates the mass of the metal−organic framework required to form the adsorbent bed. Meanwhile, the *volumetric* capacity refers to how densely the CO_2 can be stored within the material and is an equally crucial parameter, since it has a significant influence on the volume of the adsorbent bed. Both parameters also have an important role in determining the heating efficiency of the metal−organic framework, which directly impacts the energy penalty required for material regeneration and desorption of the captured CO_2.

The high internal surface areas of metal−organic frameworks provide an opportunity for large CO_2 adsorption capacities to be achieved, owing to the efficient packing and close approach of the guest molecules on the pore surface. For example, at 35 bar, the volumetric CO_2 adsorption capacity for MOF-177 reaches a storage density of 320 $cm^3(STP)/cm^3$, which is approximately 9 times higher than the quantity stored at this pressure in a container without the metal−organic framework and is higher than conventional materials used for such an application, namely, zeolite 13X and MAXSORB.[160] Note that, as mentioned earlier, the volumetric adsorption capacity of activated carbon materials at high pressures has been demonstrated to be competitive with metal−organic frameworks,[67] although we do not consider those materials in any further detail in the following discussion.

The high-pressure adsorption capacities for selected metal−organic frameworks are tabulated in Table 3. Indeed, the greatest capacities at high pressures are observed for materials exhibiting large surface areas, although excellent adsorption properties have also been demonstrated in a number of materials with modest surface areas that have a significant density of high-affinity adsorption sites, such as exposed metal cations. Owing to the particular relevance to pre-combustion CO_2 capture, which is performed at high pressures, these data will be discussed in full detail in section 4.

The lower-pressure (<1.2 bar) adsorption capacities for metal−organic frameworks collected at ambient temperatures (293−313 K) and 273 K are presented in Tables 4 and 5, respectively. At these pressures and temperatures, the adsorptive properties are predominantly dictated by the chemical features of the pore surface, and most of the high-capacity materials are those bearing highly functionalized surfaces. For post-combustion CO_2 capture, the pressure of the flue gas (∼1 bar) and the low partial pressure of CO_2 thereof ($P_{CO_2} \approx 0.15$ bar) leads to the lower-pressure region of the CO_2 adsorption isotherm being the area of interest (see section 3). Thus, maximizing the adsorption capacity specifically around 0.15 bar would be expected to lead to new materials with enhanced performance for post-combustion CO_2 capture.

2.2. Enthalpy of Adsorption

The enthalpy of adsorption of CO_2 is a critical parameter that has a significant influence over the performance of a given material for CO_2 capture applications. The magnitude of the enthalpy of adsorption dictates the affinity of the pore surface

dx.doi.org/10.1021/cr2003272 |*Chem. Rev.* 2012, 112, 724–781

Table 3. High-Pressure CO_2 Adsorption Capacities in Selected Metal−Organic Frameworks between 273 and 313 K

chemical formula[a]	common name	surface area (m^2/g) BET	surface area (m^2/g) Langmuir	capacity[b] (wt %)	pressure (bar)	temp (K)	ref
$Zn_4O(BTE)_{4/3}(BPDC)$	MOF-210	6240	10400	74.2	50	298	99
$Zn_4O(BBC)_2(H_2O)_3$	MOF-200	4530	10400	73.9	50	298	99
Cu_3(TCEPEB)	NU-100	6143		69.8[d]	40	298	161
$Zn_4O(FMA)_3$		1120	1618	69.0[d]	28	300	162
Mg_2(dobdc)	Mg-MOF-74, CPO-27-Mg	1542		68.9[c]	36	278	131
		1800	2060	39.8	40	313	87
$Zn_{3.16}Co_{0.84}O(BDC)_3$	Co21-MOF-5		2900	65.0[d]	10	273	163
$Be_{12}(OH)_{12}(BTB)_4$	Be-BTB	4030	4400	58.5	40	313	87
$Zn_4O(BDC)_3$	MOF-5, IRMOF-1		2900	58.0[d]	10	273	163
			3008	45.1[d]	40	298	164
$Zn_4O(BTB)_{4/3}(NDC)$	MOF-205	4460	6170	62.6	50	298	99
$Ni_5O_2(BTB)_2$	DUT-9			62.1[c]	47	298	165
$Zn_4O(BTB)_2$	MOF-177	4500	5340	60.8	50	298	99
		4690	5400	60.6	40	313	87
		4898	6210	56.8[d]	30	298	108
$[Cu_3(H_2O)]_3$(ptei)	PCN-68	5109	6033	57.2[c]	35	298	166
$Cr_3O(H_2O)_2F(BDC)_3$	MIL-101(Cr)	4230		56.9[d]	50	304	167
		3360	4792	50.2[d]	30	298	168
Ni_2(dobdc)	Ni-MOF-74, CPO-27-Ni	1218		54.2[c]	22	278	131
$[Cu(H_2O)]_3$(ntei)	PCN-66	4000	4600	53.6[c]	35	298	166
$Zn_4O(BDC)(BTB)_{4/3}$	UMCM-1	4100	6500	52.7[c]	24	298	169
$[Cu(H_2O)]_3$(btei)	PCN-61	3000	3500	50.8[c]	35	298	166
Cu_4(TDCPTM)	NOTT-140	2620		46.2[d]	20	293	170
$Tb_{16}(TATB)_{16}(DMA)_{24}$		1783	3855	44.2[d]	43	298	171
$Cr_3O(H_2O)_3F(BTC)_2$	MIL-100(Cr)	1900		44.2[d]	50	304	167
$Cu_3(BTC)_2$	HKUST-1	1270		42.8	300	313	172
		2211		40.1	40	303	173
		1571		35.9	15	298	174, 175
$H_3[(Cu_4Cl)_3(BTTri)_8]$	Cu-BTTri	1750	2050	42.8	40	313	87
Co(BDP)	Co-BDP	2030	2780	41.3	40	313	87
$Zn_2(BDC)_2$(DABCO)				37.6	15	298	176
$Zn(MeIm)_2$	nZif-8, *n* = nano	1264		35.0[d]	30	298	177
Al(OH)(BDC)	MIL-53(Al)			30.6[d]	25	304	178
Al(OH)(BDC-NH_2)	amino-MIL-53(Al)			30.0[d]	30	303	147
$Zn_2(BPnDC)_2$(bpy)	SNU-9		1030	29.9[c]	30	298	179
Al(OH)(ndc)	DUT-4	1308	1996	26.4	10	303	180
$Cr_3O(H_2O)_2F(BDC)_3$	MIL-101(Cr)			26.0[d]	5.3	283	181
Zn(F-pymo)$_2$	β-Zn(F-pymo)			26.0[d]	28	273	182
Mn(tpom)$(SH)_2$	MSF-2	622	816	25.0[d]	20.3	293	183
$Zn_6O_4(OH)_4(BDC)_6$	UiO-66			24.3[d]	18	303	184
$Zn(Gly\text{-}Ala)_2$				19.0[d]	15	273	185
$Al_{12}O(OH)_{18}(H_2O)_3(Al_2(OH)_4)(BTC)_6$	MIL-96(Al)			18.6[d]	20	303	186
$Cr_3O(H_2O)_2F(NTC)_{1.5}$	MIL-102			13.0[d]	30	304	187

[a] See List of Abbreviations. [b] Adsorption capacities are calculated from absolute adsorption isotherms unless otherwise noted and estimated from adsorption isotherms in cases where the values were not specifically reported. [c] Reported capacity was calculated from the excess adsorption isotherm. [d] It was not clear from the reference whether the reported isotherms were in absolute or excess adsorption.

toward CO_2, which in turn plays a crucial role in determining the adsorptive selectivity and the energy required to release the CO_2 molecules during regeneration. Precise control of the binding strength of CO_2 is essential if metal−organic frameworks are to be optimized such that they can lower the energy requirements of the capture process. Specifically, the use of a material that binds CO_2 too strongly would increase the regeneration cost owing to the large quantity of energy required in order to break the framework−CO_2 interactions. Meanwhile, if the enthalpy of adsorption is too low, although the material would be more readily regenerated, the purity of the captured CO_2 would be lowered owing to the decreased adsorption selectivity, and

dx.doi.org/10.1021/cr2003272 |Chem. Rev. 2012, 112, 724–781

Table 4. Lower-Pressure CO_2 Adsorption Capacities for Metal−Organic Frameworks at 293−319 K

chemical formula[a]	common name	surface area (m^2/g) BET	surface area (m^2/g) Langmuir	capacity[b] (wt %)	pressure (bar)	temp (K)	ref
$Mg_2(dobdc)$	Mg-MOF-74, CPO-27-Mg	1174	1733	27.5	1	298	188
				27.2	1	298	189
		1800	2060	26.7	1	298	48
				26	1.1	298	190
		1495	1905	26	1	296	150
$Cu_3(BTC)_2(H_2O)_{1.5}$	HKUST-1, (4 wt % H_2O)			27	1	298	191
$Co_2(dobdc)$	Co-MOF-74	957	1388	24.9	1	298	189
	CPO-27-Co						
		1080		23.4	1	296	150
$Ni_2(dobdc)$	Ni-MOF-74	936	1356	23.9	1	298	189
	CPO-27-Ni						
		639		22.7	1	298	192
		1083	1312	22.6	1	303	193
		1070		20.4	1	296	150
$Zn_2(dobdc)$	Zn-MOF-74			19.8	1	296	189
	CPO-27-Zn						
				19.6	1	296	150
		816		17.6	1.1	298	160
$Cu_3(BTC)_2$	HKUST-1	1400		19.8	1	293	194
			1492	18.4	1	298	191
				18.3	1	295	189
		1781		15.2	1	298	160
		1482		15	1	295	195
				10.6	0.8	298	192
				6.2	1	313	196
		857		6.2	1	295	195
$Cu_3(BTC)_3(H_2O)_3$	HKUST-1, (8 wt % H_2O)			17.4	1	298	191
$Cu_3(TATB)_2$	CuTATB-60, PCN-6	3811	4436	15.9	1	298	197
$H_3[(Cu_4Cl)_3(BTTri)_8(mmen)_{12}]$	mmen-Cu-BTTri	870		15.4	1	298	198
$Co_2(adenine)_2(CO_2CH_3)_2$	bio-MOF-11	1040		15.2	1	298	199
$H_3[(Cu_4Cl)_3(BTTri)_8]$	Cu-BTTri	1770	1900	14.3	1	298	200
$Zn_2(ox)(atz)_2$		782		14.3	1.2	293	201
$Ni_2(2\text{-amino-BDC})_2(DABCO)$	USO-2-Ni-A	1530		14	1	298	146
$Cu_2(bdcppi)(DMF)_2$	SNU-50	2300	2450	13.7	1	298	202
$Fe_3[(Fe_4Cl)_3(BTT)_8(MeOH)_4]_2$	Fe-BTT	2010		13.5	1	298	140
$Cu_3(TATB)_2$	Cu-TATB-30	2665	3065	13.4	1	298	197
$Cu(bpy)_2(BF_4)_2$	ELM-11			12.7	1	298	203
$Cu_2(bptc)(H_2O)_2(DMF)_3$	MOF-505	1547		12.6	1.1	298	160
Al(OH)(2-amino-BDC)	NH_2-MIL-53(Al), USO-1-Al-A	960		12	1	298	146
$Al(OH)(bpydc)\cdot 0.97Cu(BF_4)_2$		705		11.8	1	298	204
$Cu_4(TDCPTM)(H_2O)_4$,	NOTT-140a	2620		11.7	1	293	170
$Co(tImb)\cdot DMF\cdot H_2O$		886	1170	11.7	1	298	205
$Cu_2(TCM)$	SNU-21S		905	11.1	1	298	206
$Cu_3(BPT(N_2))_2$	UMCM-150(N2)			10.8	1	298	189
$Pd(\mu\text{-F-pymo-}N^1,N^3)_2$		600		10.7	0.86	293	207
Al(OH)(BDC)	MIL-53(Al), USO-1-Al	1300		10.6	1	298	146
		1235	1627	9.2	1	303	208
$Cu_3(BPT)_2$	UMCM-150			10.2	1	298	189
$Ni_2(BDC)_2(DABCO)$	USO-2-Ni	1925		10	1	298	146
$Ni_2(pbmp)$	Ni-STA-12			9.9	1	304	209
$Ni_3(pzdc)_2(7H\text{-ade})_2(H_2O)_4$		165		9.8	1	298	210

dx.doi.org/10.1021/cr2003272 |*Chem. Rev.* 2012, 112, 724–781

Table 4. Continued

chemical formula[a]	common name	surface area (m^2/g) BET	Langmuir	capacity[b] (wt %)	pressure (bar)	temp (K)	ref
Cu_2(TCM)	SNU-21H		695	9.7	1	298	206
Cu(BDC−OH)(H_2O)	Cu-BDC−OH	397	584	9.3	1	296	211
Fe(pz)Ni($CN)_4$				9.3	1	298	212
Zn(nbIm)(nIm)	ZIF-78	620		9.1	1	298	18, 213
Zn(cnIm)(nIm)	ZIF-82	1300		9.1	1	298	18, 213
Zn(cyanIm)$_2$	ZIF-96	960		8.8	1.1	298	214
Zn(IDC)	IMOF-3	802		8.6	1	298	215
$Zn_4O(BDC)_3$	MOF-5, IRMOF-1	2304	2517	8.5	1	296	216
		2833		4.5	1.2	298	160
				4	1.1	298	217
		1892	2784	3.5	1	298	189
			1263	3.4	1	298	218
		3320	4140	3.2	1	298	99, 219
Cr(OH)(BDC)	MIL-53(Cr)			8.5	1	304	220
Ni_3(L-TMTA)$_2$(bpy)$_4$				8.2	1	298	221
$Zn_2(BDC)_2$(DABCO)				8.1	1	296	222
$V^{(IV)}$O(BDC)	MIL-47	600	872	8.1	1	298	189
In(OH)(BDC)	USO-3-In-A	930		8	1	298	146
$Zn_4O(NO_2$-BDC$)_{1.19}((C_3H_5O)_2$-BDC$)_{1.07}$-[$(C_7H_7O)\cdot$BDC$]_{0.74}$	MTV-MOF-5-EHI	1176	1400	7.7	1.1	298	219
$Zn_4(OH)_2$(1,2,4-BTC)$_2$		408		7.6	1	295	223
Pd(μ-H-pymo-N^1,N^3)$_2$		600		7.3	0.86	293	207
$Zn_4O(PDC)_3$	IRMOF-11	2096		7.3	1.1	298	160
Mn(pmdc)			410	7.3	0.9	293	224
Pd(2-pymo)$_2$		600		7.3	0.86	293	225
Zn(cbIm)(nIm), (ZIF-69)		950	1070	8.6	1	298	18, 213, 226
Co(tImb)				7.2	1	298	205
Zn(brbIm)(nIm), (ZIF-81)		760		7.2	1	298	18, 213
$Zn_4O(BTB)_2$	MOF-177			6.5	1	298	217
		5400	4690	3.6	1	298	48
		4508		3.4	1	298	160
				3.4	1	298	189
$Zn_8(ade)_4(BPDC)_6O\cdot$2TEA	TEA@bio-MOF-1	1220		6.8	1	313	227
$Zn_8(ade)_4(BPDC)_6O\cdot$2TMA	TMA@bio-MOF-1	1460		6.7	1	313	227
Zn(almeIm)$_2$	ZIF-93	864		6.7	1	298	214
Zn(bIm)(nIm)	ZIF-68	1090	1229	6.7	1	298	18, 213, 226
Cu(pzdc)$_2$(bpy)	CPL-2	633[c]		6.6	1	298	228
Zn_2(bttb)(dpntcd)	YO-MOF			6.5	1	298	229
Cu_2(pzdc)$_2$(pyz)				6.4	1	300	230
Al(OH)(bpydc)	MOF-253	2160	2490	6.2	1	298	204
Zn_2(NDC)$_2$(diPyNI)$\cdot$Li				6.2	1	298	231
Zn(mbIm)(nIm)	ZIF-79	840		6.2	1.1	298	18, 213
$Zn_4O[(C_7H_7O)_2$-BDC$]_{2.49}(NO_2$-BDC$)_{0.51}$	MTV-MOF-5-EI	1020	1210	6.1	1.1	298	219
Zn_2(NDC)$_2$(diPyNI)				5.8	1	298	231
$Cu_4(O)(OH)_2(Me_2$trzpba$)_4$				5.8	1	298	232
$Zn_8(ade)_4(BPDC)_6O\cdot$2TBA	TBA@bio-MOF-1	830		5.7	1	313	227
$Zn(Im)_{1.13}(nIm)_{0.87}$	ZIF-70	1730	1970	5.7	1	298	18, 213, 226
$Cd_6(CPOM)_3(H_2O)_6$		231[c]		5.6	1	297	233
$H_3[(Cu_4Cl)_3(BTTri)_8(en)_{3.75}]$	en-CuBTTri	345	376	5.5	1	298	200
In(OH)(BDC)	USO-3-In	930		5.5	1	298	146
Zn_2(TCPB)(DPG)$\cdot$Li				5.4	1	298	231
$Zn_4O(TPDC)_3$		1912		5.4	1	298	234
Cu_2(hfbba)$_2$(3-mepy)$_2\cdot$2DMF$\cdot$3-mepy	F-MOF-4			5.3	1	293	235

dx.doi.org/10.1021/cr2003272 |*Chem. Rev.* 2012, 112, 724–781

Table 4. Continued

chemical formula[a]	common name	surface area (m^2/g) BET	Langmuir	capacity[b] (wt %)	pressure (bar)	temp (K)	ref
$Zn_8(ade)_4(BPDC)_6O$	bio-MOF-1	1680		5.2	1	313	227
$Zn_2(bpdc)_2(bpe)$		137.8[c]		5.2	1	298	236
$Zn_4O(BDC\text{-}NH_2)_3$	IRMOF-3	2160		5.1	1.1	298	160
				5	1	313	196
				4.7	1	298	189
$K_2(DABCO\text{-}H_2)[Zr(ox)_4]$				5.1	1	298	237
$Zn_2(bpy)(TCMO)$		1150		5	1	298	238
$Zn_2(TCMO)$				5	1	298	239
$Cu_2(TP)_3(OH)$	Cu-TP-1	258	286	5	1	298	240
$Zn_2(TCPBDA)$	SNU-30	707	740	4.9	1	298	241
Cu(dImb)		435	579	4.7	1	298	242
$Zn_2(bpdc)_2(bpee)$				4.7	1	298	243
$Zn(hymeIm)_2$	ZIF-25	1110		4.7	1	298	214
$Zn_4O(BDC\text{-}C_2H_4)_3$	IRMOF-6	2516		4.6	1.2	298	160
$Zn_2(TCPB)(DPG)$				4.6	1	298	231
$Zn(hymeIm)_2$	ZIF-97	564		4.5	1.1	298	214
$Zn_2(bcphfp)$	FMOF-2	378		4.5	1	298	244
$Zn(meIm)_2$	ZIF-8	1135	1768	4.3	1	298	189
$Cr_3O(H_2O)_2F(BDC)_3$	MIL-101(Cr)	2674		4.2	1	319	181
$Cu_2(hfbba)_2(3\text{-}mepy)_2$	Cu−F-MOF-4B			4.1	1	293	235
$Zn_3(OH)(p\text{-}CDC)_{2.5}$				4.1	1	298	245, 246
$Zn_4O(BDC)(BTB)_{4/3}$	UMCM-1	4034	5182	3.8	1	298	189
$Cu(2\text{-}pymo)_2$		350		3.8	0.86	293	225
$Zn_{20}(cbIm)_{39}(OH)$	ZIF-100	595	780	3.8	1	298	18, 247
$Zn_2(hfbba)_2(3\text{-}mepy)_2\cdot(3\text{-}mepy)$	Zn−F-MOF-4B			3.7	1	293	235
$Zn(cbIm)_2$	ZIF-95	1050	1240	3.7	1	298	18, 247
Cu(etz)	MAF-2			3.6	1	298	248
$Pd(\mu\text{-}Br\text{-}pymo\text{-}N^1,N^3)_2$				3.4	0.86	293	207
$Cd_2(ADA)_2(bpy)$	Cd-ADA-1			3.4	1	298	249
$Sc_2(BDC)_3$				3	1	303	250
$[Fe^{(III)}(Tp)(CN)_3]_2Co^{(II)}$		154		3	1	298	251
$Zn(dcIm)_2$	ZIF-71	652		2.8	1	298	214
Mg(3,5-PDC)	Mg-MOF-1			2.7	1	298	252
$Cu(hfipbb)(H2fipbb)_{0.5}$				2.6	1	298	253
$Zn_2(TCPBDA)(bpta)$	SNU-31		308	2.6	1	298	241
$Co_4(OH)_2(doborDC)_3$				2.6	1	298	254
$Zn_3(BDC)_3$	MOF-2	345		2.4	1	298	160
$Co(doborDC)_2$				2.4	1	298	254
$Pd(\mu\text{-}I\text{-}pymo\text{-}N^1,N^3)_2$				1.9	0.86	293	207
$Nd_6(OH)_9(HSCA)(SCA)$	Nd-RPF9	13.45		1.9	1	304	255
$Co(doborDC)_2(py)$				1.6	1	298	254
$Zn_2(BDC)_2(H_2O)_2$				1.4	1	296	222
$Mn_2(ADA)_2(bpy)$	Mn-ADA-1			1.4	1	298	249
$Ni(DBM)_2(bpy)$	Ni-DBM-BPY			0.9	1	298	256
$Cu(4\text{-}pymo)_2$		65		0.8	1	293	225
$Zn_3(Ge(4\text{-}carboxyphenyl)_4)_2$	Ge4A-Zn	417.7		0.5	1	297	257

[a] See List of Abbreviations. [b] Capacities were estimated from adsorption isotherms in cases where the values were not specifically reported. [c] Surface area was calculated by CO_2 adsorption.

the volume of the adsorbent beds would also be increased due to the lower density of CO_2 adsorption.

Owing to the presence of a variety of binding environments for CO_2 within the pores of metal−organic frameworks, the enthalpy of CO_2 adsorption is frequently expressed as an isosteric heat of adsorption (Q_{st}) as a function of the quantity of CO_2 adsorbed. The Q_{st} value is a parameter that describes the average enthalpy of adsorption for an adsorbing gas molecule at a

dx.doi.org/10.1021/cr2003272 |Chem. Rev. 2012, 112, 724–781

Table 5. Lower-Pressure CO_2 Adsorption Capacities in Metal−Organic Frameworks at 273 K

chemical formula[a]	common name	surface area (m^2/g) BET	surface area (m^2/g) Langmuir	capacity[b] (wt %)	pressure (bar)	ref
$Cu_2(abtc)_3$	SNU-5		2850	38.5	1	258
Dy(BTC)		655		27.2	1	259
$Cu_2(EBTC)(H_2O)_2$	Cu-EBTC	1852	2844	25.9	1	260
$Al_4(OH)_2(OCH_3)_4(BDC\text{-}NH_2)_3$	CAU-1	1268		24.1	1	261
$[Zn_2(abtc)(DMF)_2]_3$	SNU-4		1460	20.6	1	258
$Zn_2(BTetB)$		1370		19.7	1	262
$[Cu_2(abtc)(DMF)_2]_3$	SNU-5′		1260	19.2	1	258
$Cu_2(TCM)$	SNU-21		905	18.4	1	206
$[In_3O(diazDBC)_{1.5}(H_2O)_3](NO_3)$		892		17.9	1	263
$Co_4(OH)_2(p\text{-}CDC)_3$		1080		16.4	1	264
$Pd(\mu\text{-F-pymo-}N^1,N^3)_2$		600		14.2	1.2	207
$Cu(bpy)_2(BF_4)_2$	ELM-11			13.8	1	265, 266
$Cu_2(bptb)$			1217	12.6	1	267
$Zn(Pur)_2$	ZIF-20		800	12.4	1	268
$Zn_2(BTetB)(DMF)_2$		800		12.1	1	262
$Ba_2(H_2O)_4[Ln(DSbpyDO)_3(H_2O)]Cl$		718[c]		12.1	1	269
$Cd(DBNBVP)_2(ClO_4)_2$		1096[c]		12.1	1	270
$Zn_2(BDoborDC)_4$		800[c]		12.1	1	271
$Pd(\mu\text{-H-pymo-}N^1,N^3)_2$		600		11.9	1.2	207
$Ni(bpy)_2(BF_4)_2$	ELM-31			11.9	1	265
$Zn_2(TCPB)(DPG)$		740		11.6	1	272
$Cu(dhbc)_2(bpy)$				11	1	273
$Ni_2(bpy)_3(NO_3)_4$				10.6	1	274
$Cu_2(BPnDC)_2(bpy)$, (SNU-6)		2590	2910	9.9	1	275
$Cu_3(2,7\text{-NDC})_3(DEF)(H_2O)_2$	MOP-23	760	860	8.9	1	101
$Cd(nim)_2$	CdIF-9		3010	8.8	1	276
$Li(bim)(DABCO)_{0.5}(H_2O)$				8.7	1	277
$Ni(DBNBVP)_2Cl_2$		557[c]		8.1	1	278
$H[Zn_7(\mu_3\text{−}OH)_3(DBS)_3]$	UOC-1		649	8.1	1	279
$Cu_2(CNBPDC)_2(DMF)_2$, (MOF-601)			980	7.3	1	101
$In_2(OH)_2(obb)_2$		354.1	518.5	7.2	1	280
$Co_4(m\text{−}OH_2)_4(MTB)_2$	SNU-15	356[c]		7	1	281
$Ni_2(bpy)_3(NO_3)_4$, [Ethanol templated]				6.9	1	274
Zn(pydc)(dma)				6.6	1	282
$LiB(4\text{-MIm})_4$	BIF-9-Li	1523	1818	6.6	1	283
$Zn_2(BTetB)(py\text{-}CF_3)_2$		390		6.4	1	262
$CuB(4\text{-Mim})_4$, (BIF-9-Cu)		1287	1524	6.3	1	283
$Cu_2[pegBTB)](H_2O)_2$				6.3	1	267
Mn(NDC)(DEF)			191	6.2		284
$Zn_4O(BDC)_3$	(IRMOF-1, MOF-5)			6.2	1	285
$Zn_6(\mu4\text{-O})[bptb]_2[H_2bptb]$				6.1	1	267
$Cd(mim)_2$	CdIF-1		2420	5.6	1	276
$Li_2(bim)_2(DABCO)$				5.2	1	277
$Cu_2(2\text{-MeBPDC})_2(DMA)_2$	MOF-602		910	5	1	101
$Cu_2(IBPDC)_2(Py)_{1.67}(H_2O)_{0.33}$	MOF-603		460	5	1	101
$Zn_2(BPNDC)_2(bpy)$	SNU-9		1030	4.7	1	179
Cu(dhbpc)(bpy)				4.6	1	273
$Ln[(CPI)(H_2O)_2]$			147[c]	4.3	1	286
$Cd(CEbnbpy)(H_2O)_2\cdot(ClO_4)_2$		283		4.3	1	287
$Cd(eim)_2$	CdIF-4		2420	4.0	1	276
$[Na_6(H_2O)_6][Eu(DSbpyDO)_4]\cdot Cl$		426[c]		3.8	1	288
$Er_2(PDA)_3$				2.3	1	289

dx.doi.org/10.1021/cr2003272 |Chem. Rev. 2012, 112, 724–781

Table 5. Continued

chemical formula[a]	common name	surface area (m^2/g) BET	surface area (m^2/g) Langmuir	capacity[b] (wt %)	pressure (bar)	ref
Cu(atz)(benzDHP)		69		2.2	1	290
Li(bim)(4,4′-bipy)				1.8	1	277
$Co(UO_2)_6(PO_3CH_2CO_2)_3O_3(OH)(H_2O)_2$		142[c]		0.74	1	291
$Zn(DHBP)(DMF)_2$		209		0.56	1	292

[a] See List of Abbreviations. [b] Capacities were estimated from adsorption isotherms in cases where the values were not specifically reported. [c] Surface area was calculated by CO_2 adsorption.

specific surface coverage and is usually evaluated using two or more CO_2 adsorption isotherms collected at similar temperatures (usually within 10 K of each other). Usually the temperature-dependent isotherms are first fit to a high-order polynomial equation to obtain an expression for the pressure (P) in terms of the quantity of CO_2 adsorbed (N), and the Q_{st} values are subsequently computed using the Clausius−Clapeyron equation,[293] which takes the form

$$(\ln P)_N = -(Q_{st}/R)(1/T) + C \quad (1)$$

where T is the temperature, R is the universal gas constant, and C is a constant. The Q_{st} at each adsorption level is readily obtained from the slope of the plots of $(\ln P)_N$ as a function of $(1/T)$.

One further parameter of interest for evaluating the strength of CO_2 binding, particularly at the lowest CO_2 pressures, is the zero-coverage isosteric heat of adsorption. This parameter gives an indication of the strength of the strongest binding sites within the material, which, depending on its magnitude, can subsequently be attributed to certain chemical features of the pore surface, such as exposed metal cation sites or amine functionalities. The zero-coverage isosteric heat of adsorption is evaluated by first fitting the temperature-dependent isotherm data to a virial-type expression,[294] which can be written

$$\ln P = \ln N + \frac{1}{T}\sum_{i=0}^{m} a_i N^i + \sum_{i=0}^{n} b_i N^i \quad (2)$$

where a_i and b_i are virial coefficients, and m and n are the number of virial coefficients required for adequate fitting of the isotherms. The isosteric heat of adsorption can then be evaluated using the following expression:

$$Q_{st} = -R\sum_{i=0}^{m} a_i N^i \quad (3)$$

and it follows that the zero-coverage isosteric heat of adsorption is given by:

$$Q_{st} = -Ra_0 \quad (4)$$

An alternative method for calculating the isosteric heat of adsorption involves the use of a single- or dual-site Langmuir-type expression to first describe the adsorption isotherms at different temperatures. The dual-site model is particularly of benefit when performing the fit for materials featuring a combination of both strong and weak binding sites and assumes that the adsorption occurs with a Langmuir-type behavior at two separate sites.[48] Thus, the total quantity adsorbed at a given pressure is given by the sum of two single-site Langmuir isotherms:

$$N = \frac{q_{sat,A} b_A P}{1 + b_A P} + \frac{q_{sat,B} b_B P}{1 + b_B P} \quad (5)$$

where $q_{sat,A}$ and $q_{sat,B}$ are the saturation loadings and b_A and b_B are the Langmuir parameters for the sites A and B, respectively. An advantage of this type of expression is that it allows a more accurate fitting of the isotherms compared with the virial-type equations, especially when there is a large difference in the adsorption enthalpy of the adsorption sites. Once the isotherms are fit, the isosteric heat of adsorption can then be calculated by reducing eq 5 to a form in which P is expressed as a function of N, followed by the use of eq 1.[48]

Table 6 lists the zero-coverage isosteric heat of CO_2 adsorption for metal−organic frameworks reported to date. As expected, at the lowest coverages, where the magnitude of the isosteric heat of adsorption is largely a function of the binding strength of the strongest binding sites within the material, metal−organic frameworks bearing amine functionalities or highly polarizing adsorption sites display the highest values. Note that a thorough evaluation of the performance of a given metal−organic framework should consider the isosteric heat of adsorption over the entire adsorption range (not just at zero-coverage), which is greatly affected by the pressure regime in which the capture process is to be performed. Furthermore, for some metal−organic frameworks where multiple studies have been performed, the values reported for the isosteric heat of adsorption were found to vary significantly. For example, the Q_{st} values at zero-coverage reported for CO_2 adsorption within HKUST-1 range from approximately −15 to −35 kJ/mol, which presumably is a result of variations in the synthesis and activation procedures employed for preparation of the samples, and is also likely to be influenced by the method in which the value is calculated. This serves to highlight the importance of ensuring that the experimental conditions are optimized prior to evaluation of the adsorption properties of any metal−organic framework.

2.3. Selectivity for CO_2

In CO_2 capture applications, a high selectivity for CO_2 over the other components of the gas mixture is essential. This selectivity can originate from two main mechanisms. In *size-based* selectivity (kinetic separation), a metal−organic framework with small pore size may permit molecules only up to a certain kinetic diameter to diffuse into the pores, allowing the molecules to be separated based on size. For CO_2/N_2 and CO_2/H_2 separations, the relatively similar kinetic diameters of the molecules (see Table 2) would require materials operating on a size-selective mechanism to possess very small pores, which may

dx.doi.org/10.1021/cr2003272 |Chem. Rev. 2012, 112, 724–781

Table 6. Zero-Coverage Heat of CO_2 Adsorption in Metal−Organic Frameworks

material chemical formula[a]	common name	functionality type	$-Q_{st}$ (kJ/mol)	ref
$H_3[(Cu_4Cl)_3(BTTri)_8(mmen)_{12}]$	Cu-BTTri-mmen	amines	96	198
$H_3[(Cu_4Cl)_3(BTTri)_8(en)_{3.75}]$	Cu-BTTri-en	amines	90	200
Zn(DCTP)(DABCO)		amines	77	295
$Cr_3O(H_2O)_3F(BTC)_2$	MIL-100(Cr)	exposed cations	62[b]	167
$Zn_8(ade)_4(BPDC)_6O\cdot TBA$	TBA@bio-MOF-1	amines	55	227
$Al(OH)(NH_2\text{-}BDC)$	NH_2-MIL-53(Al), USO-1-Al-A	amines	50	146
			38	147
$Cu_3(TATB)_2$	CuTATB-30		48	197
$Al_4(OH)_2(OCH_3)_4(BDC\text{-}NH_2)_3$	CAU-1	amines	48	261
$Mg_2(dobdc)$	Mg-MOF-74, CPO-27-Mg	exposed cations	47	150
			41	131
			39	190
$Co_2(ade)_2(CO_2CH_3)_2$	bio-MOF-11	amines	45	199
$Cr_3O(H_2O)_2F(BDC)_3$	MIL-101(Cr)	exposed cations	44[b]	167
$Ni_2(dobdc)$	Ni-MOF-74 CPO-27-Ni	exposed cations	42	193
			37	131
$Zn_2(ox)(atz)_2$			41	201
$Pd(\mu\text{-F-pymo-}N^1,N^3)_2$			40	207
Cu(dImb)			39	242
$Pd(\mu\text{-H-pymo-}N^1,N^3)_2$			38	207
$Al_4(OH)_8$(pyromellitate)	MIL-120		38[b]	296
$Zn_2(bpdc)_2(bpe)$			38	236
$Co_2(dobdc)$	Co-MOF-74 CPO-27-Co	exposed cations	37	150
$Li@CNT@Cu_3(BTC)_2$		exposed cations	37	297
$Li@Cu_3(BTC)_2$		exposed cations	36	297
$Zn_8(ade)_4(BPDC)_6O\cdot 2Me_2NH_2$	bio-MOF-1		35	227
$Zn_8(ade)_4(BPDC)_6O\cdot 2TEA$	TEA@bio-MOF-1		35	227
$Zn_8(ade)_4(BPDC)_6O\cdot 2TMA$	TMA@bio-MOF-1		35	227
$Cu_3(TATB)_2$-catenated	CuTATB-60, PCN-6		35	197
Al(OH)(BDC)	MIL-53(Al), USO-1-Al		35[b]	178
			30	146
$Cu_3(BTC)_2$	HKUST-1	exposed cations	35	298
			15[c]	196
$Ni_3(pzdc)_2(7Hade)_2(H_2O)_4$			35 (at 5.6 wt %)	210
$CNT@Cu_3(BTC)_2$		exposed cations	34	297
$Zn_4O(BDC)_3$	IRMOF-1, MOF-5		34	216
			17	164
			15[c]	196
$Ni_2(pbmp)$	Ni-STA-12		34[b]	209
$Al_{12}O(OH)_{18}(H_2O)_3(Al_2(OH)_4)(BTC)_6$	MIL-96		33[b]	186
Cr(OH)(BDC)	MIL-53(Cr)		32[b]	178
$Er_2(PDA)_3$			30	289
$Fe(pz)Ni(CN)_4$			30	212
$Al(OH)(bpydc)\cdot 0.97Cu(BF_4)_2$			30	204
$Cu_3(BTC)_2\cdot 3H_2O$	HKUST-1 (hydrated)		30	174, 175
$Cu(hfipbb)(H_2fipbb)_{0.5}$			30	253
$Zn_2(bpdc)_2(bpee)$			29	243
$[In_3O(abtc)_{1.5}(H_2O)_3]$			29	263
Cu(etz)	MAF-2		27	248

dx.doi.org/10.1021/cr2003272 |*Chem. Rev.* 2012, 112, 724–781

Table 6. Continued

material chemical formula[a]	common name	functionality type	$-Q_{st}$ (kJ/mol)	ref
$Fe_4O_2(btb)_{8/3}$			26	299
$Cu(pzdc)_2(bpy)$	CPL-2		26	228
$Co(dpt24)_2$	MAF-25		26	300
$[Cu(BDC{-}OH)(H_2O)]$			26	211
$[Ni(Bpene)][Ni(CN)_4]$			25	301
$Sc_2(BDC)_3$			25[b]	250
$Cu_4(TDCPTM)(H_2O)_4$	NOTT-140		25	170
$NH_4[Cu_3(\mu_3{-}OH)(\mu_3\text{-4-carboxypyrazolato})_3]$			25	302
$Co(mdpt24)_2$	MAF-26		23	300
$Al(OH)(bpydc)$	MOF-253		23	204
$Zn_2(BDC)_2(DABCO)$			22	176
$[Na_6(H_2O)_6][Eu(DSbpySO)_4]Cl$			22	288
$H_3[(Cu_4Cl)_3(BTTri)_8]$	CuBTTri	exposed cations	21	200
$[Ba_2(H_2O)_4][Ln(DSbpyDO)_3(H_2O)]Cl$			21	269
$Ni_2(BDC)_2(DABCO)$			20	176
$Zn_4(OH)_2(1,2,4\text{-BTC})_2$			20	223
$Zn_2(bpy)(TCM)$			20	238
$Zn_2(BDC)_2(4,4'\text{-bpy})$	MOF-508b		19	303
			15	304
$Zn_4O(BDC\text{-}NH_2)_3$	IRMOF-3	amines	19[c]	196
$[(Tp)Fe(CN)_3]_2Co$			13	251
$Zn_4O(BDC)(BTB)_{4/3}$	UMCM-1		12	169

[a] See List of Abbreviations. Unless otherwise stated, all Q_{st} values are determined by a fitting to the adsorption isotherms, such as the virial or Clausius−Clapeyron equation. [b] Determined experimentally by microcalorimetry. [c] Determined experimentally by temporal analysis of products (TAP) method.

limit the diffusion of gases throughout the material. While some metal−organic frameworks do exhibit pore apertures in this size regime,[305] almost all materials that exhibit high surface areas and high adsorption capacities for CO_2 possess pore openings that are significantly larger than the sizes of the molecules. Thus, most studies of metal−organic frameworks rely on the separation of the molecules based on adsorptive phenomena.

The *adsorptive* selectivity (thermodynamic separation) arises owing to the difference in affinity of the various components of the gas mixture to be adsorbed on the pore surface of the metal−organic framework. For selectivity based upon a *physisorptive* adsorption mechanism, the separation relies on the gas molecules having different physical properties, such as the polarizability or the quadrupole moment, resulting in a higher enthalpy of adsorption of certain molecules over others. For example, for the CO_2/N_2 separation relevant to post-combustion CO_2 capture, the higher polarizability (CO_2, 29.1×10^{-25} cm^{-3}; N_2, 17.4×10^{-25} cm^{-3}) and quadrupole moment (CO_2, 13.4×10^{-40} C·m^2; N_2, 4.7×10^{-40} C·m^2) of CO_2 compared with N_2 results in a higher affinity of the surface of the material for CO_2.[306] As will be discussed in full detail in section 3, the selectivity can be further enhanced by installing highly charged groups, such as polar organic substituents or exposed metal cation sites, which take greater advantage of this difference in the polarizability of the molecules.[10]

Alternatively, the adsorptive selectivity can arise due to *chemical* interactions between certain components of the gas mixture and surface functionalities of the metal−organic framework. Functionalities that recognize certain molecules based on their propensity for participating in specific chemistry can result in much higher selectivities than those obtained from purely physisorptive mechanisms. For example, in the case of CO_2/N_2 separations, the susceptibility of the carbon atom in CO_2 to attack by nucleophiles has led to the investigation of materials possessing strong Lewis bases, such as amines. The interaction of CO_2 with an amine can result in a C−N bond as observed in the aqueous amine solutions, resulting in highly selective adsorption of CO_2 over N_2. For O_2/N_2 separations in oxy-fuel combustion, the ability for O_2 to participate in electron transfer reactions has led to the investigation of materials constructed from redox-active metal centers.

2.3.1. Estimation from Single-Component Isotherms. The most basic method for evaluating the adsorptive selectivity for CO_2 from a gas mixture is the calculation of a selectivity factor using the experimental single-component gas adsorption isotherms. Here, the selectivity factor is defined as the molar ratio of the adsorption quantities at the relevant partial pressures of the gases. In the case of post-combustion CO_2 capture, the partial pressures of CO_2 and N_2 are 0.15 and 0.75 bar, respectively. Additionally, selectivity factors should be normalized to the composition of the gas mixture as given by the following expression:

$$S = \frac{q_1/q_2}{p_1/p_2} \tag{6}$$

where S is the selectivity factor, q_i represents the quantity adsorbed of component i, and p_i represents the partial pressure of component i. Note that the selectivity factor does not take into account the competition of gas molecules for the adsorption sites on the pore surface owing to the fact that it originates from single-component adsorption isotherms and therefore does not

dx.doi.org/10.1021/cr2003272 |Chem. Rev. 2012, 112, 724–781

represent the actual selectivity that would result from the dosing of a mixed gas. Nevertheless, it provides a simple point of comparison for evaluating the performance of different metal−organic frameworks, and a table of selectivity factors for selected compounds in the context of post-combustion CO_2 capture will be presented in section 3.

2.3.2. Ideal Adsorbed Solution Theory (IAST). In practice, it is challenging to measure directly the adsorption selectivity of an adsorbent for gas mixtures, such as those encountered in CO_2 capture applications. However, the performance can be conveniently predicted from the single-component adsorption isotherms of the constituents of the mixed gas via modeling techniques, such as ideal adsorbed solution theory (IAST).[307] In this method, the isotherms are collected at the same temperatures, and IAST is applied in order to predict the expected selectivity of the material. Here, we briefly describe the most relevant aspects of IAST, and discuss its potential for identifying and evaluating promising CO_2 capture adsorbents and the challenges associated with its application.

First, the method used to apply IAST for modeling mixed-gas adsorption behavior from single-component isotherms will be outlined. Using a mathematical fitting of the single-component isotherms the mole fraction of each species in the adsorbed phase can be calculated by solving the expression

$$\int_0^{P\cdot y_i/x_i} \frac{\text{Isotherm fit for component } i(P)}{P}\,dp = \int_0^{P\cdot y_j/x_j} \frac{\text{Isotherm fit for component } j(P)}{P}\,dp \quad (7)$$

where x_i and y_i are the adsorbed and bulk phase mole fractions of component i, respectively, and P is the total pressure. To determine the amount adsorbed in the mixture, as opposed to the mole fraction, the following equation can be used:

$$\frac{1}{n_{\text{total}}} = \frac{x_i}{n_i^0} + \frac{x_j}{n_j^0} \quad (8)$$

where, at a given pressure, n_{total} is the total number of moles adsorbed in the mixture and n_i^0 is the amount of pure component i adsorbed per gram of adsorbent.

The two main assumptions of IAST are that the components must both mix and behave as ideal gases and that the surface of the sorbent is homogeneous. The accuracy of the theory begins to diminish at very high mixture fractions of the less-adsorbed component, since under those conditions the computation involved in an IAST calculation requires integration of the single-component of the less-adsorbed species up to extremely high pressures.[308] The behavior of gases within flexible metal−organic frameworks is also not accurately described by IAST in its usual form. It should be noted, however, that a method for applying IAST to flexible metal−organic frameworks (or any flexible solid) has recently been developed.[309,310]

The IAST method has been used to evaluate gas mixtures relevant to post-combustion[19,262,311,312] and precombustion[313−315] CO_2 capture. Additionally, IAST and grand canonical Monte Carlo (GCMC) simulations are often reported together as a method to validate the results of the IAST calculations. For example, it has been shown that IAST compares well with GCMC simulations of CH_4/H_2 selectivity in MOF-5 and HKUST-1 and CO_2/H_2 selectivity in MOF-5.[316] However, IAST was found to underpredict the CO_2/H_2 selectivity in HKUST-1, which was attributed to the differences in size between CO_2 and H_2 coupled with the varied pockets and channels present in HKUST-1. Later, it was demonstrated that CO_2/H_2 separations can be accurately modeled by IAST by substantiating the results with GCMC calculations in MOF-177.[87] A comparison of the IAST results reported for Mg_2(dobdc) to GCMC simulations found that the theory overpredicts CO_2/H_2 selectivity in metal−organic frameworks containing exposed metal cation sites.[317] Here, the differences were attributed to the fact that the configurational bias Monte Carlo (CBMC) calculations neglect orbital interactions. The validity of IAST for CH_4/H_2 separations has been validated in noninterpenetrated[318,319] and interpenetrated[320] metal−organic frameworks. Additionally, it has been demonstrated that, at least at high pressure, IAST and GCMC predict approximately the same CO_2/N_2 selectivity in HKUST-1.[321,322]

The quality and fit of the pure component data must be very good for IAST simulations to be accurate. The sensitivity of the results of IAST to the fit of the pure component data has been studied in detail,[323] and it has also been highlighted that the issue of obtaining high accuracy fits to the adsorption isotherms can be avoided by using isotherms predicted by GCMC simulations.[324] This approach, however, does not take full advantage of the principle benefit of IAST: once a class of metal−organic frameworks has been shown to be accurately described by IAST for a given gas mixture, calculus that can be solved analytically can be used to conveniently evaluate mixed-component adsorption from the experimental single-component data. As a result, determining the origin of any deviation between simulations and IAST for specific adsorbate mixtures or adsorbent types is of paramount importance for rendering IAST a routine treatment of pure-component isotherms.[325]

2.3.3. Gas Mixtures and Breakthrough Experiments. A relatively straightforward way of experimentally evaluating the performance of metal−organic frameworks in gas separations is by performing breakthrough experiments. In a typical setup, the gas mixture is flowed through a sample that has been pressed into a pellet or incorporated into a membrane, and the composition of the outgoing gas stream is monitored, usually by gas chromatography or mass spectrometry. As exemplified in Figure 9 for a CO_2/N_2 gas mixture, before the material bed becomes saturated with adsorbed gas, the downstream composition will consist of virtually pure N_2 owing to its much lower affinity for the framework surface. After the bed is saturated with CO_2 and breakthrough occurs, the downstream gas composition eventually corresponds to the input mixture. Such experiments have now been performed on metal−organic frameworks for a variety of binary gas mixtures, such as CO_2/CO,[247] CO_2/N_2,[247,303,304,326] and CO_2/CH_4,[147,190,213,247,268,302−304,327−329] as well as ternary gas mixtures, such as $CO_2/N_2/CH_4$,[303,304] $CO_2/N_2/H_2O$,[326] and $CO_2/N_2/O_2$.[330] The results provide the ultimate laboratory demonstration of the separation performance of a material prior to scale-up.

2.4. *In Situ* Characterization of Adsorbed CO_2

In situ methods are an important component of studying the relationship between the structure and chemical features of metal−organic frameworks and the observed CO_2 adsorption properties. For example, crystallographic characterization of CO_2 adsorbed in metal−organic frameworks allows direct observation of the location of the CO_2 molecules within the structure, facilitating an understanding of the interactions

dx.doi.org/10.1021/cr2003272 |*Chem. Rev.* 2012, 112, 724–781

within the material giving rise to the adsorptive behavior. Although such experiments usually require elaborate experimental facilities, *in situ* infrared spectroscopy offers a more convenient probe that can also afford information regarding the CO_2 adsorption sites. In the following sections, we describe some recent examples of the use of these techniques in elucidating the adsorption behavior of CO_2 within metal–organic frameworks.

2.4.1. Structural Observations. The most informative technique for directly obtaining structural information regarding CO_2 bound to the surfaces of metal–organic frameworks is via X-ray (or neutron) diffraction studies. Here, an activated single-crystal or powder sample of a metal–organic framework is inserted into a cell, such as a glass capillary, which is subsequently evacuated and dosed with a known (usually small) quantity of high-purity CO_2 gas.[331] Diffraction data are collected, and structural refinements are subsequently performed in order to reveal the location of the dosed CO_2 molecules. Note that although such experiments are conceptually quite simple, a number of issues complicate the full elucidation of the CO_2 adsorption sites. Indeed, from a practical point of view, absorption of X-rays by the glass capillary, sample integrity upon evacuation, and disorder of the adsorbate molecules within the void spaces of the framework can significantly affect the quality of the refinements. Here, we discuss a number of key studies in which the location of the CO_2 adsorption sites within the metal–organic framework have been elucidated by diffraction experiments.[248,332,333] Although these initial investigations were performed with pure CO_2 gas, the future use of a mixture of gases may allow the separation phenomena within metal–organic frameworks to be observed directly, enabling a greater understanding of the chemical and structural features that give rise to enhanced CO_2 capture performance.

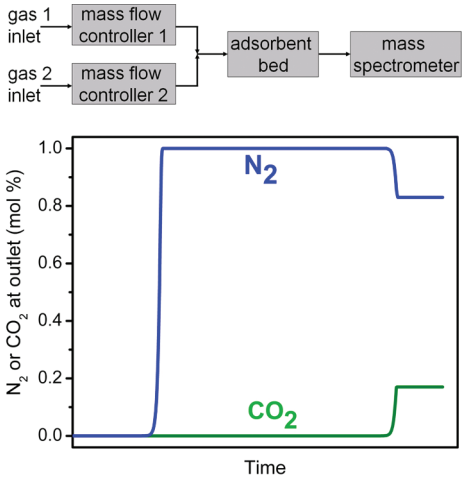

Figure 9. (top) A schematic of the configuration of an experimental breakthrough setup and (bottom) example of an idealized breakthrough curve for a mixed gas consisting of 20% CO_2 in N_2.

One of the earliest examples of an *in situ* observation of CO_2 adsorption was performed on the flexible MIL-53(Cr) system,[334] in which chains of octahedral Cr^{3+} ions are bridged by 1,4-benzenedicarboxylate linkers to form diamond-shaped one-dimensional channels. This framework exhibits a breathing behavior upon adsorption of CO_2, resulting in a dramatic change in the unit cell parameters. In the evacuated state, and at relatively low pressures of CO_2, the pores are narrow (MIL-53LP, see Figure 10). However, above a pressure of 4 bar of CO_2, the powder diffraction patterns indicate the evolution of a phase (MIL-53HP) in which the predominant low-angle peaks are shifted to lower angles, indicating an expansion of the pore dimensions. Indeed, refinement of the unit cell parameters of this phase indicate an enlargement of the cell volume by approximately 50%, which is consistent with the increased filling of the pores with guest molecules and a large step observed in the CO_2 adsorption isotherm (304 K) at approximately 5 bar. This structural transition is reversible upon lowering of the pressure, and could be cycled without loss of crystallinity. Importantly, these observations established a direct method for the characterization of the framework flexibility of this structure type, which was initially probed via temperature-dependent solid-state NMR spectroscopy for a hydrated sample of MIL-53(Al).[335]

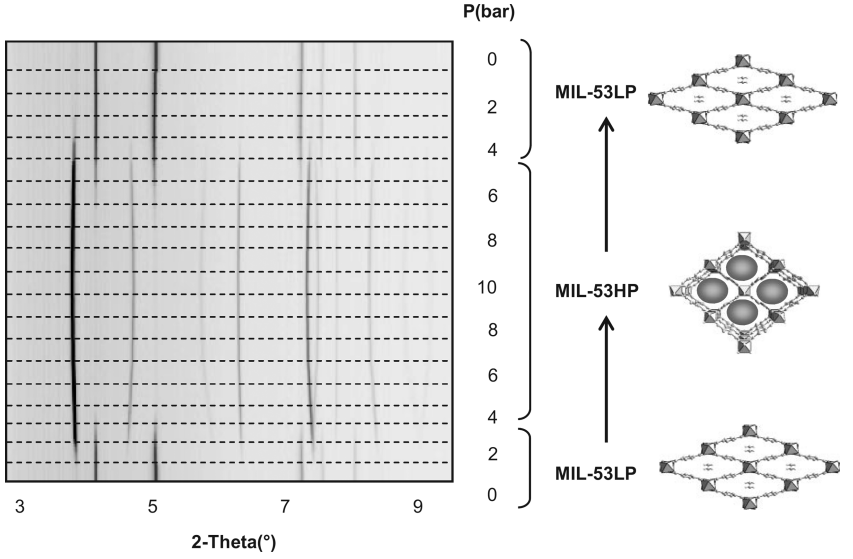

Figure 10. Powder X-ray diffraction patterns as a function of CO_2 pressure in MIL-53(Cr) recorded at 293 K. The framework undergoes a reversible structural transition upon increase of the pressure of CO_2. Reproduced with permission from ref 334. Copyright 2007 Wiley-VCH.

dx.doi.org/10.1021/cr2003272 |*Chem. Rev.* 2012, 112, 724–781

More recently, the zinc-based metal−organic framework $Zn_2(atz)_2(ox)$, with a structure comprising two-dimensional layers of Zn^{2+} ions coordinated by amine-functionalized triazolate ligands pillared by oxalate ligands, was employed in a single-crystal diffraction study in order to observe framework−CO_2 interactions.[201,336] Figure 11 shows the primary binding site for CO_2, in which the carbon atom of the CO_2 molecule and the nitrogen of the amine are in close contact, suggesting localized adsorption of CO_2 at these sites. Here, the C···N distance of 3.152(6) Å and lack of bending in the CO_2 molecule indicates that the interaction is physisorptive, with a relatively weak interaction between the amine moiety and the CO_2 molecule. It should be noted that such aromatic amines are not strongly basic and will not generally lead to a high CO_2 selectivity via chemisorption.

High-resolution powder X-ray diffraction data has been used to observe the binding sites and conformation of the CO_2 molecules in $Ni_2(dobdc)$ (Ni-MOF-74), which possesses exposed Ni^{2+} metal cation sites on the pore surface (see Figure 12).[193] Importantly, the diffraction data following dosing with CO_2 reveals that the guest molecules are indeed coordinated to the open metal sites with a bent O−C−O angle of 162(3)°. The short Ni−O_{CO_2} distance of 2.29(2) Å is indicative of a strong interaction owing to the highly polarizing nature of the Ni^{2+} adsorption sites. The disorder within the structure presents a difficulty in ascertaining the true geometry of the bound CO_2, although infrared studies performed on the same compound are indeed consistent with a perturbation of the local geometry from linear to a slightly bent conformation (see section 2.4.2).

Elucidation of the binding sites for CO_2 within a metal−organic framework provides valuable insight into the specific interactions that lead to enhanced adsorption and selectivity properties. The data obtained from structural characterization of metal−organic frameworks containing CO_2 can be used to study the structural and chemical features of the pore surface that give rise to such properties and can assist with identifying new synthetic targets that may exhibit high performance in model or pilot scale CO_2 capture processes.

2.4.2. Infrared Spectroscopy. Infrared spectroscopy has been shown to be a crucial tool for probing the local interactions between CO_2 and the surfaces of metal−organic frameworks.[209,327,334,337−341] The asymmetric stretching (ν_3, 2349 cm^{-1}) and bending (ν_2, 667 cm^{-1}) modes of CO_2 are infrared-active, while the symmetric stretching mode (ν_1, 1342 cm^{-1}) is infrared-inactive.[342] In cases where strong binding and polarization of the molecule occurs, infrared-active modes can serve as a handle for identifying the nature of the resulting CO_2 adduct.

Several studies have been performed in which the adsorption of CO_2 at exposed metal cation sites has been probed via infrared spectroscopy.[167] In the case of $Ni_2(dobdc)$ mentioned above, the adsorption of CO_2 onto the exposed Ni^{2+} adsorption sites resulted in an 8 cm^{-1} red shift of the ν_3 band due to electron donation from the oxygen lone pairs on CO_2 to the unoccupied Ni^{2+} orbitals.[193] A broad resonance at 2408 cm^{-1} was assigned to be a combination mode of $\nu_3 + \nu_{M-O}$, where ν_{M-O} is the stretching mode of the Ni^{2+}—O═C═O adduct; from this assignment ν_{M-O} was determined to be 67 cm^{-1}, in line with the expected value of ∼70 cm^{-1}. The ν_2 bending mode was split into a doublet, with an energy separation of 8 cm^{-1}. As previously discussed, refinement against powder X-ray diffraction data of the gas-loaded sample indicated that the adsorbed CO_2 adopted a bent configuration, with a large uncertainty in the O═C═O bond angle. The ν_2 doublet was presented as evidence for the bending of CO_2 and reduction of the local symmetry, despite the large geometric uncertainty.

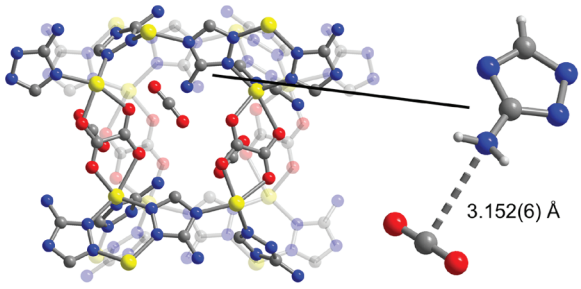

Figure 11. A portion of the single-crystal structure of $Zn_2(atz)_2(ox)$ following dosing with CO_2 as viewed along the crystallographic *a*-axis. Yellow, gray, blue, and red spheres represent Zn, C, N, and O atoms, respectively; H atoms are omitted for clarity. Inset shows interaction between the amine group and the CO_2 molecule (light gray speres represent H atoms).[201,336]

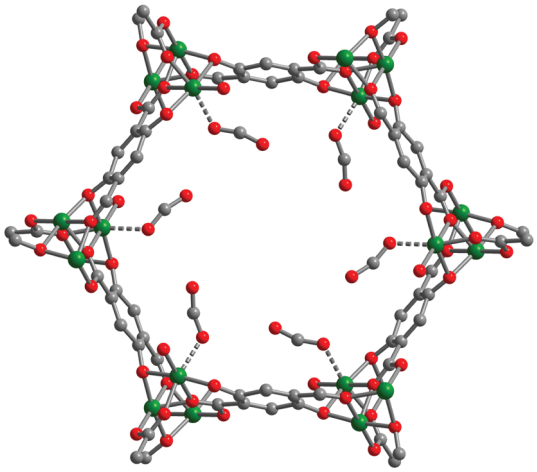

Figure 12. A portion of the crystallographic structure of $Ni_2(dobdc)$ following dosing with CO_2. Green, gray, and red spheres represent Ni, C, and O atoms, respectively; H atoms are omitted for clarity.[193]

In the related compound $Mg_2(dobdc)$, the site-specific enthalpy and entropy of adsorption of CO_2 at the exposed Mg^{2+} sites were calculated from a van't Hoff plot constructed using variable-temperature infrared spectroscopy data.[339] The calculated enthalpy of adsorption is −47 kJ/mol, which agrees well with the zero-coverage isosteric heat of adsorption (see section 2.2) obtained from the adsorption isotherms. The negative value for the entropy of adsorption is presumably a result of the efficient packing of the CO_2 molecules at the surface of the material, as well as the degrees of freedom being lowered as a result of the strong interaction with the exposed Mg^{2+} sites.

Similar studies performed on the mesoporous MIL-100 and -101 materials have revealed the direct observation of the interaction of CO_2 with the exposed Cr^{3+} cation sites within these materials.[128] In MIL-100, a strong ν_3 absorption band at 2351 cm^{-1} was observed upon dosing of CO_2 onto the evacuated material. To confirm the assignment of this band as CO_2 molecules adsorbed at the Cr^{3+} sites, the analogous experiment was performed on the solvated material (which would not be expected to possess unsaturated Cr^{3+} coordination sites), which did not reveal the evolution of such an absorption band. Several

dx.doi.org/10.1021/cr2003272 |*Chem. Rev.* 2012, 112, 724–781

bands were also observed at 2207, 2200, and 2193 cm^{-1} and were assigned as weaker Lewis acidic sites within the material. Interestingly, MIL-101 exhibited only a single band at 2196 cm^{-1}, indicating the absence of strong adsorption sites. A more recent study performed on the MIL-100(Fe) compound revealed that a portion of the Fe^{3+} metal centers in the material could be controllably reduced during the thermal activation of the compound.[343] This was attributed to the departure of one of the anionic ligands (F^- or OH^-) from the coordination sphere of the Fe^{3+} cation (presumably in the form of a radical), resulting in the generation of an exposed Fe^{2+} adsorption site. The intensity of the vibrational band corresponding to the strong binding sites at approximately 2173 cm^{-1} grows as a function of the density of Fe^{2+} ions in the material up to a concentration of approximately 14 mol %, which is approximately 40% of the available binding sites within the material.

In addition to probing of the interactions between CO_2 and exposed metal cation sites, the resolution of interactions between CO_2 and functional groups on the organic ligands has also been studied via vibrational spectra. Diffuse reflectance infrared Fourier transform spectroscopy (DRIFTS) is an effective tool for analyzing the surface chemistry of porous solids, especially when the *in situ* cell environment can be controlled. As discussed below, this technique has been applied to a handful of functionalized metal−organic frameworks to date,[344−346] revealing valuable information regarding the nature of CO_2 adsorption within the material.

The chemical adsorption of CO_2 onto basic alkylamines was recently reported in the *N*,*N*′-dimethylethylenediamine (mmen) functionalized framework $H_3[(Cu_4Cl)_3(BTTri)_8(mmen)_{12}]$ (mmen-Cu-BTTri), which will be discussed in detail in the context of post-combustion CO_2 capture in section 3.[198] The N−H stretch of mmen was followed as a 5% CO_2 in helium mixture was introduced into a high-pressure DRIFTS cell. As shown in Figure 13, the N−H stretching band of mmen at 3283 cm^{-1} disappears upon introduction of CO_2 into the cell. Regeneration by heating and vacuum restores the band to the spectrum. Chemisorption, suggested by the large isosteric heat of adsorption measured at zero coverage, was thus confirmed by infrared characterization. The presence of broad, lower energy bands, including the emergence of a band at 1669 cm^{-1}, was further suggestive of the formation of zwitterionic carbamates or carbamic acid in the absence of water.

The adsorption of CO_2 onto aromatic amines (e.g., aniline derivatives) has also been a subject of *in situ* studies using DRIFTS.[346] Although the nitrogen atom within 2-aminoterephthalic acid (NH_2-BDC) is significantly less basic than that of mmen, the formation of Lewis acid−base pairs is possible. The adsorption of CO_2 onto $Zn_4O(NH_2\text{-BDC})_3$ (IRMOF-3) and $Al(OH)(NH_2\text{-BDC})$ (NH_2-MIL-53(Al)) was first reported to result in splitting of the ν_2 band through a loss of degeneracy of the in-plane and out-of plane bends.[345] This was found for both compounds to result in the formation of electron donor−acceptor complexes, as further substantiated by the appearance of additional bands between 1000 and 1500 cm^{-1} in the case of NH_2-MIL-53(Al). Additional work, however, has shown that the mechanism of CO_2 adsorption in NH_2-MIL-53(Al) is significantly more complicated than originally thought. Density functional theory (DFT) calculations augmented additional DRIFTS measurements to elucidate a surprising flexion-based adsorption mechanism that does not involve direct interaction of CO_2 and amines. Strong Lewis acid−base interactions would be expected to significantly alter the N−H stretching frequencies and intensities of amines, as observed within mmen-CuBTTri. Thus, the negligible distortion of the N−H symmetric and asymmetric modes of IRMOF-3 and NH_2-MIL-53(Al) is a good indicator that electron transfer between the amine and CO_2 is only a minor component of the adsorption energy in those compounds.

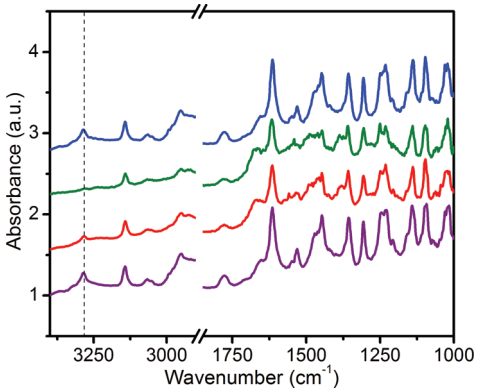

Figure 13. Infrared spectra collected for a sample of $H_3[(Cu_4Cl)_3(BTTri)_8(mmen)_{12}]$ (purple). Upon dosing of the sample with CO_2 (red, then green), the N−H stretching band of mmen at 3283 cm^{-1} disappears but is restored following regeneration of the material (blue). Reproduced with permission from ref 198. Copyright 2011 The Royal Society of Chemistry.

2.5. Computational Modeling of CO_2 Capture

Computational studies relating to the adsorption of CO_2 within metal−organic frameworks[189,234,347−351] are an important endeavor in supporting the experimental work performed in the area. In this regard, grand canonical Monte Carlo (GCMC) simulations have been widely employed in predicting the single- and mixed-component adsorption isotherms in metal−organic frameworks.[352−354] Furthermore, a number of DFT studies have emerged recently,[355,356] with many focused on determining the packing arrangement of CO_2 molecules within the pores and the associated enthalpy of adsorption,[357] and the perturbation of these as a result of the introduction of certain functionalities to the periphery of the organic ligands.[358,359] The latter is aimed at facilitating direct correlations between the electronic structure of the metal−organic framework and the observed adsorptive behavior.[360,361] Although there has been a significant amount of recent work performed in terms of developing theoretical methods for describing adsorption within metal−organic frameworks, significant challenges still exist in the area. These include the treatment of long-range interactions and adsorption of molecules at exposed metal cation sites,[362] the applicability of these methods to large-pore systems[234,363] (such as MIL-100 and MIL-101), and the development of more sophisticated algorithms that can account for flexibility within materials.[364,365] Nevertheless, computational modeling has been recently utilized in the virtual screening for metal−organic frameworks with high adsorption capacities,[189] new hypothetical structures with high performance parameters,[358] and predicting the stability of existing materials toward contaminants, such as H_2O.[155] While we do not provide a thorough coverage of the theoretical studies pertaining to CO_2 adsorption in metal−organic frameworks here, we introduce certain computational results as appropriate in the forthcoming sections.

dx.doi.org/10.1021/cr2003272 |*Chem. Rev.* 2012, 112, 724–781

3. POST-COMBUSTION CAPTURE

The combustion of coal in air generates flue gas with a relatively low CO_2 concentration (15−16%), while the bulk of the effluent is composed of N_2 and other minor components, such as H_2O, O_2, CO, NO_x, and SO_x (see Table 1).[200] The gas stream is released at a total pressure of approximately 1 bar. Since SO_x removal would precede CO_2 capture, the flue gas would be expected to enter the CO_2 scrubber at temperatures between 40 and 60 °C.[366,367] As outlined in section 1.4, an ideal adsorbent for capturing CO_2 from post-combustion flue gas would exhibit a high selectivity for CO_2 over the other flue gas components, high gravimetric and volumetric CO_2 adsorption capacities, minimal energy penalty for regeneration, long-term stability under the operating conditions, and rapid diffusion of the gas through the adsorbent material. The preparation of next-generation metal−organic frameworks that satisfy all of these requirements is currently a difficult synthetic challenge, although as discussed below, significant progress has been made in recent years.

3.1. Metal−Organic Frameworks for CO_2/N_2 Separation

The lower-pressure (<1.2 bar) CO_2 uptake capacities for all metal−organic frameworks reported to date are listed in Tables 4 (298−319 K) and 5 (273 K). Many of the frameworks exhibit large CO_2 adsorption capacities at pressures at and above 1 bar, owing to their high surface areas. However, these compounds are generally not well suited for post-combustion capture, since the adsorption capacity at lower pressures is a more relevant consideration due to the low partial pressure of CO_2.[48] Note that in these tables, the adsorption capacities at 1 bar (the most commonly reported value) are tabulated to facilitate a general comparison among different metal−organic frameworks. However, the adsorption capacities for CO_2 (0.15 bar) and N_2 (0.75 bar) at pressures relevant to post-combustion CO_2 capture are often not directly reported, and these have been carefully estimated from the literature gas adsorption isotherms and are listed in Table 7.

The selectivity calculation for CO_2 over N_2 is best performed using the adsorption capacities at pressures of approximately 0.15 bar for CO_2 and 0.75 bar for N_2. Since the total pressure of a flue gas is approximately 1 bar, selectivity calculations based upon the quantity of both CO_2 and N_2 adsorbed at 1 bar drastically overestimate the fraction of CO_2 in post-combustion flue gas and the total pressure of the gas. Table 7 lists also the calculated selectivity values for CO_2 over N_2 at 298 K for selected metal−organic frameworks, as calculated using the molar ratio of the CO_2 uptake at 0.15 bar and the N_2 uptake at 0.75 bar (eq 6). It is important to emphasize that these selectivity factors are based on pure-component adsorption isotherms and do not necessarily represent the true selectivity of the material in a CO_2/N_2 mixture. As such, the direct measurement of multicomponent isotherms, which has been recently performed for CO_2/CH_4 mixtures,[327] is necessary in order to evaluate the accuracy of selectivity factors predicted from single-component isotherms and IAST. To the best of our knowledge, there are no experimentally reported CO_2/N_2 binary isotherms yet reported. As a result, calculated selectivity factors are useful for preliminary evaluations of different materials. Note that, although gas adsorption measurements have most commonly been made at or below 298 K, it would be of benefit for a more realistic evaluation of post-combustion CO_2 capture performance if researchers were to begin reporting adsorption data in the range of 313−333 K.

In Table 7, the materials displaying the highest selectivities are generally those bearing functionalized pore surfaces. Surface functionalities that interact strongly with CO_2 (and to a lesser extent N_2) frequently increase adsorbent capacity at low pressures. Ideally, for high adsorption selectivities, the CO_2 adsorption should be maximized at pressures near 0.15 bar. Note that for metal−organic frameworks with strongly polarizing sites, the selectivity values listed in Table 7 likely underestimate the true adsorptive selectivity of the adsorbent. This is because in a realistic flue gas mixture, the strongest binding sites would be predominantly occupied by CO_2 owing to its greater polarizability and quadrupole moment. Thus, single-component isotherms overestimate the adsorption of N_2 and consequently reduce the calculated selectivity. Utilization of the IAST method (see section 2.3.2) for selectivity calculations minimizes this effect and enables more accurate selectivity values to be calculated.[317] Since using IAST to predict selectivity for a gas mixture requires accurate fits of the pure-component isotherms, selectivities are instead reported in Table 7 using the adsorption values obtained directly from the pure-component isotherms. Indeed, IAST values at the appropriate pressures have been reported for only a handful of frameworks, but values for certain adsorbents are mentioned in the discussion that follows.

It should be noted that the relevance of selectivity values calculated for flexible frameworks via the aforementioned method has not been fully established, although it is likely that the quantities calculated by this methodology would overestimate the true adsorptive selectivity. This is because flexible frameworks generally adsorb little N_2 at 0.75 bar because the apertures of the framework are not opened by N_2 in single-component gas adsorption experiments. However, if CO_2 affords the necessary gate opening pressure, the quantity of N_2 adsorbed is likely to be significantly higher than that observed during the single-component experiment. Since IAST cannot account for such effects, direct selectivity measurements of binary mixtures are likely the only accurate gauge of selectivity in flexible metal−organic frameworks. Thus, Table 7 omits selectivity values for flexible frameworks, although single-component CO_2 and N_2 capacities at the relevant pressures are tabulated.

3.2. Enhancing CO_2/N_2 Selectivity via Surface Functionalization

Tuning the affinity of the framework functionalities toward CO_2 is crucial for optimization of the adsorptive properties. In the ideal case, the appropriate pore surface properties would give rise to an adsorbent with high adsorption selectivity and capacity yet minimize the regeneration energy. In the following sections, we outline the various types of functionalities that have been explored to date for preparing materials with enhanced CO_2 capture performance, including amines, strongly polarizing organic functionalities, and exposed metal cation sites.

3.2.1. Pores Functionalized by Nitrogen Bases. Metal−organic frameworks functionalized with basic nitrogen-containing organic groups have been intensively studied for their CO_2 adsorption properties. The dispersion and electrostatic forces resulting from the interaction of the quadrupole moment of CO_2 with localized dipoles generated by heteroatom incorporation are typically responsible for the enhanced CO_2 adsorption. In some cases, acid−base type interactions between the lone-pair of nitrogen and CO_2 have been observed. The degree to which

dx.doi.org/10.1021/cr2003272 |Chem. Rev. 2012, 112, 724–781

Table 7. CO_2 and N_2 Uptake in Selected Metal−Organic Frameworks at Pressures Relevant to Post-combustion CO_2 Capture

material chemical formula[a]	common names	CO_2 uptake at 0.15 bar (wt %)[b]	N_2 uptake at 0.75 bar (wt %)[b]	selectivity[c]	temp (K)	ref
Mg_2(dobdc)	Mg-MOF-74, Mg-CPO-27	20.6	1.83	44	303	48
		18.9	1.40	52.3	313	48
		16.7	1.08	58.8	323	48
		14.5	0.87	61.1	333	48
Ni_2(dobdc)	Ni-MOF-74	16.9	2.14	30	298	131, 189
	CPO-27-Ni					
Co_2(dobdc)	Co-MOF-74	14.2			298	189
	CPO-27-Co					
$Cu_3(BTC)_2$	HKUST-1	11.6	0.41	101	293	194
$H_3[(Cu_4Cl)_3(BTTri)_8(mmen)_{12}]$	mmen-Cu-BTTri	9.5	0.20	165	298	198
$Zn_2(ox)(atz)_2$		8.3			293	201
Zn_2(dobdc)	Zn-MOF-74	7.6			296	150
	CPO-27-Zn					
Pd(μ-F-pymo-N^1,N^3)$_2$		6.5			293	207
$Cu_3(TATB)_2$	CuTATB-60	5.8	0.82	24	298	197
Co_2(adenine)$_2(CO_2CH_3)_2$	bio-MOF-11	5.4	0.28	65	298	368
$Fe_3[(Fe_4Cl)_3(BTT)_8(MeOH)_4]_2$	Fe-BTT	5.3	0.95	18	298	140
Al(OH)(bpydc)·0.97Cu$(BF_4)_2$		4.0	0.34	39	298	204
Zn(nbIm)(nIm)	ZIF-78	3.3	0.36	30	298	18, 213
Al(OH)(2-amino-BDC)	NH_2-MIL-53(Al), USO-1-Al-A	3.1			298	146
$H_3[(Cu_4Cl)_3(BTTri)_8]$	Cu-BTTri	2.9	0.49	19	298	200
Cu_2(bdcppi)$(DMF)_2$	SNU-50	2.9			298	202
$H_3[(Cu_4Cl)_3(BTTri)_8(en)_{3.75}]$	en-Cu-BTTri	2.3	0.17	44	298	200
$Zn_2(bpdc)_2$(bpee)		2.1	0.02	*d*	298	243
Ni_2(2-amino-BDC)$_2$(DABCO)	USO-2-Ni-A	2.1			298	146
$Cu_3(BPT(N_2))_2$	UMC-150(N)2	1.9			298	189, 369
$Cu_3(BPT)_2$	UMCM-150	1.8			298	189, 369
Zn_2(BTetB)		1.8	0.31	19	298	262
Al(OH)(BDC)	MIL-53(Al), USO-1-A	1.7			298	146
$Zn_2(bmbdc)_2$(4,4′-bpy)		1.4	0.01	*d*	298	370
Ni_2(BDC)$_2$(DABCO)	USO-2-Ni	1.2			298	146
$V^{(IV)}O$(BDC)	MIL-47	1.1			298	189
Al(OH)(bpydc)	MOF-253	1.0	0.37	9	298	204
Zn_{20}(cbIm)$_{39}$(OH)	ZIF-100	1.0	0.15	22	298	247
$Zn_4O(NO_2$-BDC$)_{1.19}((C_3H_5O)_2$-BDC$)_{1.07}$-$((C_7H_7O)_2$-BDC$)_{0.74}$	MTV-MOF-5-EHI	1.0			298	219
Zn_2(BTetB)(py-$CF_3)_2$		0.9	0.06	50	298	262
Zn$(MeIM)_2$	ZIF-8	0.6			298	189
$Zn_4O(BDC$-$NH_2)_3$	IRMOF-3	0.6			298	160, 189
$Zn_4O(BTB)_2$	MOF-177	0.6	0.39	4	298	48
$Zn_4O(BDC)(BTB)_{4/3}$	UMCM-1	0.5			298	189
$Zn_4O(BDC)_3$	MOF-5, IRMOF-1	0.5			298	189
$Co_4(OH)_2$(doborDC$)_3$		0.5	0.08	18	298	254

[a] See List of Abbreviatons. [b] When not directly reported, values were estimated from adsorption isotherms in the corresponding reference. [c] Selectivities were calculated from the pure-component isotherms by dividing the mass of CO_2 adsorbed at 0.15 bar by the mass of N_2 adsorbed at 0.75 bar according to eq 6 in section 2.3.1. [d] Single-component isotherms are not expected to be meaningful predictors of mixed-component selectivity for these flexible materials.

nitrogen incorporation enhances CO_2 adsorption depends significantly on the nature of the functional group. To date, three major classes of nitrogen-functionalized metal−organic frameworks have been synthesized: heterocycle (i.e., pyridine) derivatives, aromatic amine (i.e., aniline) derivatives, and alkylamine (i.e., ethylenediamine) bearing frameworks.

Perhaps owing to the ease of synthesis, a particularly large number of metal−organic frameworks with organic bridging units derived from nitrogen-containing heterocycles have been studied in the context of CO_2 capture.[140,200,202,205,215,224,228,230,232,235,241,248,251,268,269,277,288,329] However, the incorporation of these heterocycles generally improves capacity only modestly at low pressures. Among the

dx.doi.org/10.1021/cr2003272 |*Chem. Rev.* 2012, 112, 724–781

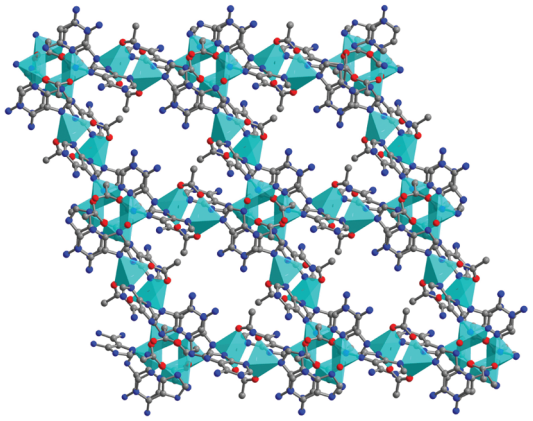

Figure 14. A portion of the crystal structure of $Co_2(adenine)_2(CH_3CO_2)_2$ (bio-MOF-11).[368] Turquoise, gray, blue, and red spheres represent Co, C, N, and O atoms, respectively; H atoms are omitted for clarity. The turquoise tetrahedra represent the coordination sphere of the Co^{2+} ions.

best-performing metal−organic frameworks featuring nitrogen-containing heterocycles are those incorporating biologically relevant moieties.[210,227] The ratio of heteroatoms to carbon atoms in these frameworks can be quite large, resulting in pore surfaces with significant surface polarization. For example, bio-MOF-11 was synthesized from adeninate and acetate linkers (see Figure 14).[368] Its CO_2 adsorption capacity is ca. 5.8 wt % at 298 K and 0.15 bar, with a corresponding isosteric heat of adsorption at zero-coverage of −45 kJ/mol. The large initial isosteric heat is likely partially attributable to the presence of an aromatic amine that also decorates the pore surface. However, the effects of the nitrogen heterocycle are considerable because the CO_2 capacity of bio-MOF-11 exceeds that of any other aromatic amine functionalized framework reported to date at 1 bar, despite a surface area of only 1040 m^2/g.

The commercial availability of aromatic amine containing linkers, especially 2-aminoterephthalic acid (NH_2-BDC), and the expected affinity of amino groups toward CO_2 has generated significant interest in aromatic amine functionalized frameworks.[146,201,258,263,290,371,372] In particular, the IRMOF series of frameworks provides a basis for elucidating the effects of aromatic amines within metal−organic frameworks. At 298 K and 1.1 bar, $Zn_4O(BDC)_3$ (IRMOF-1 or MOF-5) adsorbs approximately 4.6 wt % CO_2, while the amine-functionalized variant $Zn_4O(NH_2\text{-BDC})_3$ (IRMOF-3) adsorbs 5.0 wt % CO_2, despite a decrease in the BET surface area from 2833 to 2160 m^2/g.[160] The reduced surface area of IRMOF-3 decreases the high-pressure CO_2 adsorption capacity, but the higher uptake observed within the material at lower pressures leads to it being a higher-performance material compared with IRMOF-1 in the context of post-combustion CO_2 capture. We note that there has been a report of significantly greater adsorption of CO_2 in IRMOF-1 (8.5 wt % at 1 bar).[216] However, this anomalous result stands in contrast to the lower value more frequently reported and has yet to be reproduced to the best of our knowledge.

Amine functionalization has been shown to enhance CO_2 capacity in a number of other metal−organic frameworks, including $Ni_2(NH_2\text{-BDC})_2(DABCO)$, $Al(OH)(NH_2\text{-BDC})$ (NH_2-MIL-53(Al)) and $In(OH)(NH_2\text{-BDC})$, when their low-pressure capacities are compared with that of the parent material.[146] However, the amine may not always be directly responsible for the enhanced adsorption. It was recently shown for the well-studied compound $Al(OH)(NH_2\text{-BDC})$ (NH_2-MIL-53(Al)) that the aromatic amine has little direct interaction with adsorbed CO_2 at low pressures.[346] However, the presence of the amine favors the formation of a flexed, narrow-pore structure upon evacuation. This same narrow-pore structure, in which hydrogen bonding is observed between the aromatic substituents and the Al-based clusters, is not observed for the parent MIL-53(Al) framework until the material is cooled to temperatures below 150 K. In the narrow-pore structure, CO_2 molecules can interact with multiple pore surfaces simultaneously. Furthermore, DFT calculations showed that interactions between CO_2 and hydroxyl groups that line the pore surfaces were stronger in the amino functionalized material because of the increased acidity of the hydroxyl moieties. While enhanced adsorption of CO_2 in NH_2-MIL-53(Al) was originally attributed to direct interactions between the amino functionality and CO_2,[147] *in situ* infrared spectroscopy experiments showed that the N−H resonances of NH_2-MIL-53(Al) were only slightly perturbed by CO_2 adsorption. Amines are generally expected to enhance CO_2 adsorption in porous materials by acid−base chemistry, electrostatic forces, or enhanced dispersion forces. In this case, however, the actual mechanism of binding, when fully elucidated, was shown to be quite different from those observed in other frameworks.

Table 8. Select pK_a Values for the Dissociation of Protonated Amine Complexes in Water[373]

parent amine	pK_a
aniline	4.60
pyridine	5.23
benzylamine	9.38
ethylamine	10.79

For heterocycle- and aromatic amine-based frameworks, enhanced adsorption at low pressures is likely only partially attributable to the basicity of the nitrogen donor atom. The pK_a values of ammonium complexes can help explain the basicity differences between different classes of amines. Table 8 lists the pK_a values for selected ammonium complexes. Note that the conjugate acids of pyridine and aniline are significantly more acidic than the conjugate acids of benzylamine or ethylamine. The presence of electron-withdrawing carboxylate functionalities *ortho* or *para* to the amine would be expected to further reduce the basicity of aniline derivatives. Thus, the enhanced adsorption of CO_2in metal−organic frameworks containing pyridine and aniline derivatives is likely primarily attributable to the increased number of polarizing sites that decorate the pore walls. Without the formation of Lewis acid−base pairs, the binding of CO_2 is still physisorptive and regeneration conditions are generally very mild.

In order to mimic the chemisorptive interactions that are observed in aqueous amine scrubbers, more basic amine species need to be incorporated onto the pore surfaces of metal−organic frameworks. Very strong adsorption of CO_2 has indeed been shown to be possible via incorporation of alkylamines into metal−organic framework pores. As illustrated in Figure 15, alkylamine incorporation onto the open metal sites of Cu-BTTri was found to be an effective method for postsynthetically modifying this metal−organic framework to enhance the CO_2 binding.[198,200] Note that although not explored initially for CO_2 adsorption, the grafting of amine moieties onto exposed

dx.doi.org/10.1021/cr2003272 |*Chem. Rev.* 2012, 112, 724–781

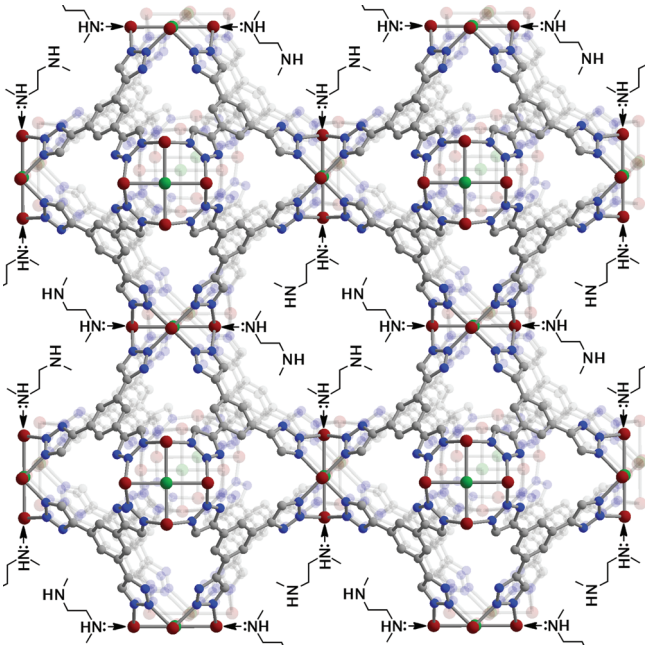

Figure 15. Functionalization of the metal−organic framework Cu-BTTri through binding *N,N′*-dimethylethylenediamine (mmen) to the open metal coordination sites; dark red, green, gray, and blue spheres represent Cu, Cl, C and N atoms, respectively. The basic amine groups dangling within the framework pores lead to strong CO_2 adsorption, with a zero-coverage isosteric heat of adsorption of −96 kJ/mol. Reproduced with permission from ref 198. Copyright 2011 The Royal Society of Chemistry.

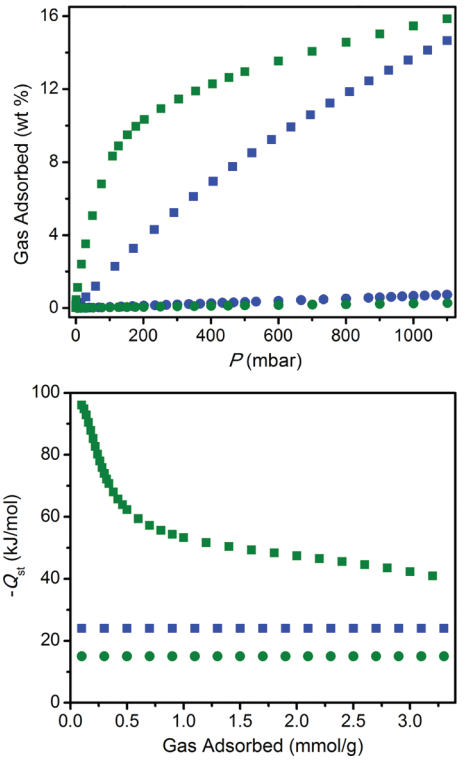

Figure 16. (top) CO_2 (■) and N_2 (●) adsorption isotherms collected at 298 K for mmen-Cu-BTTri (green symbols) and Cu-BTTri (blue symbols) and (bottom) a plot of the isosteric heat of adsorption of CO_2 (■) and N_2 (●) in mmen-Cu-BTTri (green symbols) and Cu-BTTri (blue symbols). Reproduced with permission from ref 198. Copyright 2011 The Royal Society of Chemistry.

metal cations was also previously demonstrated in the MIL-101 system,[374] indicating that this approach may indeed be applicable to a wide range of materials with pores that are furnished with such sites.

The compound $H_3[(Cu_4Cl)_3(BTTri)_8(mmen)_{12}]$ (mmen-Cu-BTTri) was synthesized by stoichiometric functionalization of Cu-BTTri with the sterically encumbered secondary amine *N,N′*-dimethylethylenediamine (mmen).[198] A 3.5-fold increase in gravimetric capacity at 0.15 bar (to ∼9.5 wt %) compared with the nonfunctionalized Cu-BTTri framework replete with open metal sites (see Figure 16, upper) was achieved. The highly selective chemisorptive process in this framework strongly affects only CO_2 adsorption. Indeed, N_2 adsorption decreased at all pressures compared with the parent framework, because of the significantly reduced surface area resulting from the pore modification. Thus, the IAST selectivity of mmen-Cu-BTTri for CO_2 at conditions relevant to post-combustion carbon capture is 327 at 298 K. This high selectivity is associated with a large isosteric heat of CO_2 adsorption at low pressures, approaching −96 kJ/mol at zero-coverage, which is substantially higher than the ca. −15 kJ/mol observed over the entire sorption range for N_2 (see Figure 16, lower). In the case of CO_2, the isosteric heat initially sharply decreases with CO_2 adsorbed, which is consistent with the highest-affinity amine sites becoming occupied with CO_2 molecules. However, despite this decrease, the magnitude is significantly higher than that observed for the parent framework, which exhibits an almost constant isosteric heat of approximately −23 kJ/mol. Although the large initial adsorption enthalpy in mmen-Cu-BTTri suggests that high temperatures would be required for desorption of the CO_2 from the amines, the regeneration conditions were shown to be mild. Following activation, the material adsorbed nearly 7 wt % CO_2 from a 15% CO_2 in N_2 mixture. Complete regeneration was accomplished with a N_2 purge and fast temperature ramp to 60 °C, with no capacity loss observed over the course of 72 cycles (27 min per cycle). More detailed work, such as optimization of the amine, and the consideration of the effect of the temperature increase expected from the large quantity of heat originating from the high isosteric heat of adsorption, and the influence of the other minor impurities of the post-combustion flue gas on the performance of the material, would allow the promise of this approach for industrial applications to be further evaluated.

3.2.2. Other Strongly Polarizing Organic Functional Groups. In addition to the amine and other nitrogen-based functionalities discussed in the previous sections, organic linkers with heteroatom functional groups (other than amines) have also been investigated in detail for their effects on the CO_2 adsorption behavior.[18,101,179,206,211,213,214,225,226,231,233,235,238,239,244,253,255,262,267,270,272,273,275,276,278−280,286,287,292,347] These functional groups include hydroxy, nitro, cyano, thio, and halide groups, and the degree to which CO_2 adsorption is enhanced in these cases depends largely upon the extent of ligand functionalization and the polarizing strength of the functional group. In general, more strongly polarizing groups will influence CO_2 adsorption more favorably.

A systematic understanding of polarization strength is perhaps best observed via the large number of functionalized zeolitic imidazolate frameworks that have been reported to date.[18,213,226]

dx.doi.org/10.1021/cr2003272 |*Chem. Rev.* 2012, 112, 724–781

This subclass of metal−organic frameworks is convenient for understanding the effects of different functional groups, because all frameworks incorporate imidazolate-based organic linkers and most have tetrahedral Zn^{2+} cation nodes. While there are important topological differences between the many frameworks, a wide number of isostructural compounds with different functional groups have also been reported, allowing comparisons to be made between the compounds. For example, a number of mixed-linker frameworks of the GME topology were studied for functional group and pore size effects on adsorption.[213] Linkers containing various functional groups afforded a series of frameworks with drastically different pore sizes. Adsorption was found not to correlate with the pore size, which varied between 7.1 and 15.9 Å. Different functional groups, however, appear to impact volumetric adsorption capacity. The compound Zn(nbIm)(nIm) (ZIF-78) exhibits the largest volumetric capacity because every imidazolate and benzimidazolate linker was modified with a polarizing nitro group. Frameworks synthesized from cyano- and nitro-functionalized (ZIF-82), chloro- and nitro-functionalized (ZIF-69), and bromo- and nitro-functionalized (ZIF-81) imidazolate linkers performed similarly to each other but slightly worse than ZIF-78. Frameworks partially functionalized with alkyl groups adsorbed the least quantity of CO_2 on a volumetric basis. As expected, the greater the surface polarization engendered by the functional group in the framework, the higher the CO uptake capacity is at low pressures.

The foregoing conclusion is not immediately apparent if framework performance is only benchmarked by gravimetric capacity. On a gravimetric basis, less-functionalized, lighter frameworks outperformed the more functionalized, heavier materials. The compound ZIF-70, composed of nonfunctionalized and nitro-functionalized imidazolate linkers (see Figure 17), exhibits a higher gravimetric capacity than ZIF-78. For the latter materials, the presence of benzimidazolate linkers increases the molecular weight significantly, but with the same connectivity, the unit cell volumes of ZIF-78 (11 514 $Å^3$)[213] and ZIF-70 (11 386 $Å^3$)[226] are very similar. Thus, the best comparison between ZIF-70 and ZIF-78 is the quantity of CO_2 adsorbed within a fixed volume. Assuming void spaces between crystallites are similar, a particular volume of ZIF-78 would adsorb 33% more CO_2 than the same volume of ZIF-70, which for a stationary application like carbon capture is relevant to infrastructure costs. For isostructural materials, volumetric capacity calculations can elucidate the effects of functional groups without discriminating against the additional mass.

The IRMOF series of metal−organic frameworks are similarly suitable for investigating functional group effects on CO_2 adsorption in a controlled manner. In one study, multiple functional groups from different types of organic linkers were incorporated into individual IRMOF crystallites.[219] Volumetric CO_2 adsorption capacities were again utilized to account for mass differences between frameworks. Two potential benefits of this mixed linker technique are apparent. First, mixed ligand frameworks can incorporate functional groups (like 2-nitroterephthalic acid) into the IRMOF structure that could not be incorporated when used alone. In particular, the nitro functionality was a common feature among the best performing frameworks synthesized. Second, the presence of multiple functional groups along a single pore surface can afford properties that exceed those expected from a simple linear combination of the individual components. This was demonstrated by the synthesis of $Zn_4O(NO_2\text{-BDC})_{1.19}((C_3H_5O)_2\text{-BDC})_{1.07}\text{-}((C_7H_7O)_2\text{-BDC})_{0.74}$ (MTV-MOF-5-EHI) (see Figure 18),

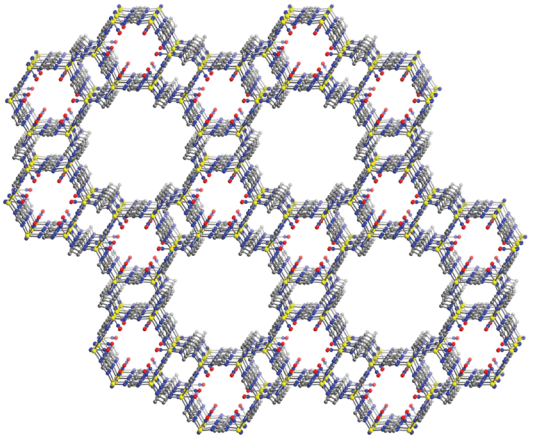

Figure 17. A portion of the crystal structure of Zn(Im)(nIm) (ZIF-70) as viewed along the [001] direction. Yellow, gray, blue, and red spheres represent Zn, C, N, and O, respectively; H atoms are omitted for clarity.[226]

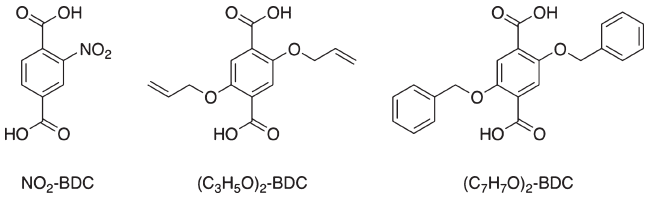

Figure 18. MTV-MOF-5-EHI is composed of the three ligands shown.[219] The incorporation of multiple ligands within a single crystallite was reported to improve CO_2 adsorption capacity at low pressures.

which adsorbs 7.7 wt % CO_2 at 1 bar and has a CO_2/CO selectivity at 298 K that is over 4 times greater than that observed within MOF-5, which does not possess any substitutions on the organic backbone. While the performance and stability of the IRMOF series of metal−organic frameworks may ultimately make them unsuitable for CO_2 capture applications, mixed ligand and mixed functionality frameworks could potentially lead to materials with finely tunable properties.

Theoretical work has also modeled the effects of certain functional groups on CO_2 adsorption.[360] For example, a series of functionalized zirconium metal−organic frameworks based upon the UiO-66 structure-type with substituted BDC^{2-} ligands were constructed via DFT calculations.[375] GCMC simulations were used to predict isotherms for CO_2 and CH_4. The authors concluded that strongly polarizing groups enhanced CO_2 adsorption through increased isosteric heats of adsorption. Futhermore, it was observed that confinement effects attributable to reduced pore volumes could further enhance CO_2 adsorption. Among the most promising materials of this class, the sulfonic acid and carboxylic acid functionalized materials displayed the largest selectivity enhancement in the separation of CO_2 from CH_4.[375]

3.2.3. Exposed Metal Cation Sites. Another strategy that has been explored as a means for improving the affinity and selectivity of metal−organic frameworks toward CO_2 over N_2 is the generation of structure types bearing exposed metal cation sites on the pore surface.[128−132] These sites are usually obtained following desolvation of the material, where one of the solvent molecules in the coordination sphere of the metal center is removed *in vacuo* at elevated temperatures. Such metal binding

dx.doi.org/10.1021/cr2003272 |*Chem. Rev.* 2012, 112, 724–781

sites have been previously shown to facilitate close approach of guest molecules to the pore surface, which is of benefit for raising the adsorption enthalpy and storage density of gases, such as H_2 and CH_4,[13,376,377] and in Lewis acid catalysis.[378] In the context of post-combustion CO_2 capture, the open metal cation sites serve as charge-dense binding sites for CO_2, which is adsorbed more strongly at these sites owing to its greater quadrupole moment and polarizability compared with N_2.

The earliest studies of metal−organic frameworks possessing exposed metal cation sites were performed predominantly on $Cu_3(BTC)_2$ (HKUST-1, Figure 7).[133,337,379] Here, the solvent molecules present on the axial sites of the paddlewheel units can be removed to afford open Cu^{2+} adsorption sites. These sites interact more strongly with CO_2 due to the high charge density of the Cu^{2+} cation, resulting in a zero-coverage isosteric heat of adsorption of −29.2 kJ/mol. A number of independent studies have reported the adsorption isotherms for this compound, wherein adsorption capacities range from 15.0 to 18.4 wt % at 1 bar and 298 K.[160,189,191,192,194] The difference in these values likely stems from the degree of purity of the material or the degree of activation (desolvation) of the compound. Note that the adsorption properties of metal−organic frameworks containing bound solvent molecules are highly dependent upon the desolvation conditions. Furthermore, careful handling of the materials following activation is essential, as a result of the propensity of the exposed metal cation sites to become hydrated as a result of even brief exposure to atmospheric moisture.[115]

The adsorption of CO_2 within the chromium-based metal−organic frameworks $Cr_3O(H_2O)_3F(BTC)_2$ (MIL-100) and $Cr_3O(H_2O)_2F(BDC)_3$ (MIL-101) has been studied.[167] These materials exhibit BET surface areas of 1900 and 4230 m^2/g, respectively, and feature exposed Cr^{3+} sites following removal of the H_2O molecules originally bound to the metal centers.[128] Accordingly, the high charge density of the metal ion affords a zero-coverage isosteric heat of adsorption of −62 kJ/mol in the case of MIL-100 and −44 kJ/mol for MIL-101. The storage capacities were probed at high pressures, and CO_2 uptakes of over 40 wt % were observed for both compounds at 50 bar and 304 K. Although no low-pressure (<1.0 bar) data were reported, one advantage of these materials is their high chemical and thermal stability. Indeed, both compounds are water-stable and can be heated to temperatures approaching 300 °C without degradation of the framework structure, a crucial characteristic for post-combustion CO_2 capture where significant quantities of H_2O are present in the flue gas.

The $M_2(dobdc)$ structure type represents one of the most well-studied families of materials with regard to metal−organic frameworks bearing exposed metal cation sites (see Figure 8).[150,380−384] The high density of binding sites decorating the hexagonal one-dimensional pores endow the materials with high adsorption capacities for CO_2 at 1 bar and 296 K, ranging from 19.8 to 26.0 wt % within $Zn_2(dobdc)$ and $Mg_2(dobdc)$, respectively.[150] In fact, the value for $Mg_2(dobdc)$ represents the highest low-pressure gravimetric and volumetric adsorption capacity for CO_2 in a metal−organic framework, despite its relatively low surface area (SA_{BET} = 1495 m^2/g), demonstrating the importance of furnishing the pores with a large number of high-affinity binding sites. The zero-coverage isosteric heat of CO_2 adsorption across this series is significantly affected by the metal cation, wherein $Mg_2(dobdc)$ was observed to display the highest affinity (Q_{st} = −42 kJ/mol), while $Zn_2(dobdc)$ exhibited the weakest interactions (Q_{st} = −26 kJ/mol) among the compounds studied. The isosteric heat of adsorption plot

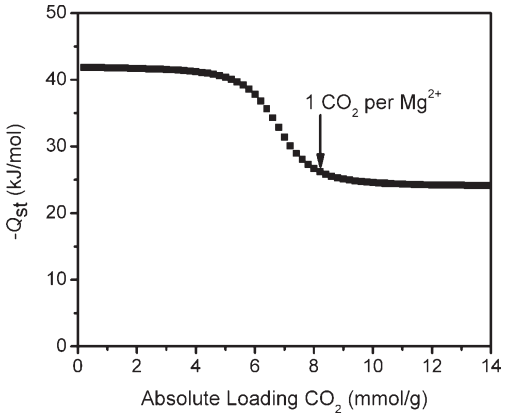

Figure 19. Isosteric heat of adsorption, Q_{st}, as a function of loading of CO_2 for $Mg_2(dobdc)$ calculated at 40 °C using a dual-site Langmuir model. Reproduced with permission from ref 48. Copyright 2011 The Royal Society of Chemistry.

shown in Figure 19, calculated using a dual-site Langmuir expression, shows a significant drop at a surface coverage that is consistent with the occupation approaching one CO_2 molecule per Mg^{2+} site, which would be expected as a result of only weaker binding sites being vacant at this loading level. Note that the considerable difference in the isosteric heat of adsorption between the compounds is attributed to the higher ionic character of the Mg−O bonds in $Mg_2(dobdc)$ compared with the Zn−O bonds within $Zn_2(dobdc)$, leading to a higher partial positive charge on the Mg^{2+} metal centers, which consequently facilitates a greater degree of polarization on the adsorbed CO_2 molecules.[150] Importantly, the increased affinity for CO_2 within $Mg_2(dobdc)$ leads to a higher CO_2 uptake at low pressures and high temperatures (16.2 wt % at 0.15 bar and 323 K), which is crucial for post-combustion CO_2 capture.

More recently, $Mg_2(dobdc)$ and MOF-177 were evaluated for use in a temperature swing adsorption-based process by collecting single-component CO_2 and N_2 adsorption isotherms across a temperature range of interest for such a process (25−200 °C; see Figure 20).[48] The working capacity of the materials was calculated as a function of the desorption temperature as the difference between the quantity of CO_2 adsorbed at a partial pressure of 0.15 bar at the flue gas temperature (40 °C), and the corresponding value at 1 bar at the desorption temperature. For $Mg_2(dobdc)$, it was demonstrated that the working capacity for CO_2 (shown in Figure 21) reaches 17.6 wt % for a 200 °C desorption temperature. The increase in working capacity with desorption temperature arises from the fact that the quantity of CO_2 adsorbed is reduced at higher temperatures, leading to more complete evacuation of the pores during regeneration. A similar analysis performed on MOF-177 resulted in a negative CO_2 working capacity across the entire temperature range. This is ascribed to the relatively limited CO_2 adsorption capacity at low pressures due to the lack of strong binding sites within the pores, which affords a near-linear isotherm that steadily increases up to the desorption pressure. Even at the higher temperatures, a relatively high quantity of CO_2 is retained at 1 bar, leading to a poor working capacity even at a desorption temperature of 200 °C. The results highlight the importance of selecting a structure containing a high density of strong binding sites within the pores, making $Mg_2(dobdc)$ a suitable candidate for further testing.

While most metal−organic frameworks possessing exposed metal cation sites are obtained by removing solvent molecules

dx.doi.org/10.1021/cr2003272 |Chem. Rev. 2012, 112, 724–781

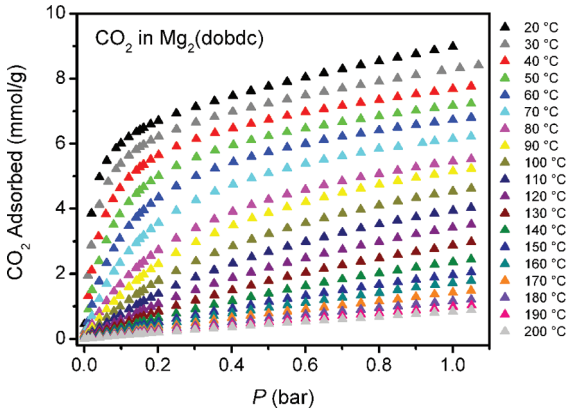

Figure 20. CO_2 adsorption isotherms for Mg_2(dobdc) collected over a temperature range of 20−200 °C. Reproduced with permission from ref 48. Copyright 2011 The Royal Society of Chemistry.

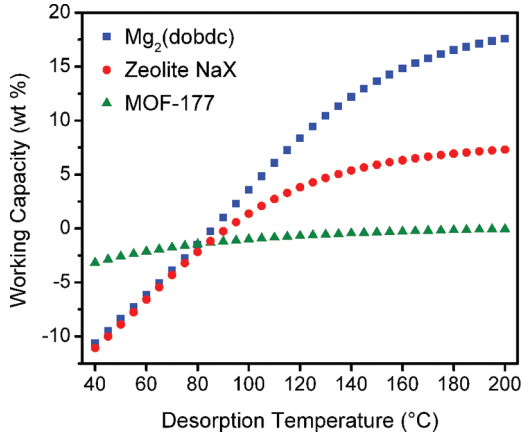

Figure 21. Estimated working capacity as a function of desorption temperature (T_d) for MOF-177, Mg_2(dobdc), and zeolite NaX. The working capacity is calculated as the difference between the amount of CO_2 adsorbed at 0.15 bar at a flue gas temperature of 40 °C and the amount of CO_2 adsorbed at 1 bar at the desorption temperature. Reproduced with permission from ref 48. Copyright 2011 The Royal Society of Chemistry.

from the metal centers after synthesis of the framework structure, one alternative strategy that has been pursued is the postsynthetic insertion of metal ions. For example, an aluminum-based metal−organic framework Al(OH)(bpydc) (MOF-253, $bpydc^{2-}$ = 2,2′-bipyridine-5,5′-dicarboxylate) was synthesized, which exhibits the same network topology as Al(OH)(BDC) (MIL-53) and possesses open bipyridine sites along the one-dimensional pores.[204] Owing to the low affinity of the bipyridine moieties toward the Al^{3+} ions used to construct the framework, these sites are vacant following synthesis, allowing metal ions to be selectively bound postsynthetically. The framework was loaded with a variety of transition metal salts, and the resulting products were screened for their CO_2 adsorption properties. Of the compounds studied, the Cu^{2+}-loaded material, Al(OH)(bpydc)·0.97$Cu(BF_4)_2$, exhibited the best performance, where the quantity of CO_2 adsorbed at 1 bar at 298 K increased from 6.2 wt % in the bare framework to 11.7 wt % following metal insertion, despite a decrease in the BET surface area from 2160 to 705 m^2/g. The increased uptake is accompanied by a dramatic increase in the CO_2/N_2 selectivity from 2.8 to 12.0, highlighting the success of this approach. While the chemical origin of the high performance of the Al(OH)(bpydc)·0.97$Cu(BF_4)_2$ compound has not yet been established, the increased affinity of the framework for CO_2 is also demonstrated by an increase in the magnitude of the zero-coverage isosteric heat of adsorption from −23 to −30 kJ/mol, suggesting that a more suitable chemical environment for CO_2 binding is facilitated by the insertion of $Cu(BF_4)_2$ into the channels of the framework.

3.3. Considerations for Application

Many studies involving the synthesis and evaluation of metal−organic frameworks for post-combustion CO_2 capture applications focus exclusively on the CO_2/N_2 separation performance of the material, neglecting other important aspects of actual flue gas. While CO_2 and N_2 account for around 90% of the flue gas composition, understanding the effects of the gases present in the remaining 10% is critical to properly evaluating any material for use in a realistic CO_2 capture process. Here, we discuss a number of studies that have aimed to study the performance of metal−organic frameworks under more realistic conditions, including the use of humidified gas mixtures.

3.3.1. Stability to Water Vapor. While the primary challenge of CO_2 capture is the separation of CO_2 and N_2, the detailed study of metal−organic frameworks for post-combustion CO_2 capture must take into account the fact that flue gas is saturated with H_2O (5−7% by volume).[11,31] While partial dehydration of the effluent may be possible, drying the flue gas completely prior to extracting CO_2 is costly and most likely not feasible on such a large scale.[31,367] As such, adsorbents used in CO_2 capture from flue gas must be stable in the presence of at least some water vapor. In evaluating metal−organic frameworks for applications in post-combustion CO_2 capture processes, it is important to consider not only the stability of the framework to water vapor but also the effect of water vapor on the separation of CO_2 from N_2.

With regard to water stability, the metal−ligand bond is typically the weakest point of a metal−organic framework, and hydrolysis can lead to the displacement of bound ligands and collapse of the framework structure (eq 1).[155] This was first observed in the zinc-carboxylate based MOF-5, which is water-sensitive and begins to lose crystallinity upon exposure to small amounts of humidity.[115,385−387] Molecular dynamics simulations were used to show that the mechanism of hydrolysis for MOF-5 likely involves the direct attack of H_2O at the tetrahedral Zn^{2+} centers to displace bound BDC^{2-} ligands and destroy the framework structure.[388]

$$ML + H_2O \rightarrow M(OH) + LH \quad (9)$$

Several attempts have been made at understanding the differences in relative water stability of metal−organic frameworks. High-throughput screening of frameworks exposed to different temperatures of steam was used to suggest that the strength of the metal−oxygen bonds within the framework correlates with resistance to hydrolysis, with strong metal−oxygen bonds imparting greater hydrothermal stability on the resulting framework.[155] In a different study, representative metal−organic frameworks were tested in different ratios of H_2O to DMF, and the resulting differences in stability were attributed to the metal nodes within the framework.[389] In agreement with previous work, it was found that the basic zinc acetate clusters characteristic of most zinc

dx.doi.org/10.1021/cr2003272 |Chem. Rev. 2012, 112, 724–781

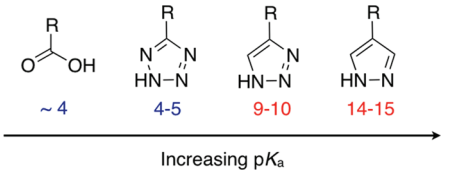

Figure 22. The general trend of increasing pK_a for ligands built from carboxylic acids, tetrazoles, triazoles, and pyrazoles. The metal–ligand bond is expected to be stronger as the pK_a increases.

carboxylate metal–organic frameworks, such as the IRMOF series and MOF-177, are most susceptible to hydrolysis.[390] The trinuclear chromium clusters found in many of the MIL series of frameworks are the most stable of the studied building units, while the copper-paddlewheel carboxylate clusters found in HKUST-1 exhibit intermediate stability.

One of the primary efforts to increase the water stability of metal–organic frameworks has been through the use of azolate-based linkers rather than the typical carboxylate linkers.[200,391−397] The azolate linkers can bind metals with a similar geometry to carboxylate ligands, but their greater basicity typically leads to stronger M–N bonds and greater thermal and chemical stability in the resulting framework. The relative M–N bond strengths can be predicted based on the pK_a values associated with the deprotonation of the free ligand. As such, stability typically decreases with the pK_a: pyrazole (pK_a = 14.4) linkers exhibit the greatest stability, imidazole (pK_a = 10.0) and triazole (pK_a = 9.3) are intermediate, and tetrazole (pK_a = 4.6) linkers are the most labile (see Figure 22).[398,399] Illustrating the remarkable stability of some of these frameworks, $Ni_3(BTP)_2$ (H_3BTP = 1,3,5-tris-1*H*-pyrazol-4-yl)benzene) is stable in boiling water at pH 2–14 for at least 14 days.[397]

An alternative strategy for increasing the metal–ligand bond strength in metal–organic frameworks is through the use of tri- or tetravalent metal cations.[155] In general, frameworks containing Cr^{3+}, Al^{3+}, Fe^{3+}, and Zr^{4+} cations display a high degree of stability in water. Specifically, MIL-53 (M(OH)(BDC), M = Cr^{3+}, Fe^{3+}, Al^{3+}) is a flexible framework that expands or contracts based on the absence or presence of water.[119,144,335] Here, the structural transition is reversible, and the overall framework scaffold remains intact upon repeated exposure to water. MIL-100 and MIL-101 are rigid trivalent frameworks built from trinuclear metallic clusters that have shown a high stability in both boiling water and steam.[400−404] Similarly, the zirconium-(IV)-based metal–organic framework UiO-66, which contains extremely robust $Zr_6O_4(OH)_4(CO_2)_{12}$ cluster units (see Figure 23), has been shown to be very water-stable.[117]

Aside from increasing the metal–ligand bond strength, other strategies have been successfully employed to synthesize metal–organic frameworks with intrinsic functionalities designed to protect the material from hydrolysis. For instance, several Zn^{2+}- and Cu^{2+}-based frameworks have been synthesized with highly hydrophobic surfaces that adsorb only very small amounts of water at low pressures.[405−408] Additionally, several metal–organic frameworks have been synthesized with water-repellant groups incorporated directly into the organic ligands as a means of protecting the metal core from water.[409−411] In one promising study, a metal–organic framework (Banasorb-22) isostructural to MOF-5 was synthesized, wherein each of the terephthalic acid linkers was modified with a trifluoromethoxy substituent.[409] The resulting material demonstrated improved stability with regard to

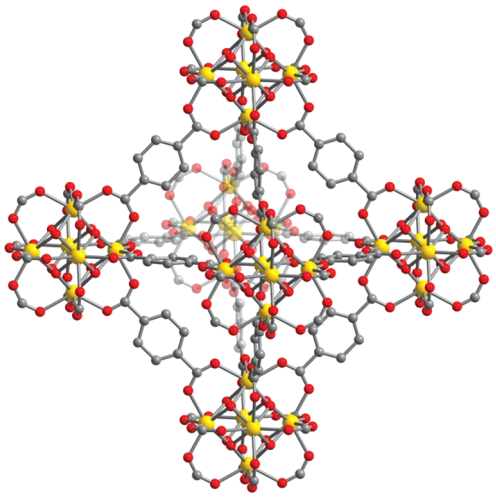

Figure 23. A portion of the crystal structure of the high-stability metal–organic framework UiO-66.[117] Yellow, gray, and red spheres represent Zr, C, and O atoms, respectively. H atoms are omitted for clarity.

unmodified MOF-5. X-ray powder diffraction patterns indicated only minor changes to the framework structure after exposure to steam from boiling water for 1 week, while MOF-5 was shown to decompose into $Zn_3(OH)_2(BDC)_2$ (MOF-69C) after just 2 h of exposure to steam.

There have been several investigations of metal–organic framework stability in liquid water, but few with regard to different levels of humidity and temperature. Note that due to the temperature and composition of the flue gas, stability to water vapor (rather than liquid water) is more relevant to CO_2 capture applications.[11] While several studies have reported water adsorption isotherms for various metal–organic frameworks, most do not rigorously evaluate the stability of the framework upon repeated exposure to water vapor.

In addition to the structural and chemical stability of metal–organic frameworks in the presence of water vapor, evaluating any new compound for use in a post-combustion CO_2 capture process also requires knowledge of the impact of water on the CO_2/N_2 separation performance. Indeed, small amounts of water can significantly affect the CO_2 adsorption properties of many zeolites due to its strong adsorption on the highly hydrophilic surface, which prevents CO_2 from interacting with many of the strong adsorption sites in the material.[412]

Initial efforts at understanding the effect of water on CO_2/N_2 separations in metal–organic frameworks have focused on HKUST-1. It is well-known that this framework can reversibly bind water, and there have been extensive studies, both theoretical and experimental, on this topic.[133,175,191,192,298,404,413,414] In its fully hydrated form, one water molecule is bound as a terminal ligand to each axial Cu^{2+} site. By heating of the material to 100 °C, these water molecules can be desorbed, generating the activated form of the framework as evidenced by a color change from turquoise (hydrated) to dark blue (dehydrated).[133] The effect of water coordination on the CO_2 adsorption properties of HKUST-1 was examined.[191] In the fully hydrated form, less than 1 mmol/g of CO_2 was adsorbed at 1 bar, compared with near 5 mmol/g for the dehydrated form. This is in agreement with a similar study that found that after exposure to 30% relative humidity, HKUST-1 experiences a decrease in CO_2 uptake to

dx.doi.org/10.1021/cr2003272 |*Chem. Rev.* 2012, 112, 724–781

about 75% of its original value and a concurrent loss of some crystallinity.[192]

Surprisingly, when HKUST-1 was loaded with 1 equiv of water per every two Cu^{2+} sites, the CO_2 adsorption increased to around 8 mmol/g, representing one of the highest CO_2 uptakes of any metal−organic framework at 1 bar (see Table 4).[191] The increased CO_2 capacity is attributed to electrostatic interactions between water bound to Cu^{2+} sites and the quadrupole moment of CO_2. Unfortunately, a loading of one H_2O molecule per two Cu^{2+} sites corresponds to such a low partial pressure of water that this form of HKUST-1 is unlikely to be realized in any realistic application.

In a similar study, CO_2 adsorption isotherms were measured at different water loadings for HKUST-1 and Ni_2(dobdc).[192] Both metal−organic frameworks retained some capacity for CO_2 at low water loadings but exhibited essentially no capacity for CO_2 above 70% relative humidity (RH). Significantly, water adsorption resulted in a much faster decrease in CO_2 uptake for zeolites 5A and NaX than for either metal−organic framework.

The effects of humidity on the performance of the M_2(dobdc) (M = Zn, Ni, Co, and Mg) series of metal−organic frameworks was studied in order to evaluate their CO_2/N_2 separation performance under conditions more relevant to post-combustion capture.[326] A flow-through apparatus was used to measure the breakthrough CO_2 capacity of each material in a 5:1 N_2/CO_2 mixture. The samples were then exposed to the same mixture at 70% RH, followed by regeneration at high temperatures. The breakthrough CO_2 uptake capacity after regeneration was then measured (see Figure 24). The compound Mg_2(dobdc), which has the highest reported capacity for CO_2 at low pressures, performed the worst out of the series with a recovery of only 16% of its initial CO_2 capacity after regeneration. Interestingly, this result stands in sharp contrast to previous reports that Mg_2(dobdc) can be fully regenerated after exposure to water without any effect on its CO_2 adsorption performance.[190] The reason for these different results is not yet established, though the observations could be consistent with incomplete dehydration, which would dramatically lower the CO_2 adsorption capacity. Nevertheless, Ni_2(dobdc) and Co_2(dobdc) performed far better with recoveries of 61% and 85% of their initial CO_2 capacity, respectively. This is in agreement with a similar study that found Ni_2(dobdc) was able to maintain its CO_2 capacity after steam conditioning and long-term storage, while Mg_2(dobdc) suffers a significant loss in capacity.[415] The work serves to highlight the importance of looking at the effect of water on the CO_2 adsorption properties of metal−organic frameworks, because the uptake of CO_2 as determined from single-component isotherms may not be the best indicator of material performance in a real-world post-combustion CO_2 capture process.

While strong adsorption sites, such as the exposed metal cations present in the M_2(dobdc) series, can be poisoned by small amounts of water, some flexible metal−organic frameworks have shown promising CO_2 adsorption properties in the presence of water.[266] In one report, water induced structural changes in MIL-53 that promoted a higher selectivity for CO_2 over CH_4.[220] Similarly, the breakthrough CO_2 adsorption of the flexible framework NH_2-MIL-53(Al) in the presence of 5% water vapor was also studied.[346] At low pressures, this material adopts a narrow-pore conformation that prevents the adsorption of certain gas molecules and improves its selectivity. Interestingly, CO_2 is selectively retained by the framework even in the presence of water.

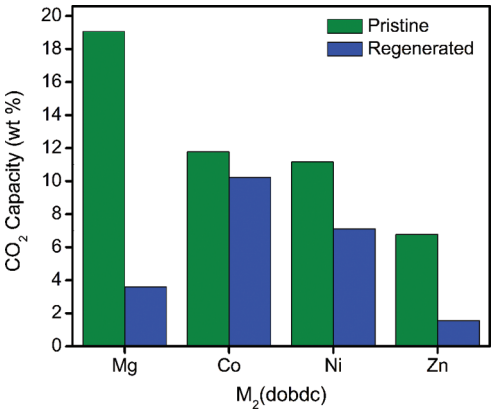

Figure 24. Comparison of the flow-through CO_2 capacities, as determined from breakthrough experiments using a 5:1 N_2/CO_2 mixture, for pristine M_2(dobdc) and regenerated M_2(dobdc) after exposure to 70% RH. Reproduced with permission from ref 326. Copyright 2011 American Chemical Society.

All of the studies presented here have involved either the measurement of single-component CO_2 adsorption isotherms after exposure to water or the measurement of breakthrough curves. While these experiments are crucial for the initial assessment of metal−organic frameworks for post-combustion CO_2 capture, multicomponent adsorption isotherms are of high priority for evaluating and understanding the performance under conditions likely to be encountered in an actual capture system.[11] To the best of our knowledge, there are no direct measurements of multicomponent isotherms involving CO_2 and H_2O in metal−organic frameworks to date.

3.3.2. Other Minor Components of Flue Gas. Although the gases CO_2, N_2, and H_2O account for greater than 95% of the flue gas mixture, the other minor components (mostly O_2, SO_x, NO_x, and CO) present cannot be ignored in assessing metal−organic frameworks for post-combustion CO_2 capture. While the exact amount of each species present in flue gas varies based on the type of coal burned and the specific configuration of a given power plant, a representative flue gas composition for a power plant burning low-sulfur eastern bituminous coal is reproduced in Table 1. Significantly, the effects of these trace gases on the CO_2/N_2 separation performance of metal−organic frameworks remains unknown. Future research must also address this issue if metal−organic frameworks are to be implemented in an actual post-combustion CO_2 capture process.

4. PRE-COMBUSTION CAPTURE

Pre-combustion CO_2 capture is a process in which fuel is decarbonated prior to combustion, resulting in zero carbon dioxide production during the combustion step (see Figure 3). Here, coal is gasified, generally at high temperature and pressure, to produce synthesis gas or "syn gas", which is a mixture of mostly H_2, CO, CO_2, and H_2O (see Table 9).[416] This gas mixture is then run through the water−gas shift reaction to produce H_2 and CO_2 ("shifted syn gas") at high pressure and slightly elevated temperature (5−40 bar and 40 °C, depending on the production plant).[417−420] Pre-combustion CO_2 capture, which refers to the separation of CO_2 from H_2 within this gas mixture, can then be performed to afford pure H_2, which is subsequently combusted in a power plant to generate electricity.

dx.doi.org/10.1021/cr2003272 |Chem. Rev. 2012, 112, 724–781

Table 9. Composition of Shifted Product of Coal Gasification[421]

component	approximate percentage (vol %)
CO_2	25−35
CO	0.5−0.7
H_2	30−50
CH_4	0
H_2O	15−40
H_2S	0.1−0.2
N_2	0.3−2.3
Ar	0.04

4.1. Considerations for Pre-combustion CO_2 Capture

Solid adsorbents, membrane materials, and liquid absorbers are currently under consideration as potential candidates for use in pre-combustion CO_2 capture.[422] With regard to industrial applications, pre-combustion CO_2 capture systems based upon CO_2-absorbing solvents are the closest to being realized,[423,424] and a number of power plants incorporating such systems are being constructed.[425,426] Furthermore, the use of solid adsorbents in pressure-swing adsorption-based processes is currently under intense investigation. Here, the high-pressure gas mixture is transported through a packed bed of a porous adsorbent incorporated into a PSA process. The CO_2 within the flue gas is selectively adsorbed along with other minor impurities of the mixture, such as CO, and following a series of concurrent and countercurrent pressurization and depressurization steps, the adsorbed gases can be removed, and the capture material can be regenerated for subsequent CO_2 capture cycles.[427]

4.1.1. Advantages of Pre-combustion Capture. In comparison to post-combustion CO_2 capture and oxy-fuel combustion-based processes, pre-combustion CO_2 capture carries a number of advantages that may be of benefit for its rapid industrial implementation. Perhaps most significantly, the gases are produced at high pressure, and the partial pressure of CO_2 in the mixture is high compared with post-combustion flue gas. As a result, regeneration of the loaded adsorbent can occur through a drop to atmospheric pressure, which is energetically favorable and is more practical compared with a temperature or vacuum swing-based process. Furthermore, the CO_2/H_2 separation is inherently easier to perform than CO_2/N_2 or O_2/N_2 separations, owing to the greater differences in the polarizability and quadrupole moment of the molecules.[10] Thus, for purely physisorption-based separations, a greater selectivity for CO_2 over H_2 can be anticipated, which may allow next-generation precombustion CO_2 capture materials to be more rapidly developed than new adsorbents for post-combustion CO_2 capture or oxy-fuel combustion.

4.1.2. Hydrogen Purification. Pressure-swing adsorption separation of shifted syn gas is a mature technology because of its wide use in hydrogen purification. Hydrogen used for industrial applications is generally synthesized from methane reformation followed by the water−gas shift reaction, which is very similar to coal gasification. The same processes as for coal gasification are applied, although the composition of the final products differ in the partial pressures of the gases (see Table 10), owing to the differences in carbon content between methane and coal. While liquid solvents such as Selexol are often used,[428] PSA columns employing solid adsorbent beds are also common and are responsible for the purification of millions of tons of hydrogen annually.[418] This hydrogen is used for ammonia synthesis and large industrial-scale reactions such as the Fischer−Tropsch synthesis of hydrocarbons.

Table 10. Components of the Shifted Products of Steam Methane Reformation[417]

component	approximate percentage (vol %)
H_2	70−80
CO_2	15−25
CO	1−3
CH_4	3−6

The ubiquitous nature of hydrogen purification via pressure-swing adsorption motivates the use of this separation process in the context of pre-combustion processes in two ways. First, because the technology is already in use, pre-combustion CO_2 capture would only require slight modifications or extensions to existing processes rather than a complete process overhaul. Second, from a practical point of view, the tremendous scale of H_2 purification (50 million tons of H_2 annually) suggests that even slight enhancements in the efficiency of this process would have significant benefits on the energy infrastructure as a whole. For example, if the energy cost of purification (7.3 MW·h per ton of H_2) can be reduced by 10%, the energy savings would represent the equivalent of shutting down 18 average-sized coal-fired power plants.[418,429] Thus, the development of next-generation materials for pre-combustion CO_2 capture that exhibit improvements in energy efficiency over existing materials would also have a significant impact on the economic and environmental costs associated with H_2 production worldwide.

Zeolites and activated carbons (see section 1.4.2) remain the most well studied solid adsorbents for H_2 purification of gas streams from steam-methane reformation.[430,431] Zeolite 13X possesses a high selectivity for CO_2, CO, and CH_4 over H_2 compared with BPL activated carbon,[417] although the capacity of activated carbons is generally greater than that of zeolites. Considering that these are the state-of-the-art porous solid adsorbents used for hydrogen purification, we compare the performance of these materials with metal−organic frameworks in the following sections to evaluate the potential of the latter to become the materials of choice for this application.

4.1.3. Metrics for Evaluating Adsorbents. In pressure-swing adsorption processes, the performance of adsorbents is evaluated using the selectivity for CO_2 over H_2 (eq 6), sometimes in the presence of other gases, such as CO. Although the selectivity value is the most important factor for determining the purity of the respective gas phases following the separation process, an equally important metric for evaluating an adsorbent is the CO_2 working capacity. This parameter is evaluated by taking the difference between the quantity adsorbed at flue gas pressure and the quantity adsorbed at the lower purge pressure. A high working capacity is particularly favorable in that less adsorbent is needed to form the PSA bed that performs the separation, which in turn decreases initial capital costs and, more importantly, lowers the long-term energy requirements for adsorbent regeneration.

An increase in either the selectivity or the working capacity would decrease the cost of a pressure-swing adsorption-based CO_2 capture system, and indeed, it has been reported that

dx.doi.org/10.1021/cr2003272 |Chem. Rev. 2012, 112, 724–781

optimization of both of these parameters is essential for developing promising candidates for PSA processes.[432,433]

4.1.4. Non-CO_2 Impurities in CO_2/H_2 Streams. In both hydrogen purification and pre-combustion CO_2 capture applications, the two main gas components are CO_2 and H_2. As can be seen in Tables 9 and 10, both product gases also contain CO, and in the case of steam-methane reformation, CH_4 is also present. Thus, discovery of materials that selectively capture CO and CH_4 in the presence of H_2 is also of high importance, since the impurity gases adsorb onto surfaces less strongly than CO_2 and conseqently break through the end of the column with H_2.[434] Both of these impurities must be removed owing to the implications of CH_4 as a greenhouse gas[435] and the high toxicity of CO. Other trace impurities, such as H_2O and H_2S, may also influence the performance of the material over time, and at the very least, the materials should be robust toward these components. The stability of metal−organic frameworks toward H_2O was considered in the context of post-combustion CO_2 capture in section 3.3.1. There is relatively little known regarding the effect of H_2S on metal−organic frameworks, although initial studies have demonstrated strong (irreversible) adsorption within materials with exposed metal cation sites, such as MIL-100.[436,437]

4.1.5. Metal−Organic Framework-Containing Membranes for pre-combustion CO_2 Capture. Membrane separation is an exceptionally promising strategy for precombustion CO_2 capture.[438] This is primarily because the high pressure of a pre-combustion gas mixture is an excellent driving force for membrane separation of CO_2 and H_2. The same properties that make metal−organic frameworks promising precombustion adsorbents are preserved in a membrane separation scenario. In a MOF-5 membrane, the CO_2/H_2 selectivity is theoretically higher than the CO_2/N_2 selectivity.[313] The high capacities for CO_2 in bulk metal−organic frameworks are not necessarily lowered when these materials are incorporated into membranes, since, for example, mixed-matrix membranes of MIL-53 have been shown to adsorb as much as 6 mol/kg of CO_2 at 25 bar.[439]

Diffusion is a property of gases that is pertinent to membrane separations that is frequently not discussed for bulk nanoporous adsorbents. This important characteristic has been thoroughly studied and can be harnessed in CO_2/H_2 membrane separations in metal−organic frameworks.[440] In MOF-5, the self-diffusivity of H_2 is much higher than that of CO_2, a requisite property for a H_2-selective membrane.[441] H_2 diffusion in MIL-47(V) and MIL-53(Cr) has been shown to be 2 orders of magnitude higher than the highest values recorded within a zeolite, which is a potential advantage in incorporating metal−organic framework-containing membranes into pre-combustion CO_2 capture systems. Additionally, CO_2 diffusion is slower than H_2 in MIL-47 just as in MOF-5,[442] preserving the selectivity of the separation materials. In section 6, we will discuss membrane applications of metal−organic frameworks in more detail.

4.2. Metal−Organic Frameworks as Adsorbents

Metal−organic frameworks have recently been investigated as potential next-generation adsorbents for pressure-swing adsorption-based separation of CO_2 from H_2. Their high surface areas afford enhanced gas adsorption capacities compared with porous solids conventionally employed in multilayer beds within current PSA systems, namely, activated carbons and zeolites, and their tunable surface chemistry is anticipated to facilitate further optimization of the material properties. Here, optimization refers to creating adsorption characteristics that are ideal for the CO_2/H_2 separation with the aim of reducing the regeneration cost of the PSA adsorbent, while maintaining a high gas adsorption working capacity and selectivity for CO_2 over H_2.[419]

Despite the opportunity for the development of metal−organic frameworks as pre-combustion CO_2 capture adsorbents (and H_2 purification adsorbents), relatively few reports have emerged in this regard. Although evaluation of the performance of candidate frameworks can be well-approximated via the collection of high-pressure, single-component CO_2 and H_2 isotherms at near-ambient temperature, there are only a small number of examples where such experiments have been performed. In cases where they have been reported, the isotherms have seldom been discussed and analyzed in the context of pre-combustion capture. Note that in this section, we consider CO_2/H_2 separations only in the context of pressure-swing adsorption-based processes in which the separation of the gases is achieved by a thermodynamic equilibrium that results from the bulk adsorptive properties of the material. As mentioned above, an alternative strategy for achieving the separation would be to make use of the difference in the kinetic diameters or diffusion properties of the two molecules in a kinetic-based separation using metal−organic framework membranes, and a thorough discussion of CO_2/H_2 separations (and other gas separations relevant to CO_2 capture) using such materials can be found in section 6. It should further be noted that, although the present discussion predominantly addresses CO_2/H_2 separations, CO_2/CO separation is also highly relevant to pre-combustion CO_2 capture (see section 4.1.4) and has been investigated in metal−organic frameworks such as ZIF-100[247] and mixed-linker MOF-5 variants (multivariate "MTV" metal−organic frameworks).[219] The separation of CH_4 and H_2 is also highly relevant to hydrogen purification and has been investigated in metal−organic frameworks in a number of studies.[320,443−445]

Table 3 provides high-pressure adsorption data for metal−organic frameworks representing many structure types and surface chemistries, and in general the data demonstrate the tremendous CO_2 adsorption capacity owing to the high surface areas and pore volumes found within the materials. In evaluating these materials for pre-combustion carbon dioxide capture, an initial step would be to calculate the maximum PSA working capacity of the potential adsorbent, which requires knowledge of its saturation capacity for CO_2. While the adsorption capacity at the lower (purge) pressure is a crucial parameter for maximizing the working capacity, a high saturation capacity is a necessity since it serves as an upper limit of the working capacity.

The selectivity of the material is also a crucial parameter when considering a material for pre-combustion CO_2 capture. There can be a trade-off between the working capacity and the selectivity, since more selective materials will tend to have a steeper initial portion in the CO_2 isotherms ($P < 1$ bar). This leads to a lower working capacity because the CO_2 adsorbed at the lowest pressures will not be removed at the purge pressure. Thus, since the working capacity is highly sensitive to the lower-pressure region of the adsorption isotherm, a single high-pressure CO_2 isotherm is not sufficient to evaluate a material for pre-combustion CO_2 capture. For example, among the more promising metal−organic frameworks listed in Table 3 are the MOF-74

dx.doi.org/10.1021/cr2003272 |Chem. Rev. 2012, 112, 724–781

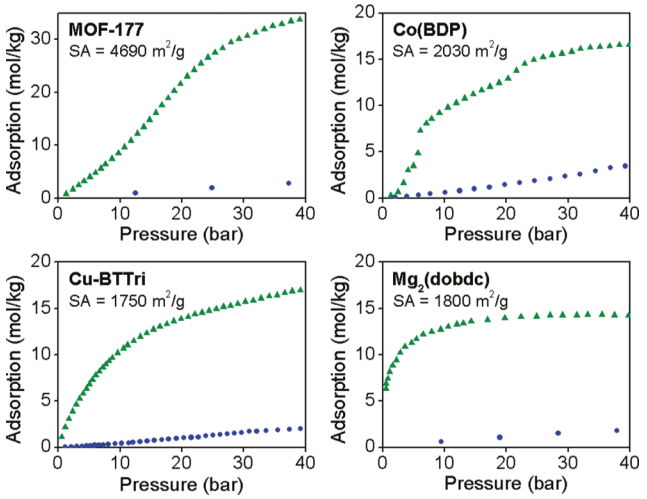

Figure 25. Single-component CO_2 (green triangles) and H_2 (blue circles) adsorption isotherms for the metal−organic frameworks MOF-177, Co(BDP), Cu-BTTri, and Mg_2(dobdc) at 313 K. Reproduced with permission from ref 87. Copyright 2011 American Chemical Society.

structure types (Mg- and Ni-MOF-74), which possess exposed metal cation sites (see section 3.2.3). These materials do not have the highest CO_2 saturation capacity and also have a relatively steep CO_2 adsorption isotherm, but as will be discussed in section 4.2.1, the balance between selectivity and working capacity renders them extremely promising for pre-combustion CO_2 capture. In contrast, MOF-177 has a high CO_2 capacity and a shallow initial rise in its CO_2 adsorption isotherm. However, its internal surface imparts little CO_2/H_2 selectivity and after further investigation, MOF-177 is shown to be a poor pre-combustion CO_2 capture material. These two examples serve to stress that while metal−organic frameworks adsorb large amounts of CO_2 at high pressures, they need to be carefully evaluated in order to elucidate the most promising candidates for pre-combustion CO_2 capture.

4.2.1. Investigations Based on Single-Component Isotherms. To date, very few experimental studies explicitly investigating metal−organic frameworks or pre-combustion CO_2 capture have been reported. In one recent example, high-pressure CO_2 and H_2 adsorption isotherms were measured at 40 °C for five rerpresentative metal−organic frameworks, and the selectivities and working capacities were calculated using IAST.[87] Two rigid, high-surface area frameworks (MOF-177 and Be-BTB),[446,447] one flexible framework (Co(BDP)),[448] and two materials bearing exposed metal cation sites (Mg_2(dobdc) and Cu-BTTri)[150,200] were studied. Figure 25 shows the isotherms for four of the five frameworks (the isotherms for Be-BTB were similar to those obtained for MOF-177).

In terms of adsorption selectivity, Mg_2(dobdc) was the best out of the materials studied, including two activated carbons and zeolite 13X (see Figure 26). These selectivities were calculated by applying IAST (section 2.3.2) to the single-component isotherms and assuming an 80:20 H_2/CO_2 mixture. All porous materials with localized charges in the pores (Mg_2(dobdc) and Cu-BTTri) and zeolite 13X demonstrated selectivities between 100 and 1000, as did activated carbons with strong van der Waals interactions with CO_2 due to their small pores. The metal−organic frameworks having largely aromatic internal surfaces without significant surface charges (MOF-177, Be-BTB, and

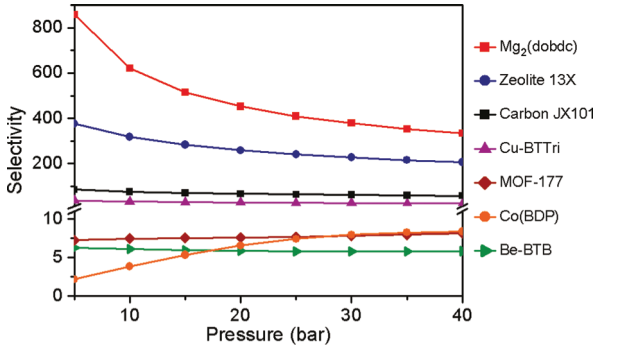

Figure 26. CO_2/H_2 selectivities for an 80:20 H_2/CO_2 mixture at 313 K as calculated using IAST methods. Reproduced with permission from ref 87. Copyright 2011 American Chemical Society.

Co-BDP) were found to display low CO_2/H_2 selectivities in the range of 5−10.

In terms of working capacity for the same gas composition, all of the metal−organic frameworks exhibited higher volumetric and gravimetric working capacities compared with zeolite 13X and activated carbon JX101 (see Figure 27). The high CO_2 saturation capacities of the metal−organic frameworks, especially coupled with strong polar interactions (such as in the case of Mg_2(dobdc) and Cu-BTTri) lead to their high working capacities. Note that the materials with large pores (MOF-177 and Be-BTB) have a high gravimetric capacity but a low volumetric capacity, highlighting the importance of structural considerations when selecting a metal−organic framework for pre-combustion CO_2 capture.

The results of this study suggest that metal−organic frameworks with open metal sites or other sources of localized charge are particularly promising as pre-combustion CO_2 capture adsorbents. They offer high CO_2/H_2 selectivities as well as high working capacities. Due to the delicate balance between strong CO_2 binding and the need for low CO_2 adsorption at low pressures (in order to increase working capacity), screening a wide variety of this class of metal−organic frameworks is of high importance for identifying the best materials for this application.

4.2.2. Computational Studies. While the performance of metal−organic frameworks can be probed by collecting high-pressure CO_2 and H_2 isotherms, an alternative option for screening the vast number of materials would be to simulate the adsorption of a pre-combustion gas mixture to predict the separation performance. This can be performed by using only the crystal structure of a porous material, making it a very powerful tool. While such a methodology would allow a large number of structures to be rapidly screened, it should be noted that synthetic limitations (such as obtaining a perfectly desolvated sample) make theoretical results a best-case scenario that require experimental substantiation in the case of the most promising materials.

In a similar situation to the experimental studies discussed above, simulation-based investigations of CO_2/H_2 separations are also limited to a relatively small number of reports. One of the earliest reports involved an indium-based metal−organic framework, $[In_3O(abtc)_{1.5}(H_2O)_3](NO_3)\cdot 3H_2O$, consisting of 3,3′,5,5′-azobenzenetetracarboxylate (abtc) organic bridging units and charge-balancing nitrate anions in the pores.[449] The predicted selectivity for CO_2 over H_2 in a 15:85 CO_2/H_2 mixture introduced at 298 K increases from approximately 300 to 600

dx.doi.org/10.1021/cr2003272 |Chem. Rev. 2012, 112, 724–781

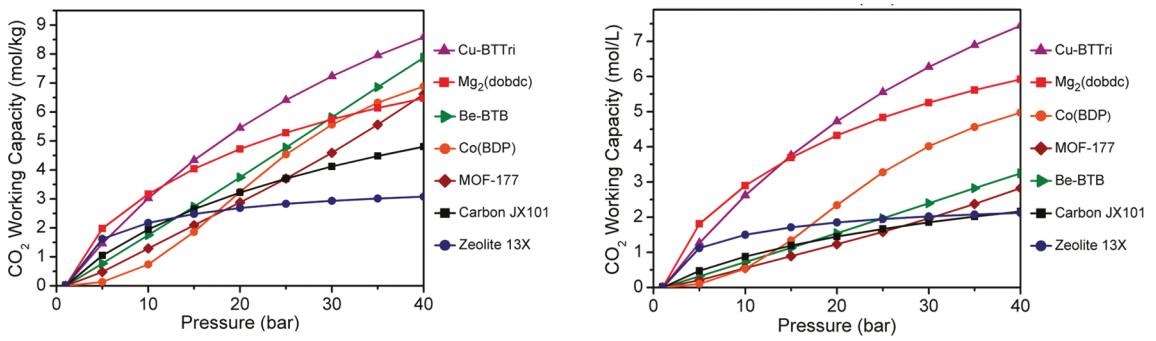

Figure 27. Gravimetric (left) and volumetric (right) CO_2 working capacities calculated using IAST for an 80:20 H_2/CO_2 mixture at 313 K, assuming a purge pressure of 1 bar. Reproduced with permission from ref 87. Copyright 2011 American Chemical Society.

between 0 and 5 bar and then gradually decreases to 450 up to 30 bar. While the authors did not report the CO_2 working capacity for this material, the high-pressure CO_2 adsorption of a 15:85 CO_2/H_2 mixture was reported and from this isotherm a maximum working capacity of 7 mmol/g can be approximated. This is similar to the highest performing metal−organic frameworks discussed in section 4.2.1, and therefore, if the nitrate anions are accessible to gas molecules in the experimentally prepared material, this compound would be very promising for pre-combustion CO_2 capture.

Quaternary and quinary mixtures were also simulated in this study. The quaternary mixture was composed of 15:75:5:5 $CO_2/H_2/CO/CH_4$ and the quinary mixture was 15:75:5:5:0.1 $CO_2/H_2/CO/CH_4/H_2O$. These were included to better model pre-combustion carbon capture mixtures as discussed in section 4.1. Both selectivity curves maintain the same shape as the binary mixture; however, the maximum selectivity drops by approximately 20 for the quaternary and another 30 for the quinary mixture. The selectivity continues to decline from 5 to 30 bar, and as such, the quaternary mixture drops to approximately 375 and the quinary selectivity to 350. In the context of pre-combustion CO_2 capture, this work suggests that a modest amount of water in the gas mixture could significantly decrease the selectivity for CO_2 due to selective binding of H_2O over CO_2 due to its stronger polarizability. Interestingly, between 0 and 2 bar the highest selectivity was observed for the quinary mixture,which was attributed to bound water promoting the adsorption of CO_2.

The same four- and five-component mixtures were employed in evaluating a second cationic metal−organic framework with charge-balancing nitrate anions.[450] The copper-based material, $Cu_6O(TZI)_3(H_2O)_9(NO_3)\cdot 15H_2O$ (*rht*-MOF), was shown to be much less selective for CO_2 in both the quaternary and quinary mixtures, and the initial selectivity of ca. 42, drops to 40 at 1 bar, increases to 60 at 40 bar, and then approximately plateaus until 50 bar. The authors attributed this difference to the large pore volume of *rht*-MOF.

A tetracarboxylate-linked indium-based metal−organic framework was also investigated for CO_2/H_2 separation.[451] This anionic framework with formula $Li_{0.5}(H_3O)_{0.5}[In(C_{16}H_6O_8)]$ contains charge-balancing Li^+ cations in the pores, which are shown theoretically to be the primary binding site for CO_2. The selectivity for CO_2 in a 15:85 CO_2/H_2 mixture decreases from 1100 to 600 between 0.01 and 1 bar, increases slightly until 10 bar, and then decreases back down to 500 at 50 bar (see Figure 28). These three regions are attributed to strong binding sites becoming unavailable with increasing CO_2 loading, followed by cooperative

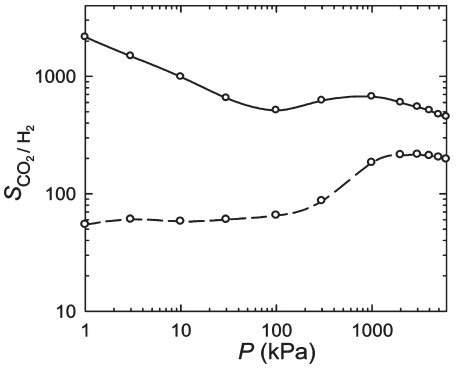

Figure 28. Selectivities calculated from simulations for a 15:85 CO_2/H_2 mixture at 298 K in $Li_{0.5}(H_3O)_{0.5}[In(C_{16}H_6O_8)]$ shown with (solid line) and without (dashed line) inclusion of electrostatic interactions. Reproduced with permission from ref 451. Copyright 2011 American Chemical Society.

CO_2-CO_2 interactions becoming predominant, and last the entropic favorability of H_2 binding at high pressures. This entropic effect has been observed previously for other porous materials.[452]

Simulations for CO_2/H_2 separations were further reported within an indium-based metal−organic framework, $In_{48}(C_5N_2O_4H_2)_{96}$-$Na_{48}(C_2H_5OH)_{96}(H_2O)_{192}$ (*rho*-ZMOF), formed from 4, 5-imidazoledicarboxylic acid as the linker.[453] This framework is anionic and contains charge-balancing Na^+ cations in the pores, which bind CO_2 strongly and preferentially. Only at high pressures when the cations are completely solvated by CO_2 does the CO_2 begin to bind at other surfaces. This strong Na^+-CO_2 interaction leads to an initial selectivity of 200 at 10 bar, which remains steady until 30 bar for a 15:85 CO_2/H_2 mixture. A maximum working capacity of 4 mmol/g can be estimated from the high-pressure CO_2 adsorption of a 15:85 CO_2/H_2 mixture. This is approximately half that of other metal−organic frameworks with exposed metal sites (see Section 4.2.1). Interestingly, the Na^+ cations shift locations slightly with CO_2 adsorption.

The effect of replacing the protons on 1,4-benzenedicarboxylate (BDC) in MOF-5 (see Section 1.4.1, Figure 6) with O^-Li^+ groups was studied computationally in a recent report.[350] Upon exposure to a 20:80 CO_2/H_2 mixture, this structure reaches predicted CO_2/H_2 selectivities of 10 000 at infinite dilution, compared with approximately 10 for unmodified MOF-5. This was determined to be solely from electrostatic interactions by turning these forces off and examining the changes in selectivity.

dx.doi.org/10.1021/cr2003272 |*Chem. Rev.* 2012, 112, 724–781

The selectivity for CO_2 in a 50:50 CO_2/H_2 mixture in HKUST-1 (see Figure 7) and MOF-5 were compared via simulations.[316] In MOF-5, the authors found that the selectivity slowly increases from less than 10 to approximately 30. HKUST-1 demonstrates a selectivity curve similar to *rht*-MOF, with an initial decrease from 100 to 80 by 1 bar, an increase to 150 by 15 bar, and then a decrease to 100 at 50 bar. The last decrease is ascribed to the favorable packing of the small hydrogen molecules when gas molecules are filling the pores, as opposed to physisorption onto the surface. This effect is not seen in MOF-5, because at 40 bar the pores are not fully occupied. The authors also compared these selectivities to those generated using IAST and found that for MOF-5 the prediction is reasonably accurate but in HKUST-1 IAST underestimates the selectivity with a drop from 100 at 0 bar to 70 at 50 bar. An additional insight was the composition-dependence of selectivity, which was shown to be minimal as the selectivity did not change more than 10% upon increasing the amount of CO_2 in the mixture from 10% to 90%.

A compound with a neutral framework structure, $Co_2(ade)_2(CO_2CH_3)_2 \cdot 2DMF \cdot 0.5H_2O$ (bio-MOF-11), was studied theoretically for pure-component CO_2 and H_2 adsorption and a 15:85 CO_2/H_2 mixture.[315] Radial distribution functions demonstrated that CO_2 binds at Lewis basic sites of the adenine linker and not near the framework cobalt atoms. The selectivity of the gas mixture increases from 270 to 370 between 0 and 5 bar, then decreases to 220 at 30 bar. The addition of 0.1 mol % H_2O to the mixture had a negligible effect on the selectivity, in contrast to the results of the cationic materials discussed above.

Some researchers have focused on comparing groups of porous solids to extract meaningful trends in CO_2/H_2 separations. Simulated breakthrough curves (see section 3.2.3) of CH_4/H_2, CO_2/H_2, and $CO_2/CH_4/H_2$ mixtures of five metal−organic frameworks (as discussed in section 4.2.1), as well as zeolite 13X, were published recently.[434] A packed bed of metal−organic framework was simulated and both the composition of the gas mixture exiting the bed as a function of time and the amount of CO_2 adsorbed were evaluated. The metric τ_{break}, the time at which a specified fraction of impurity (either CO_2 or CH_4) is present in the gas leaving the bed, was used to characterize the adsorbents. In terms of τ_{break} and the amount of CO_2 adsorbed at τ_{break}, Mg_2(dobdc) was determined to be the best material of those studied (see Figure 29). Note that this method provides an important means of ranking materials via a single metric, which takes into account both selectivity and working capacity.

The effect of catenation (interpenetration) on CO_2/H_2 selectivity was examined computationally, and it was found that catenated IRMOFs are much more selective than the noncatenated materials.[454] Looking at five different mixture compositions (5:95, 30:70, 50:50, 70:30, and 95:5 CO_2/H_2), the catenated metal−organic frameworks all displayed selectivites between approximately 40 and 110, whereas the three noncatenated materials were much lower (below 20). The shapes of the selectivity curves differed for the different compositions, with the three steps discussed above for $Li_{0.5}(H_3O)_{0.5}$[In(abtc)] becoming more apparent with more CO_2 in the mixture. This substantiates the attribution of $CO_2 \cdots CO_2$ interactions to the increase in selectivity after an initial decrease, as this increase is not apparent in the 5:95 CO_2/H_2 mixture. Furthermore, turning off electrostatic interactions between CO_2 molecules *only* resulted in the loss of this feature in the selectivity trace. The adsorption sites of the gas molecues of the mixture gas

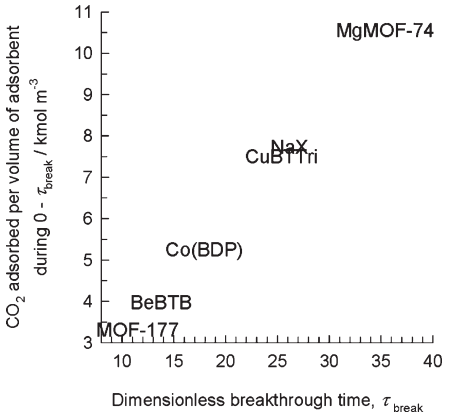

Figure 29. Amount of CO_2 adsorbed as a function of breakthrough time (τ_{break}), where the breakthrough concentration of CO_2 is 0.05% and the conditions are 313 K, 48 bar adsorption, and 12 bar desorption pressures. Reproduced with permission from ref 434. Copyright 2011 American Chemical Society.

demonstrated that selective CO_2 adsorption happens in the small channels of the catenated frameworks.

A study in which the CO_2/H_2 selectivity for two ZIF materials, ZIF-3 and ZIF-10, was compared with those of IRMOF-1, -8, -10, and -14 has been recently reported.[308] In a 10:90 mixture of CO_2/H_2, ZIF-3 exhibited the three-step adsorption selectivity behavior discussed above, with a selectivity factor between 100 and 200, while ZIF-10 increased linearly in selectivity from 25 to 60 between 0 and 50 bar. All of the IRMOF selectivities were approximately constant with pressure, varying between 7 and 12. The difference in selectivity between the two classes of frameworks was attributed to the smaller pore size in ZIFs and confinement effects, which is a result of the higher degree of overlap of the van der Waals forces associated with opposing wall surfaces.

In a separate study, six metal−organic frameworks were compared with six covalent-organic frameworks (COFs). These are porous crystalline solids that consist of only covalent bonds and are typically assembled from the co-condensation of boronic acids.[314] The six COFs studied are very similar with respect to their properties since they are composed of the aromatic units connected by boron oxide rings. Five of the six metal−organic frameworks studied are from the IRMOF series and the sixth was HKUST-1. Two materials, HKUST-1 and COF-6, were found to be much more selective than the other materials. The selectivity in COF-6 was attributed to the small pore size, and the concomitant confinement effects. Both materials had large differences in the heats of adsorption of CO_2 compared with H_2, and HKUST-1 exhibited a significantly higher electrostatic contribution to the selectivity.

A compilation of previously published data obtained from configurational-bias Monte Carlo (CBMC) simulations was recently reported.[317] The CO_2/H_2 selectivity for a 15:85 CO_2/H_2 mixture was compared for zeolites NaX, NaY, AFX, CHA, and FAU-Si in addition to the metal−organic frameworks *rho*-ZMOF, Mg_2(dobdc), Zn_2(dobdc), HKUST-1, ZIF-8, and MOF-177. The most selective was zeolite NaX followed by NaY, AFX, *rho*-ZMOF, and Mg_2(dobdc). The working capacities assuming a 1 bar purge pressure were also plotted for these materials and the same gas mixture, and Mg_2(dobdc), Zn_2(dobdc), HKUST-1, ZIF-8, and zeolite AFX were the top five

dx.doi.org/10.1021/cr2003272 |*Chem. Rev.* 2012, 112, 724–781

in terms of working capacity, with Mg_2(dobdc) being consistently significantly higher than all of the other materials (see Figure 30a). In addition, selectivity as a function of working capacity was also plotted at a pressure of 10 bar to demonstrate which materials maintained a high working capacity and were also selective (Figure 30b). Here, Mg_2(dobdc) stands out as clearly the most attractive metal−organic framework candidate for pre-combustion CO_2 separation.

Taking all of the simulation work published to date relating to metal−organic frameworks for pre-combustion CO_2 capture into consideration, Mg_2(dobdc) is expected to provide the best overall performance out of the materials studied so far. Importantly, this is consistent with the conclusions from the few experiments performed thus far (see section 4.2.1). Strategies for improving upon the performance of Mg_2(dobdc) are urgently required, although the synthesis of new metal−organic frameworks with pore surfaces decorated with a high concentration of exposed high-valent (trivalent or tetravalent) cations would be one approach for achieving higher capacities and selectivities. As discussed in section 4.1.4, examining the effects of impurity components (H_2O, CO, H_2S, and CH_4) in the pre-combustion gas stream on the stability and separation performance in Mg_2(dobdc) as well as other metal−organic frameworks is an area in which a greater understanding is urgently needed.

5. OXY-FUEL COMBUSTION

Oxy-fuel combustion refers to the ignition of pulverized coal or other carbon-based fuels in a nearly pure O_2 environment and represents a relatively new process for mitigating CO_2 emissions compared with pre-combustion and post-combustion CO_2 capture. The significant advantages of this process stem from the fact that the flue gas (following removal of particulates, water, and trace impurity gases) is almost entirely CO_2, which greatly simplifies the capture step, and that most existing power plants could be readily retrofitted with an oxy-fuel combustion system. Although there are no full-scale plants currently using oxy-fuel combustion, theoretical studies along with laboratory and pilot-scale studies have provided an understanding of important design parameters and operational issues.

A schematic of a typical oxy-fuel combustion process is presented in Figure 3. Here, in a conventional set up, O_2 (purity >95%) is fed into the plant from a cryogenic separation unit, which separates O_2 from the other components of dry air by a distillation process. The O_2 inlet gas is diluted with CO_2 from the flue stream to a partial pressure of 0.21 bar in order to control the temperature of fuel combustion and to reduce the formation of NO_x impurities that frequently form when coal is burned in an O_2-enriched atmosphere.[455] The exhaust gas, which is essentially pure CO_2, can then be directly subjected to sequestration using the techniques discussed in detail in section 1.3. Indeed, in addition to CO_2 (55−65 wt %), the other major component of the gas stream is water vapor (25−35 wt %), which is easily condensed and removed.[456] In fact, CO_2 capture rates higher than 95% have been achieved by this method, a level not currently possible with pre-combustion and post-combustion separations.[457] A further advantage related to combustion in an O_2/CO_2 mixture lies in the fact that compared with a process utilizing air, which is rich in N_2, the formation of NO_x is largely inhibited, allowing for a smaller, cheaper NO_x removal step than required in current power plants.

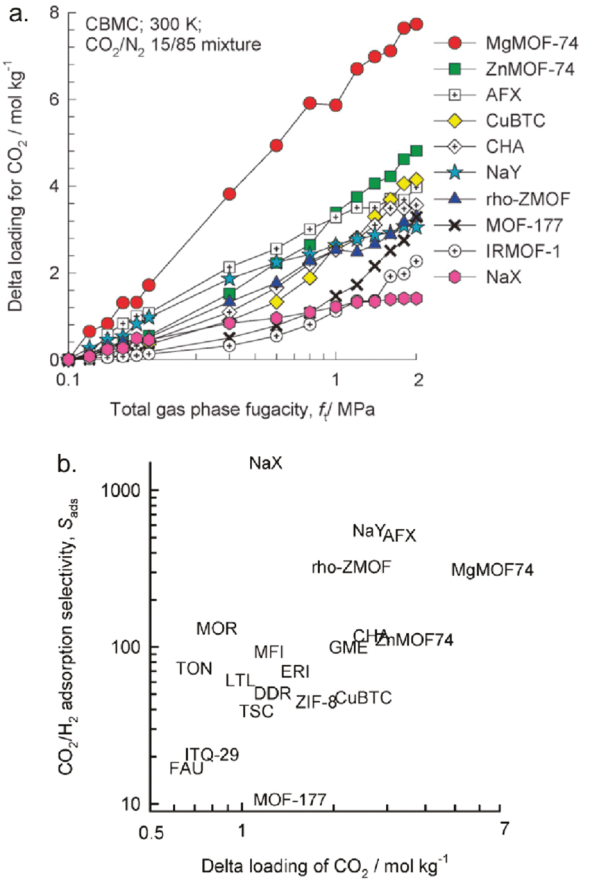

Figure 30. (a) Working capacities ("delta loadings") of selected metal−organic frameworks and zeolites, as calculated for a 15:85 CO_2/H_2 mixture at 300 K with a purge pressure of 1 bar. (b) The CO_2/H_2 adsorption selectivity as a function of working capacity ("delta loadings") of selected metal−organic frameworks and zeolites. The selectivities and working capacities are calculated for a 15/85 CO_2/H_2 mixture at at 300 K, with a purge pressure of 1 bar. Reproduced with permission from ref 317. Copyright 2011 The Royal Society of Chemistry.

A significant challenge for the implementation of oxy-fuel combustion methods is in the large-scale generation of pure O_2 from air. This separation is currently carried out on a scale of over 100 Mt/year,[458] but the large energy requirement for this process creates an urgent need for alternative separation methods if oxy-fuel combustion is to be widely used in mitigating carbon emissions. Microporous solids that selectively adsorb O_2 from the air could potentially significantly reduce this energy cost. Indeed, zeolites have been used in this separation on an industrial scale and in portable medical devices,[459] although the separation performance and energy efficiency is considered to be insufficient for use in oxy-fuel combustion applications. In this regard, metal−organic frameworks hold tremendous promise for delivering high-performance materials that are specifically optimized for the removal of O_2 from the air. As will be discussed, this separation is essentially an O_2/N_2 separation, for which metal−organic frameworks exhibiting high selectivities, and O_2 adsorption capacities have been recently reported.

dx.doi.org/10.1021/cr2003272 |Chem. Rev. 2012, 112, 724–781

5.1. Metal−Organic Frameworks for O_2/N_2 Separation

As discussed in previous sections, microporous metal−organic frameworks are typically selective for the adsorption of CO_2 over N_2 or CO_2 over H_2, based on the large differences in the quadrupole moments and polarizabilities between the molecules. However, owing to the very similar physical properties of O_2 and N_2, their separation using a purely physisorptive adsorption mechanism is expected to yield very limited selectivity factors. In fact, because of the higher quadrupole moment and polarizability of N_2 compared with O_2 (see Table 2), many of the metal−organic frameworks for which O_2 isotherms have been measured at room temperature are slightly selective for the adsorption of N_2 over O_2. For example, O_2 and N_2 adsorption isotherms recorded at 298 K for MOF-177 and UMCM-1, which are both high-surface area frameworks with BET surface areas of greater than 4000 m^2/g, yield a selectivity factor (calculated as the number of moles of O_2 adsorbed at 0.21 bar divided by the number of moles of N_2 adsorbed at 0.79 bar) of less than 1.[169,228,298,390] Furthermore, although small-pore zeolites have been employed for O_2/N_2 separations based on the differing kinetic diameters of these molecules, it is unlikely that metal−organic frameworks could offer the significant improvements needed for an efficient kinetic-based O_2/N_2 separation process. Instead, an effective separation of O_2 from N_2 within metal−organic frameworks is expected to be achieved through harnessing the differences in chemical properties of the molecules, and this has indeed been the focus of recent work in which high adsorption selectivities have been reported.

The high propensity for O_2 to accept electrons from redox-active metal centers is one feature that can be exploited to perform the separation of O_2 from N_2 within metal−organic frameworks. Indeed, such interactions are crucial in nature for biological functions such as O_2 transport, and a large volume of biomimetic molecular chemistry has emerged through coordination complexes containing metal ions such as Fe^{2+} or Cu^{+}.[460−468] Thus, if the surfaces of metal−organic frameworks can be decorated with electron-rich, redox-active metals with open coordination sites, these sites may engage in a reversible electron transfer to O_2, but not N_2.

Metal−organic frameworks containing such accessible redox-active metal centers have recently emerged,[140,254,469−471] and these display considerable promise as next-generation O_2 capture materials. Note that metal−organic frameworks are expected to possess several advantages over zeolites, since their larger pores are expected to facilitate higher gas permeability, and the adjustable character of the pore surfaces are anticipated to allow the enthalpy of O_2 adsorption to be finely tuned for specific working conditions. Additionally, since the exposed metal sites are immobilized and separated from each other on the pore surface by virtue of the framework structure, two metal sites cannot combine to form O_2-bridged species, a reactivity pathway that is known to diminish the performance of molecular complexes investigated for O_2 binding.[472−474]

Recently, a metal−organic framework bearing exposed Cr^{2+} adsorption sites, $Cr_3(BTC)_2$, a framework isostructural to HKUST-1 was studied for selective binding of O_2 over N_2.[134] The Cr^{2+} sites are available for binding guest molecules and exhibit a tremendous affinity for O_2, leading to an O_2 adsorption of 11 wt % at 298 K and a pressure of just 2 mbar (see Figure 31). At the same temperature, the quantity of N_2 adsorbed is just 0.58 wt % at a pressure of 1 bar. The steep initial rise in the O_2 adsorption isotherm is indicative of a strong (chemical) interaction between

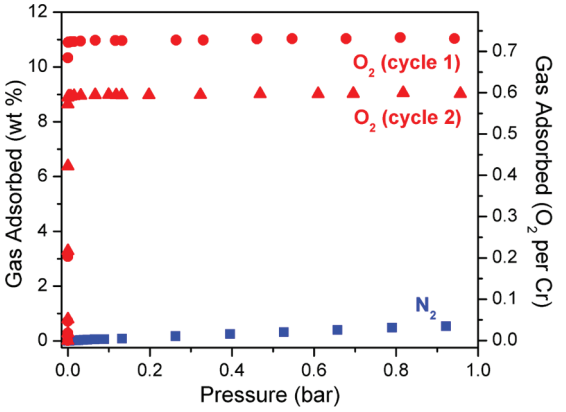

Figure 31. Uptake of O_2 (red symbols) and N_2 (blue squares) by $Cr_3(BTC)_2$ at 298 K. The compound saturates with O_2 at approximately 2 mbar but shows little affinity for N_2. Upon evacuation, the O_2 isotherm for a second cycle reveals a slightly reduced capacity. Reproduced with permission from ref 134. Copyright 2010 American Chemical Society.

the Cr^{2+} sites and O_2 molecules, and the saturation uptake corresponds to the adsorption of dioxygen at approximately 80% of available Cr^{2+} sites within the framework. Indeed, UV−vis−nIR spectroscopy and X-ray absorption spectra confirmed the partial electron transfer from Cr^{2+} to the bound O_2 molecule to give roughly a Cr^{3+}−superoxide adduct. The charge transfer gives rise to a significantly stronger interaction compared with the physisorptive adsorption of N_2 molecules, resulting in an O_2/N_2 selectivity factor of 19.3. This selectivity is significantly higher than that observed for most previously investigated porous solid materials,[475] such as a carborane-based porous Co^{2+}-based framework, which displays a selectivity factor of 6.5 at low pressure.[254] Importantly, $Cr_3(BTC)_2$ displays reversible O_2 uptake, and heating of the framework to just 50 °C liberates the majority of the bound O_2. However, following 14 adsorption/desorption cycles, approximately 35% of the O_2 adsorption capacity of the material is lost, presumably as a result of framework decomposition owing to the highly exothermic nature of the chromium−O_2 interaction.

More recently, selective O_2 adsorption has been studied in $Fe_2(dobdc)$, a metal−organic framework featuring one-dimensional hexagonal channels lined with five-coordinate Fe^{2+} centers (see Figure 8).[476] Gas adsorption isotherms measured at 298 K indicate that this material binds O_2 at a capacity of 10.4 wt % at 1.0 bar. The N_2 uptake under these conditions is considerably lower, reaching just 1.3 wt % at 1.0 bar. Although this material exhibits a selectivity factor of 6.6, the adsorption of O_2 at 298 K was irreversible. Remarkably, at 211 K, O_2 adsorption was nearly doubled to 18.2 wt % and fully reversible. Under these conditions, the material showed negligible loss in adsorption capacity after 13 cycles. Initial isosteric heats of N_2 (−35 kJ/mol) and O_2 (−41 kJ/mol) adsorption in $Fe_2(dobdc)$, calculated from dual-site Langmuir−Freundlich fits to isotherms measured at 201, 211, 215, and 226 K, reflect the higher propensity for O_2 to accept charge from Fe^{2+}. Accordingly, $Fe_2(dobdc)$ exhibits high O_2/N_2 selectivity at these temperatures ranging from 4.4 to 11, reaching a maximum of 11.4 at 201 K and about 0.4 bar. Application of IAST to simulate breakthough curves indicate $Fe_2(dobdc)$ is a promising material for the separation of O_2 from air at temperatures well above those currently used for cryogenic distillations.

dx.doi.org/10.1021/cr2003272 |*Chem. Rev.* 2012, 112, 724–781

Mössbauer spectroscopy, in conjunction with neutron powder diffraction and infrared spectroscopy, was employed to elucidate the mechanism of O_2 adsorption in $Fe_2(dobdc)$. At low temperatures, $Fe_2(dobdc)$ was found to adsorb O_2 reversibly at a capacity corresponding to the adsorption of one O_2 molecule per Fe center. At higher temperatures O_2 adsorption becomes irreversible and decreases to one O_2 molecule per two Fe centers. Mössbauer spectroscopy indicated that in the absence of O_2, the spectrum of $Fe_2(dobdc)$ exhibits a simple quadrupole doublet, with isomer shifts and quadrupole splitting indicative of high-spin Fe^{2+} in a square pyramidal coordination environment. Upon dosing the material with O_2 at 94 K nearly all of the iron centers display a substantially reduced isomer shift, which lies between typical values expected for high-spin Fe^{2+} and high-spin Fe^{3+}, suggesting partial charge transfer to the adsorbed O_2. Warming the material above 222 K in the presence of O_2 results in spectra with isomer shifts and quadrupole splittings typical of high-spin Fe^{3+}. The combination of data from O_2 adsorption experiments and Mössbauer spectroscopy suggests that O_2 binds to the exposed iron sites in $Fe_2(dobdc)$ by two different coordination modes depending on the temperature of adsorption. At low temperatures, partial charge transfer from iron to O_2 results in a material with weakly bound, partially reduced O_2 at every Fe center. At higher temperatures, the initial electron transfer step is followed by a second electron transfer from an adjacent Fe center. In this scenario, all of the iron centers are oxidized to Fe^{3+}, half being irreversibly coordinated by an O_2^{2-} anion, while the other half remain five-coordinate.

Infrared spectroscopy and neutron powder diffraction were utilized to confirm the proposed mechanism of O_2 binding in $Fe_2(dobdc)$. Upon dosing the sample with O_2 at 100 K, a number of new bands were apparent in the difference IR spectra. Most notable was the component present at 1129 cm^{-1}, which, in conjunction with the first overtone of this stretching mode appearing at 2238 cm^{-1}, is indicative of partially reduced (near superoxo) O_2 species coordinated to the Fe centers. Additionally, upon warming the sample to room temperature, the superoxo band at 1129 cm^{-1} disappears while a new component at 790 cm^{-1} (indicative of metal-bound O_2^{2-}) appears. These assignments are consistent with the model developed from O_2 adsorption experiments and Mössbauer spectroscopy.

Direct structural evidence for temperature-dependent binding of O_2 to the iron centers in $Fe_2(dobdc)$ was provided by neutron powder diffraction. Refinement of powder diffraction data collected on a sample at 4 K that was dosed with 2 equiv of O_2 per iron at 100 K indicate three different O_2 adsorption sites (Figure 32). The first site to be populated by O_2 is the open Fe-based binding site. Interestingly, the O_2 molecule binds in a symmetric side-on coordination geometry, with an Fe−O distance of approximately 2.10(1) Å. The refined O−O separation distance of 1.25(1) Å is approximately halfway between the internuclear distance observed for typical superoxide (1.28 Å) and free O_2 (1.207 Å).[477] The second and third O_2 adsorption sites occur within the pores of the material at occupancies of 0.857(9) and 0.194(8) Å, respectively. Refinement of data collected at 4 K on a sample that had been dosed with O_2 at room temperature confirmed coordination of a peroxide species to approximately half of the iron centers in the framework. Specifically, O_2 was found to coordinate to iron in an asymmetric side-on mode with a refined occupancy of 0.46(2) and a substantially elongated O−O distance of 1.6(1) Å.

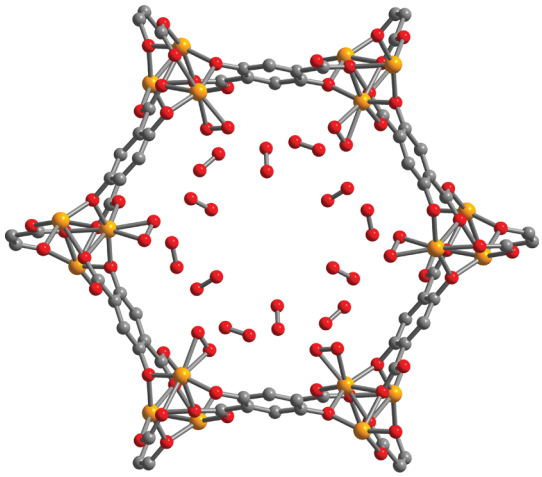

Figure 32. A portion of the structure of $Fe_2(O_2)_2(dobdc)\cdot O_2$ as viewed down the (001) direction. Orange, gray, and red spheres represent Fe, C, and O atoms, respectively; H atoms are omitted for clarity.[477]

The O_2 adsorption characteristics of $Fe_2(dobdc)$ and $Cr_3(BTC)_2$ highlight the importance of exposed redox-active metal centers for the development of new metal−organic frameworks that exhibit selective O_2 adsorption. A simple strategy for preparing new metal−organic frameworks with potential utility for O_2/N_2 separations is exemplified by the synthesis of these materials. Although $Cu_3(BTC)_2$[478] or $Mo_3(BTC)_2$[137] do not selectively adsorb O_2 over N_2, replacement of the metal cations in the structure of these materials with Cr^{2+} effectively resulted in a material with unprecedented O_2/N_2 selectivity. This approach of preparing frameworks of known structure types with redox-active metals could potentially be expanded to other families of materials.

In addition to preparing new metal−organic frameworks for O_2/N_2 separations, modifications can be made to existing frameworks to optimize the O_2 adsorption selectivity. The compound $Fe_2(dobdc)$, for example, exhibits reversible O_2 adsorption up to 226 K, above which electron transfer reactions result in irreversible O_2 adsorption. Modification of the bridging ligand by incorporating electron-donating or -withdrawing groups would presumably alter the electronics of the material and could result in a framework that demonstrates reversible room-temperature O_2 adsorption. Additionally, a number of metal−organic frameworks have been shown to be amenable to the postsynthetic insertion of metal cations.[204,479−483] Incorporation of redox-active metals into these frameworks may lead to materials with selective/reversible O_2 binding properties. As compared with CO_2 capture and storage, O_2/N_2 separations with metal−organic frameworks are still relatively new. However, rapid progress has been made in this area, and further work is expected to lead to a large class of O_2 separation materials that operate with high capacity at room temperature.

6. METAL−ORGANIC FRAMEWORK-CONTAINING MEMBRANES

Gas separation using membranes is a kinetics-based process that relies on differences in the diffusion rates of gas molecules within the membrane materials. In addition to the chemical interactions between gas molecules and the surfaces of the

dx.doi.org/10.1021/cr2003272 |Chem. Rev. 2012, 112, 724–781

sorbent, which is the primary determinant of the efficiency of sorption-based separations, the sizes of the gas molecules and the microstructure of the membrane play a crucial role in the separation performance. Membrane-based gas separations have been effectively used in many industrial-scale processes, such as H_2/CO, H_2/CH_4, and H_2/N_2 separations, N_2 separation from air, and natural gas sweetening, and may potentially be applicable for use in CO_2 capture under the scenarios mentioned previously, namely, post-combustion CO_2 capture (CO_2/N_2 separation), pre-combustion CO_2 capture (CO_2/H_2 separation), and oxy-fuel combustion (O_2/N_2 separation). Although membrane-based separations of these pairs of gases have previously been demonstrated, the membranes must be further improved to function effectively under the specific operating conditions required for these CO_2 capture processes. As mentioned in previous sections, the separations are often also complicated by the presence of minor components within the gas mixture. For example, in post-combustion CO_2 capture, the partial pressure of CO_2 within the feed stream is relatively low (~0.15 bar) and the flue gas contains many other components, including H_2O, SO_x, and NO_x. These relatively harsh conditions may limit the opportunity of membrane processes for application in post-combustion CO_2 capture compared with sorption-based separation processes. However, recent work has suggested several membrane process designs for CO_2 separation from flue gas mixtures along with detailed calculations on the energy requirements for each process.[484] An excellent discussion on the desired membrane separation performance is also presented in the work.

The performance of a membrane is usually described by its permeability (or permeance) and selectivity. The permeability, P_i, of gas component i in a given membrane can be calculated by the following expression in gas permeation experiments:

$$P_i = \frac{J_i \times l}{\Delta p_i} \tag{11}$$

where J_i is the molar flux of component i, l is the thickness of the membrane, and Δp_i is the partial pressure difference across the membrane. The selectivity or permselectivity of a gas pair, $\alpha_{i/j}$, which is a measure of separation efficiency, can be expressed as the ratio of gas permeabilities:

$$\alpha_{i/j} = \frac{P_i}{P_j} \tag{12}$$

Note that when membranes have asymmetric structures, the permeance is used more frequently than the permeability:

$$\text{permeance}_i = \frac{J_i}{\Delta p_i} \tag{13}$$

Owing to their well-defined pore structures, the values of these parameters can be higher within crystalline microporous materials compared with polymeric membranes, where the gas transport is governed by a solution-diffusion behavior. Analogously, zeolite membranes with various topologies have demonstrated a significantly enhanced separation performance when compared with polymeric membranes. The high surface area and tunable pore functionalities available in metal−organic frameworks presents an opportunity to further enhance the performance of membrane materials, although their use within membranes is still in a very preliminary stage.[485] In this section, we discuss membranes containing metal−organic frameworks either as a pure film, or as one component within a mixed-matrix membrane. Although our focus will be predominantly on those separations that would be of high importance for reducing CO_2 emissions from power plants, a number of other CO_2 separations, such as CO_2/CH_4 separations, that illustrate the important considerations for the development of next-generation membrane materials for CO_2 capture, will also be discussed as needed.

6.1. Continuous Films of Metal−Organic Frameworks

A growing number of continuous metal−organic framework thin films have been fabricated for applications in a variety of areas, such as supported catalysts, molecular sensors, and gas separation membranes.[486,487] In the context of gas separations, the studies to date have been limited to membranes with low surface areas, although significant advances have been made with regard to the investigation of their gas transport properties and the fabrication methods of these membranes on porous substrates.

Initial efforts on the fabrication of metal−organic framework continuous films have been made on nonporous supports such as uniformly functionalized organic self-assembled monolayers (SAM) and silicon wafers. For example, Fe-MIL-88B crystal layers were grown on a gold substrate functionalized with mercaptohexadecanoic acid by a solvothermal treatment with a synthesis mixture for MIL-53.[488] In fact, two metal−organic frameworks appeared after the reaction; the MIL-53 framework formed in the homogeneous solution, and MIL-88B framework was heterogeneously grown on the substrate. Uniformly distributed organic functional groups on the substrate allowed metal−organic framework crystals to grow in an oriented fashion. In other studies, thin MIL-89[489] and MIL-101[490] layers were deposited on silicon wafers by a dip-coating method using a metal−organic framework nanoparticle colloidal solution. Continuous metal−organic framework films, however, should be fabricated on porous supports if they are to be used as gas separation membranes.

The synthesis of layers of MOF-5 on a porous substrate has been accomplished by microwave heating,[491] wherein a conductive layer such as graphite was deposited on a porous alumina substrate followed by selective and rapid formation of crystals of the metal−organic framework on the coated surface. However, upon close examination of the morphology of the resulting films, it was determined that the metal−organic framework layers were not continuous and were therefore not suitable for applications in gas separations. Nevertheless, continuous films were obtained through the conventional solvothermal method, and the resulting membranes deposited on an alumina support showed Knudsen diffusion behavior (H_2/CO_2 selectivity of 4.7) for all gases studied.[492] Films of MOF-5 were fabricated using the seeded growth method assisted by microwave heating, and these also exhibited gas transport behavior consistent with a Knudsen-type diffusion mechanism.[493] Note that the specific gas transport mechanism observed for a given continuous metal−organic framework film is derived predominantly from the structural features of the framework. Here, the large pore openings and channel dimensions (>10 Å in diameter) within MOF-5 presumably leads to a relatively low contribution of collisions of gas molecules with the pore walls, resulting in a Knudsen-type diffusion mechanism. However, one complicating factor in the analysis was the fact that intercrystalline boundary defects could not be excluded. The presence of such defects can lead to a significant contribution to the overall transport mechanism via

dx.doi.org/10.1021/cr2003272 |Chem. Rev. 2012, 112, 724–781

diffusion of the gas molecules between the individual MOF-5 crystallites within the membrane, although such macroscopic defects were not observed using scanning electron microscopy (SEM).

An HKUST-1 membrane has been fabricated on a copper surface via the hydrothermal method.[494] The resulting membrane exhibited a higher H_2 permeance than conventional zeolite membranes, with selectivity of ~7 for H_2 over CO_2 at 25 °C and 1 bar of feed pressure. This can be attributed to the more rapid diffusion of H_2 through the structure compared with CO_2, which displays a relatively high affinity for the pore surface (particularly the Cu^{2+} sites) due to its greater quadrupole moment and polarizability.

For the foregoing examples, the pore diameters within the metal−organic framework structures are significantly larger than the kinetic diameters of the gas molecules, too large for size exclusion-based gas separation to be realized. However, a number of frameworks with smaller pores have been utilized in membranes to demonstrate size-based separations. For example, a continuous membrane has been fabricated from Cu(hfipbb)-$(H_2hfipbb)_{0.5}$, which exhibits narrow one-dimensional channels with small pore windows (3.5 × 3.2 $Å^2$ in diameter), comparable to those in small-pore zeolites, such as LTA, CHA, and DDR.[495] Here, although continuous films could not be formed directly on bare alumina supports using solvothermal methods, submicrometer-sized crystals of the framework could be anchored to the surface after treatment of the substrate with a polyethyleneimine coating. The membrane was then fabricated by secondary growth from the seeded support and showed good gas selectivity, especially at high temperature (190 °C), with a selectivity of ca. 6 for CO_2 over N_2, and ca. 23 for H_2 over N_2 at 1 bar of feed pressure. However, the observed permeance within the membrane was very low, presumably as a result of the incorrect orientation of the one-dimensional channels of the structure with respect to the membrane.

The gas transport properties of several continuous films of zeolitic imidazolate frameworks (ZIFs), including ZIF-8,[496−498] ZIF-7,[499−501] ZIF-22,[502] and ZIF-90,[503] were recently reported. Initially, films composed of ZIF-8 were fabricated on titania supports through a microwave-assisted solvothermal synthesis.[496] As shown in Figure 33, a well-intergrown layer of ZIF-8 crystals was produced on the top of the support. The successful formation of continuous ZIF-8 layers was also visualized with a sharp transition between Zn and Ti signals in an energy-dispersive X-ray spectroscopy (EDX) map. The gas separation properties of the resultant membranes were investigated for various gases. Surprisingly, despite the pore diameter of 3.4 Å for ZIF-8 falling between the kinetic diameters of CO_2 and CH_4, the membrane showed a very low selectivity for CO_2 over CH_4 (α = 4−5) at 25 °C and 1.1−2 bar. The membrane also showed limited selectivity for CO_2 over N_2, and the selectivity for H_2 over CO_2 of ca. 4.5 is close to the Knudsen selectivity, although the membranes did show a higher H_2 permeance compared with the Cu(hfipbb)$(H_2hfipbb)_{0.5}$ membranes.

Continuous membranes of ZIF-7, which exhibits a pore diameter of approximately 3 Å, were fabricated by seeding of the alumina support with nanocrystals of the framework, followed by microwave-assisted solvothermal growth.[499] Polyethyleneimine was added to the aqueous seed solution not only to stabilize the nanoparticles in the suspension but also to enhance the linkage between the seeds and the support through hydrogen bonding interactions. As shown in Figure 34, a well-intergrown

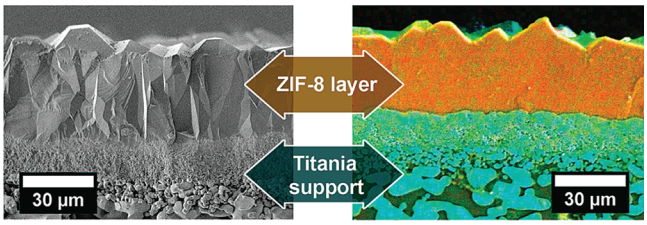

Figure 33. SEM image (left) and corresponding EDX mapping (right) of a cross section of a ZIF-8 membrane. In the EDX map, orange and cyan represent Zn and Ti, respectively, clearly showing the clean formation of the ZIF-8 layer on the titania support. Reproduced with permission from ref 496. Copyright 2009 American Chemical Society.

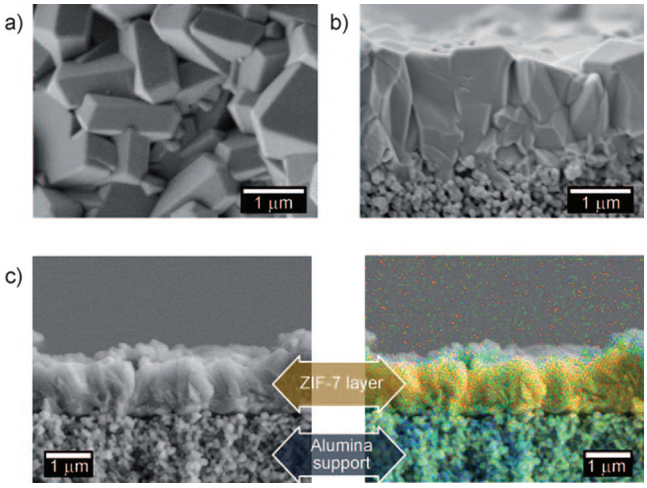

Figure 34. (a) Top down and (b) cross-section SEM images of a ZIF-7 membrane. (c) Cross-section SEM image of the ZIF-7 membrane (left) and the same image overlaid with an EDX mapping (right). In the EDX mapping, orange and cyan represent Zn and Ti, respectively, and the results clearly show the clean formation of the ZIF-7 layer on the alumina support. Reproduced with permission from ref 500. Copyright 2010 Wiley-VCH.

ZIF-7 crystal layer was deposited on the support. Due to the thin nanoseed layer and the short secondary growth time during which microwave heating was performed, a ZIF-7 membrane with a thickness of just 1.5 μm, representing one of the thinnest metal−organic framework-based membranes reported to date, could be readily prepared. This membrane showed relatively modest selectivities of 6.7 (single-component) and 6.5 (mixed-component) for H_2 over CO_2 at 200 °C and 1 bar. Here, it was hypothesized that the permeance of molecules with a diameter greater than the pore diameter, namely, CO_2, N_2, and CH_4, is due to a contribution arising from non-size-selective mass transport through the imperfect sealing of the membrane or through the grain boundaries of the polycrystalline ZIF-7 film. Indeed, in a more detailed gas transport study within ZIF-7 membranes, an improved selectivity for H_2 over CO_2 of 13.6 was observed from an equimolar binary mixture at 220 °C and 1 bar.[501] Significantly, the gas separation performance of the membrane did not deteriorate in the presence of steam, which is an important consideration for applications in post-combustion CO_2 capture.

In a more recent study, membranes of ZIF-22, which possesses the zeolite LTA topology with 3 Å pore windows, were fabricated

dx.doi.org/10.1021/cr2003272 |Chem. Rev. 2012, 112, 724–781

Scheme 2. Surface Modification of Al_2O_3 with 3-Aminopropyltriethoxysilane Moieties, Which Can Then Be Used in Covalently Grafting Imidazolate Functionalities for Anchoring ZIF-90 Crystals onto the Surface[503]

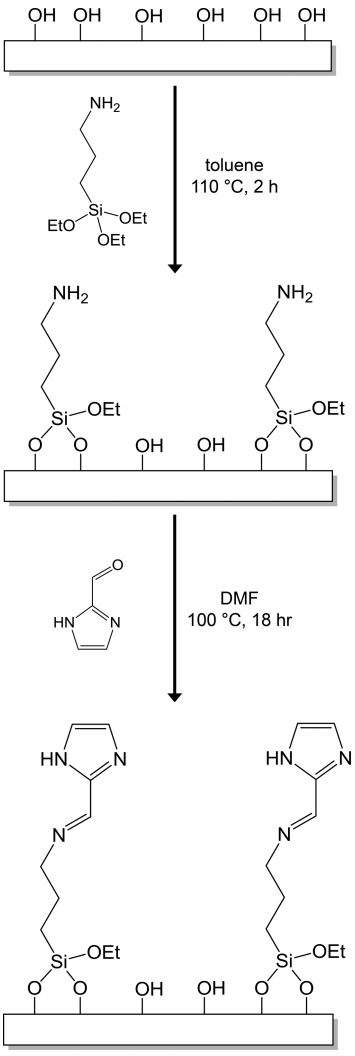

on porous titania supports treated with 3-aminopropyltriethoxysilane (APTES).[502] Here, it was speculated that the 3-aminopropylsilyl groups could coordinate to the exposed Zn^{2+} centers on the surface of the nanocrystals, enabling them to be directly tethered to the substrate surface, where they could then act as seeds for further film growth. However, in a similar case to the ZIF-7 films, the permeation of molecules larger than the pore diameter of 3 Å was large, and the membrane showed only a modest selectivity for H_2 over CO_2 of 7.2 at 50 °C and 0.5 bar. When the feed pressure was increased to 1 bar, the H_2/CO_2 selectivity decreased to 5.1.

Continuous films of ZIF-90, which is isostructural to ZIF-8 but with aldehyde groups on the organic bridging unit, have also been fabricated on an alumina support treated with APTES.[503] In this work, the aldehyde groups within the organic linker were utilized for the covalent anchoring of the framework onto the surface through a reaction with the aminopropyl group installed on the support (see Scheme 2). Subsequent nucleation and film growth of ZIF-90 about these sites resulted in a high-quality membrane displaying selectivity for H_2 over CO_2 of 7.3 at 200 °C and 1 bar. However, permeation of molecules with a kinetic diameter larger than the crystallographic pore size of 3.5 Å led to low selectivities for CO_2 over N_2 and CO_2 over CH_4.

Membranes comprising ZIF materials have also been reported using a variety of other substrate types. For example, a ZIF-8 film was deposited on a tubular porous alumina support seeded with ZIF-8 nanoparticles of ~45 nm diameter.[504] The resulting membrane showed very high CO_2 permeance $[(1.7-2.5) \times 10^{-5}$ mol/m^2·s·Pa$]$ with a selectivity for CO_2 over CH_4 of 4−7 at 22 °C and 1.4 bar.

Another method for ZIF membrane synthesis involves modification of the surface of the support with the organic ligand of the metal−organic framework of interest followed by conventional solvothermal synthesis.[505] Here, it has been found that performing the synthesis at an elevated pH can play a crucial role in forming dense, well-intergrown membranes. In the presence of sodium formate, the imidazole units on the surface of the ZIF crystals are thought to be fully deprotonated due to the increase in pH (see Figure 35), resulting in isotropic growth in all crystal directions to yield large, high-quality crystals. In contrast, at low pH, random crystal branching and growth were observed, presumably as a result of only partial deprotonation of the surface imidazole groups. The permselectivities of the resulting ZIF-8 membranes were 11.6 for H_2 over N_2 and 3.9 for H_2 over CO_2 at 25 °C and 1 bar.

More recently, ZIF-8 films were prepared on a flexible nylon substrate via a contra-diffusion of metal and imidazole linker solutions at room temperature.[506] Here, two reagent solutions were initially separated by a porous nylon sheet within a U-tube, and then, following diffusion of the reagents through the nylon barrier, ZIF-8 crystals formed on both sides of the nylon sheet at the interfaces where the reagents combine. Unfortunately, the resulting membranes exhibited a selectivity for H_2 over N_2 of just 4, suggesting that their quality is relatively low compared with those fabricated using other methods of growth.

Table 11 summarizes the CO_2 separation performance of all of the continuous-film membranes formed from metal−organic frameworks reported to date. Although some membranes exhibit very high gas permeabilities, significant improvements in the selectivities are required if they are to be adapted for use in a viable CO_2 capture process. Significantly, the performance in the context of H_2/CO_2 selectivity is generally just slightly improved over the selectivity that would be expected from a Knudsen-type diffusion mechanism. Furthermore, metal−organic framework membranes capable of performing CO_2/N_2 and O_2/N_2 separations have not yet been reported. However, the numerous examples of high-quality continuous-film membranes formed from zeolites and exhibiting attractive separation performances highlights the crucial need for the development of improved preparative methods for metal−organic framework membranes. In particular, advances in control over the microstructure of the membranes, such as the minimization of intercrystalline grain boundary defects[507,508] and control of the orientation of the crystallites,[507,509] are important for the realization of high-performance membranes for CO_2 capture applications. The formation of high-quality films is also crucial for fully characterizing the performance of metal−organic framework-based membranes.

Efforts to better characterize the intrinsic capabilities of metal−organic frameworks in membrane-based separation processes have also begun to emerge. Recently, the gas transport

dx.doi.org/10.1021/cr2003272 |Chem. Rev. 2012, 112, 724–781

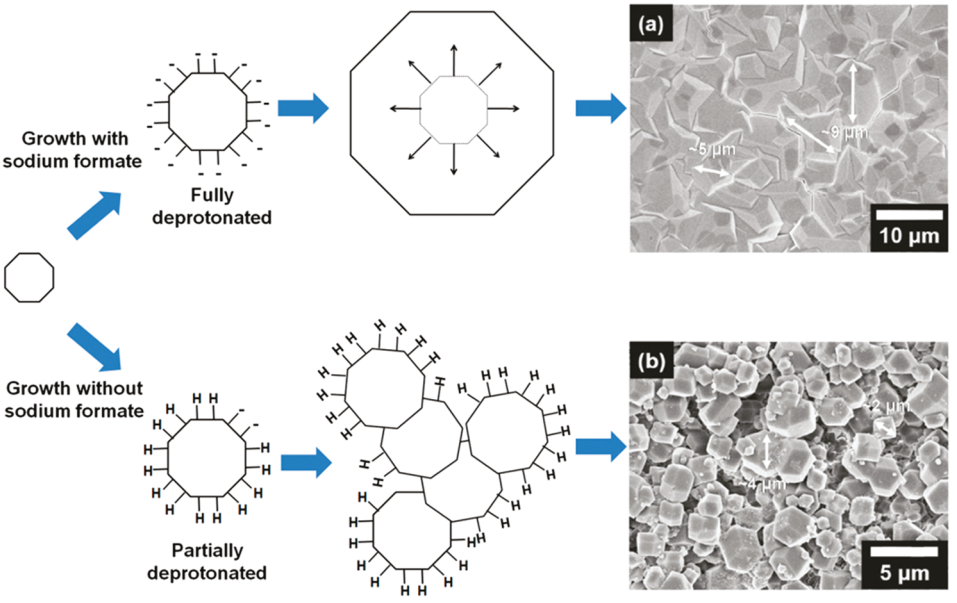

Figure 35. A schematic of the proposed role of sodium formate in promoting the growth of large ZIF-8 particles through complete deprotonation of the surface imidazole functionalities. Top-view SEM images of ZIF-8 films after secondary growth are also shown (a) in the presence of sodium formate and (b) without addition of sodium formate. The larger crystal sizes in panel a result in a more dense membrane, which is essential for good performance in gas separation applications. Reproduced with permission from ref 505. Copyright 2010 American Chemical Society.

Table 11. CO_2 Separation Performance of Metal−Organic Framework Continuous Films

metal−organic framework	gas permeance (mol/m^2·s·Pa)	selectivity	testing conditions	ref
Cu(hfipbb)-(H_2hfipbb)$_{0.5}$	H_2, 2×10^{-8}	H_2/CO_2, ~4	25−190 °C, 1 bar	495
$Cu_3(BTC)_2$	H_2, $(1.0-1.3) \times 10^{-6}$	H_2/CO_2, ~7	25 °C, 1 bar	494
$Zn_4O(BDC)_3$	H_2, 4.7×10^{-6}	H_2/CO_2, 4.7	25 °C, 1 bar	492
SIM-1	H_2, 8×10^{-8}	H_2/CO_2, ~2.5	50 °C, 0.5−3.0 bar	512
ZIF-7	H_2, $(7.5-8.0) \times 10^{-8}$	H_2/CO_2, ~7	200 °C, 1 bar	500
ZIF-7	H_2, 4.5×10^{-8}	H_2/CO_2, 13	220 °C, 1 bar	501
ZIF-8	H_2, 5.1×10^{-8}	H_2/CO_2, 4.5	25 °C, 1.1−2.0 bar	496
ZIF-8	CO_2, $1.7-2.5 \times 10^{-5}$	CO_2/CH_4, 4−7	22 °C, 1.4 bar	504
ZIF-22	H_2, 2.0×10^{-7}	H_2/CO_2, 7.2	50 °C, 0.5 bar	502
ZIF-90	H_2, 2.5×10^{-7}	H_2/CO_2, 7.3	200 °C, 1 bar	503

properties have been measured through a single crystal of $Cu_2(bza)_4(pyz)$ (bza^- = benzoate; pyz = pyrazine), the structure of which exhibits a pore size of about 4 Å.[510] The high dependence of the gas transport properties on the orientation of the metal−organic framework crystal (see Figure 36) illustrates the importance of controlling the growth direction within polycrystalline films. In addition, the gas selectivities observed for this particular single-crystal membrane are greater than for any other metal−organic framework membrane reported to date, with a CO_2/N_2 selectivity of 14, and a CO_2/CH_4 selectivity of 25. Interestingly, CO_2 is more permeable than H_2 in this structure, suggesting an adsorption-selective mechanism rather than a simple diffusion-selective mechanism. Such studies clearly indicate that the gas transport performance of metal−organic framework membranes can indeed be high, but only upon incorporation within high-quality structures.

For the preparation of high-performance membranes, the metal−organic framework should be wisely chosen to suit the target separations. To this end, computational studies on mass transport properties in metal−organic frameworks can be used to predict the performance of the resultant membranes. For

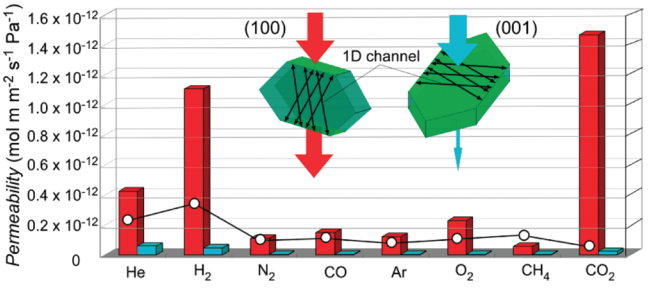

Figure 36. Single-component gas permeabilities of a $Cu_2(bza)_4(pyz)$ single-crystal membrane when the crystal orientation is controlled such that the one-dimensional channels within the structure of the framework are aligned (red) and perpendicular (turquoise) with respect to the direction of the incoming gas flow. Reproduced with permission from ref 510. Copyright 2010 American Chemical Society.

dx.doi.org/10.1021/cr2003272 |*Chem. Rev.* 2012, 112, 724–781

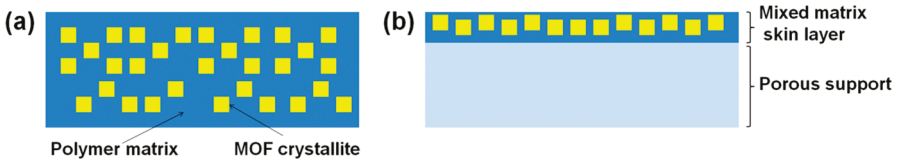

Figure 37. Schematic illustration of mixed-matrix membranes (a) incorporating metal−organic framework crystallites within a dense film and (b) in an asymmetric membrane geometry.

example, a recent study predicted an excellent CO_2 separation performance in a Mg_2(dobdc) membrane.[511] The permselectivity of 200 estimated for a CO_2/H_2 mixture at 27 °C and 10 bar was higher than that of any other metal−organic framework studied, as well as the experimental result for the SAPO-34 membrane, which possesses the zeolite CHA topology with 3.8 Å pore window. The selectivity estimated for the CO_2/N_2 mixture was also higher than 40 in this material. This outstanding performance arises from the chemical and structural properties of Mg_2(dobdc), in which, as discussed in section 3.2.3, a large concentration of open metal sites allows CO_2 to be selectively adsorbed onto the pore channels over other species. Then, in the one-dimensional channels of the framework, CO_2 molecules bound to pore walls can effectively slow the more mobile partner species (H_2 and N_2), resulting in a high CO_2 permselectivity in the mixture. The CO_2 permeance in the Mg_2(dobdc) membrane was also predicted to be much higher than that of the SAPO-34 membrane, owing to its larger pore dimension (11 Å), further emphasizing the outstanding performance of Mg_2(dobdc) and its potential as a membrane material for applications in CO_2 capture.

6.2. Mixed-Matrix Membranes

An alternative approach to the formation of metal−organic framework-based separation membranes is through the incorporation of crystals into a polymeric membrane matrix, as depicted in Figure 37. One key advantage of such "mixed-matrix" membranes is the ability to combine the processability and mechanical stability of polymers with the excellent gas separation properties of crystalline, microporous solids. Zeolite molecular sieves have been most widely employed for this purpose so far, but reports of studies with mixed-matrix membranes containing metal−organic frameworks have also begun to appear.[15] The incorporation of metal−organic frameworks is particularly attractive due to their high surface areas, adjustable pore dimensions, and tunable surface functionality, which might enable the fabrication of membranes exhibiting properties that are optimized for a specific separation. Furthermore, the high processability originating from the polymer phase could allow large-scale fabrication of high-quality membranes for industrial applications using conventional methods. Similar to the continuous metal−organic framework membranes described in section 6.1, their mixed-matrix counterparts are still in the early stages of investigation, and many improvements are required in the selection of materials and development of fabrication methods in order to realize high-performance membranes.

Composite membranes incorporating the three-dimensional metal−organic framework $Cu_2(PF_6)(NO_3)(bpy)_4 \cdot 2PF_6 \cdot 2H_2O$ confined within an amorphous glassy polysulfone polymer have been investigated.[513] The very narrow channels within this framework structure, measuring 4×3 Å^2 in the crystallographic *b*-direction and 3×3 Å^2 in the *c*-direction, should be suitable for applications in size-exclusion based gas separations. The gas permeability measured at 35 °C and 1 bar was found to decrease slightly as a function of the amount of metal−organic framework loaded within the polymer matrix, although membranes containing 5 wt % of the framework did show an enhanced selectivity of ca. 200 for H_2 over CH_4 versus ca. 50 for the pure polymeric membrane. Unfortunately, the CO_2 transport properties of this system were not reported.

Mixed-matrix membranes have also been studied with varying amounts of HKUST-1 incorporated within two different polymers: a rubbery polydimethylsiloxane (PDMS) and a glassy polysulfone.[514] The polysulfone membrane showed a gradual increase in CO_2 permeability with increasing HKUST-1 loading, up to 10 wt %. Membranes containing 5 wt % of HKUST-1 exhibited further enhanced selectivity of ca. 25 for CO_2 over N_2, as compared with ca. 20 for pure polysulfone membranes. The selectivity dropped significantly when the framework loading was increased to 10 wt %. Meanwhile, a 10 wt % HKUST-1/PDMS membrane showed a substantial enhancement in CO_2 permeability from 2500 to 3000 barrers, with a modest increase in the selectivity from 8.2 to 8.8. Here, again, the performance was not improved when the metal−organic framework loading was further increased.[514]

Mixed-matrix membranes containing $CuSiF_6(bpy)_2$ and MOF-5 within a commercial polyimide (Matrimid) have been fabricated and tested.[515] Gas permeation measurements performed at 35 °C and 2 bar revealed that incorporating the copper-based framework, which exhibits a structure with 8 Å pore windows, within the polymer increased the CO_2 permeability but decreased the selectivity for CO_2 over N_2. In contrast, the selectivity for CH_4 over N_2 was enhanced. This can be rationalized on the basis that the framework has a high affinity for CH_4, presumably due to its large surface area and relatively large pore windows. The Matrimid membranes incorporating MOF-5 showed increased CO_2 permeability with a modest increase or no change in gas selectivity, according to pure gas permeation tests conducted at 35 °C and 2 bar.[516] As the best example, in a membrane containing 30 wt % MOF-5, the CO_2 permeability was almost doubled with a 10% increase in the selectivity for CO_2 over N_2 compared with the pure polymer membrane. Disappointingly, the mixed gas permeation tests for this membrane formulation revealed H_2/CO_2 and CO_2/CH_4 selectivities lower than the corresponding values of the pure polymeric membrane.

One of the major challenges for mixed-matrix membrane studies is the issue of nonideality at the interface between the dispersed microporous crystals phase and the polymer matrix, particularly when glassy polymers are employed. To overcome this problem, a mixed-matrix membrane based on a low-T_g (glass transition temperature) polymer, polyvinylacetate (PVAc) was fabricated in an attempt to achieve a defect-free morphology.[517] Mixed-matrix membranes containing

dx.doi.org/10.1021/cr2003272 |*Chem. Rev.* 2012, 112, 724–781

Cu(BDC) showed enhanced separation performance compared with the pure PVAc membrane when tested at 35 °C and 4.5 bar. Membranes containing 15 wt % of Cu(BDC) exhibited a 34% increase in the CO_2 permeability and a 10% increase in the selectivity for CO_2 over N_2. This rather modest gas separation enhancement can be attributed to both a molecular sieving effect from the relatively small pores of the framework (5.2 Å pore windows) and improved adhesion between the metal−organic framework and polymer phases.

A number of ZIF-based mixed-matrix membranes have also been reported. In particular, the CO_2 transport properties of ZIF-8/polysulfone mixed-matrix membranes have been investigated via gas permeation measurements and pulsed-field gradient NMR techniques.[518] The CO_2 self-diffusion coefficient measured by NMR spectroscopy at 25 °C increased with ZIF-8 content, from 2.1×10^{-8} cm^2/s for pristine membranes to 9.3×10^{-8} cm^2/s for membranes containing 30 wt % ZIF-8. Gas permeation tests confirmed the significantly improved CO_2 permeability for the mixed-matrix membrane. Detailed analysis further revealed that the ZIF-8 particles also contribute greatly to the CO_2 permeation by increasing the gas solubility within the composite membranes. Additionally, ZIF-8/Matrimid mixed-matrix membranes were tested with various single-component and mixed gases at 35 °C and 2.7 bar.[519] Gas permeability increased with the loading of ZIF-8 up to a level of 40 wt %. Noticeable increases in selectivities, as evaluated from both single-component and mixed gas permeation, were observed at a loading level of 50 wt % for gas pairs including small molecules, such as H_2/CH_4, CO_2/CH_4, H_2/C_3H_8, and CO_2/C_3H_8, suggesting that the ZIF-8 phase may act as a molecular sieve for smaller gas molecules.

Membranes comprising ZIF-90 dispersed within various polyimides have also been investigated.[520] As shown in Figure 38, the ZIF-90 crystals were evenly distributed within the polymer matrix and interfacial voids were not observed by SEM. Gas permeation tests revealed that when less permeable polymers such as Ultem and Matrimid were used as the matrix, the membrane displayed an increase in the CO_2 permeability with no change in the selectivity for CO_2 over CH_4. However, an enhancement in both permeability and selectivity was observed when a highly permeable polyimide 6FDA−DAM (6FDA = 2,2-bis(3,4-carboxyphenyl)hexafluoropropane dianhydride, DAM = diaminomesitylene) was employed as the matrix. This result highlights the importance of a careful selection of both the polymer and metal−organic framework phases based on gas permeabilities, such that the performance of the resulting mixed-matrix membrane is optimized for a given separation. Indeed, one of the most promising membranes displayed excellent performance for post-combustion CO_2 capture; exhibiting a CO_2 permeability of ca. 700 barrers with a selectivity for CO_2 over N_2 of 22 at 25 °C and 2 bar.

Most recently, in order to improve the CO_2 separation performance of polymeric membrane, an amino-functionalized metal−organic framework, NH_2-MIL-53, was incorporated into polysulfone.[439] Presumably due to the hydrogen bonding interactions between the amine functionalities within the metal−organic framework crystal and the sulfone groups of the polymer, high NH_2-MIL-53 loadings of up to 40 wt % were achieved. However, the best CO_2/CH_4 separation performance was observed in 25 wt % NH_2-MIL-53 loaded membranes. In the gas permeation study at 35 °C and 3 bar, although there was no significant improvement in CO_2 permeability,

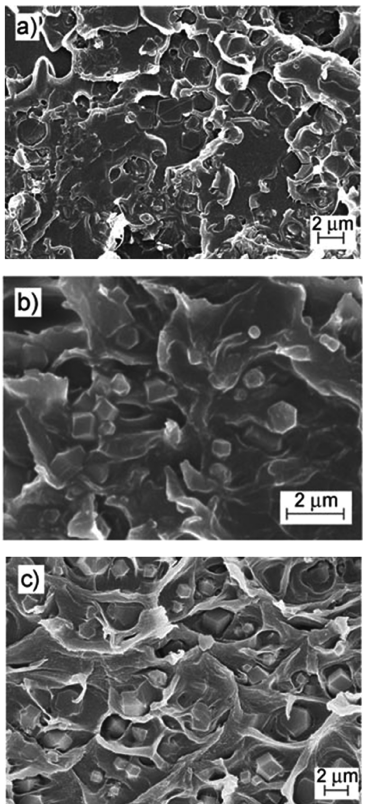

Figure 38. SEM images of cross-sections of mixed-matrix membranes incorporating ZIF-90 within (a) Ultem, (b) Matrimid, and (c) 6FDA−DAM. Reproduced with permission from ref 520. Copyright 2010 Wiley-VCH.

CO_2/CH_4 selectivity was almost doubled in the mixed-matrix membranes as compared with pure polysulfone membranes. Even higher selectivity (ca. 110) was observed at −10 °C and 10 bar, although the CO_2 permeability decreased significantly.

The aforementioned mixed-matrix membranes were all measured in a dense film form to investigate their intrinsic gas transport properties. However, such membranes should ideally be fabricated in an asymmetric form in which a thin active surface layer is supported by a porous sublayer to minimize the mass transport resistance (see Figure 37b). Only a very limited number of studies investigating the gas separation performance of asymmetric mixed-matrix membranes containing metal−organic frameworks have been reported to date. Asymmetric HKUST-1/Matrimid mixed-matrix membranes have been fabricated via the phase inversion method.[521] Here, to seal the defects within the membrane, the metal−organic framework/polymer thin surface layer was coated with the highly permeable polymer PDMS. The resultant membrane showed a substantial increase in CO_2 permeance with modest enhancement in the selectivity for CO_2 over N_2 compared with pure Matrimid membranes. Asymmetric membranes with HKUST-1 crystallites embedded within a polyimide matrix have been prepared in a hollow fiber form, a capillary geometry with a small diameter.[522] These displayed an enhancement in both the H_2 permeability and selectivity for H_2 over CO_2, although the CO_2/N_2 separation performance was not improved by incorporating the metal−organic framework into the polymer.

dx.doi.org/10.1021/cr2003272 |*Chem. Rev.* 2012, 112, 724–781

Table 12. CO_2 Separation Performance of Metal−Organic Framework Mixed-Matrix Membranes

MOF and polymer	gas permeability (barrers)[a]	selectivity	testing conditions	ref
Cu(BDC), PVAc	CO_2, 3.3	CO_2/N_2, 35	35 °C, 4.5 bar	517
HKUST-1, PDMS	CO_2, 3000	CO_2/N_2, 9	not reported	514
HKUST-1, polysulfone	CO_2, 6−8	CO_2/N_2, 25	not reported	514
$CuSiF_6(bpy)_2$, Matrimid	H_2, 17−26	H_2/CO_2, 2	35 °C, 2 bar	515
	CO_2 8−15	CO_2/N_2, 30−33		
MOF-5, Matrimid	H_2, 30−54	H_2/CO_2, 2−3,	35 °C, 2 bar	516
	CO_2, 11−20	CO_2/N_2, 35−40		
ZIF-8, Matrimid	H_2, 29−71	H_2/CO_2, 3−4	35 °C, 2.7 bar	519
	CO_2, 9−24	CO_2/N_2, 23−30		
ZIF-90, 6FDA-DAM	CO_2, 600−800	CO_2/N_2, 22	25 °C, 2 bar	520
		CO_2/CH_4, 37		
HKUST-1, Matrimid[b]	CO_2, 12−18 GPU[c]	CO_2/N_2, 23−27	35 °C, 10 bar	521
HKUST-1, polyimide[b]	H_2, 876 GPU	H_2/CO_2, 10	25 °C, 2 bar	522
	CO_2, 88 GPU	CO_2/N_2, 9		

[a] 1 barrer = 3.348×10^{-16} mol·m/(m^2·s·pa). [b] Asymmetric membranes. [c] Gas permeation unit, 10^{-6} cm^3(STP)/(cm^2·s·cm Hg).

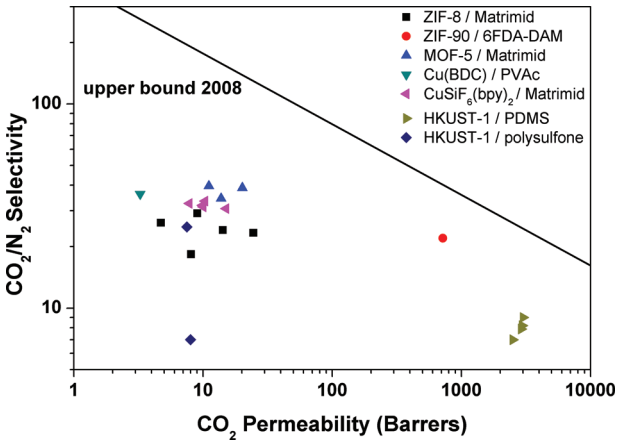

Figure 39. CO_2/N_2 separation performance of metal−organic framework mixed-matrix membranes. The solid line represents the upper bound of polymeric membranes, as determined in 2008.[524] ZIF-8/Matrimid from ref 519; ZIF-90/6FDA-DAM from ref 520; MOF-5/Matrimid from ref 516; Cu(BDC)/PVAc from ref 517; $CuSiF_6(bpy)_2$/Matrimid from ref 515; HKUST-1/PDMS from ref 514; HKUST-1/polysulfone from ref 514.

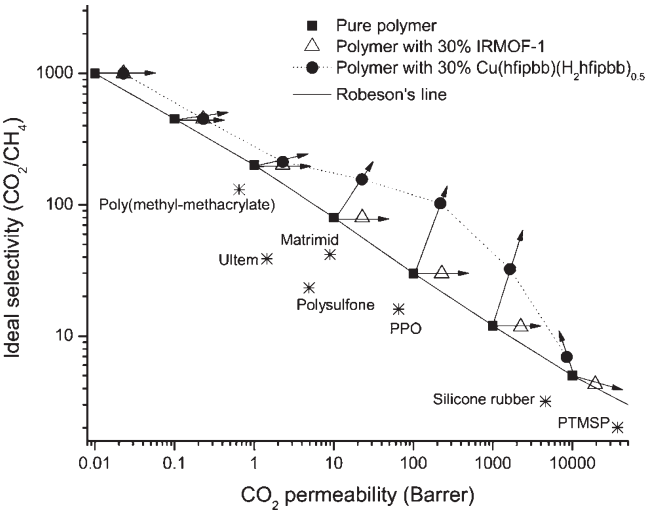

Figure 40. Predicted CO_2/CH_4 separation performance of hypothetical mixed-matrix membranes. Squares represent hypothetical pure polymer membranes on the upper bound limit (Robeson line). Triangles and circles show the predictions for a mixed-matrix membrane with a 30% volume fraction of IRMOF-1 (MOF-5) and Cu(hfipbb)-(H_2hfipbb)$_{0.5}$, respectively. The performance of several well-known polymer membranes are also shown. Reproduced with permission from ref 523. Copyright 2010 The Royal Society of Chemistry.

The CO_2 separation performance of metal−organic framework-based mixed-matrix membranes is summarized in Table 12. Due to the properties of the polymer matrix, these membranes generally exhibit enhanced gas selectivity compared with the pure metal−organic framework films, especially in the case of CO_2/N_2 separations. Figure 39 shows the CO_2/N_2 separation performance of the mixed-matrix membranes reported to date. Although many membranes exhibit enhanced characteristics compared with pristine polymers, no metal−organic framework mixed-matrix membrane in which the performance exceeds that of the best polymers has been demonstrated to date. As mentioned above, the preparation of high-performance membranes relies on the careful selection of both the polymer and the metal−organic framework phases.[520,523] This is also highlighted in a computational study on metal−organic framework mixed-matrix membranes.[523]

As shown in Figure 40, CO_2/CH_4 selectivity cannot be improved compared with pristine polymers when MOF-5, possessing much larger pores than the kinetic diameters of both CO_2 and CH_4, is incorporated into the polymer matrix. In contrast, mixed-matrix membranes comprised of a small-pore metal−organic frameworks, such as Cu(hfipbb)(H_2hfipbb)$_{0.5}$, can show higher gas separation performance than pure polymeric membranes. The properties of the resulting mixed-matrix membranes can also be tuned depending on the selection of the polymer. In particular, when the gas permeabilities of both phases are well-matched, the enhancement in gas separation performance can be maximized. In addition, a high degree of control over the interfacial morphology between the metal−organic

dx.doi.org/10.1021/cr2003272 |Chem. Rev. 2012, 112, 724–781

framework and the polymer is also a prerequisite for the fabrication of high-performance mixed-matrix membranes. Many efforts have been made to obtain improved morphologies, including particle/polymer adhesion and the uniform distribution of particles. The methodologies developed for zeolites or other molecular sieves do not necessarily apply to metal−organic frameworks, but it is likely that new and improved fabrication techniques customized specifically for these materials will soon afford membranes with enhanced gas separation properties.

7. CONCLUDING REMARKS AND OUTLOOK

The foregoing sections have described the recent progress made in the investigation of metal−organic frameworks as potential new solid adsorbents to be used within CO_2 capture systems. Indeed, tremendous CO_2 adsorption capacities have been demonstrated in the highest surface area materials, and high adsorptive selectivities have also begun to emerge in materials furnished with functionalized surfaces. With regard to the prospects of creating new materials suitable for real-world applications, the high degree of control over the structural and chemical features of metal−organic frameworks is particularly promising for optimization of their properties, not only for the type of CO_2 capture to be performed but also for the specific composition of the flue gas of a particular power plant. Such a precise tuning of the material characteristics is expected to result in considerable improvements in the sorbent performance, leading to reduced energy requirements for the capture process compared with current technologies. In this section, we briefly outline the main issues that need to be addressed in order to achieve next-generation materials capable of fulfilling the criteria required for the gas separations relevant to post-combustion CO_2 capture, pre-combustion CO_2 capture, and oxy-fuel combustion.

In the area of post-combustion CO_2 capture, the primary need is for more chemically and thermally robust materials capable of withstanding the high levels of water present in the flue gas stream, while also tuning the temperature required for regeneration. Increasing the strength of the metal−ligand bonds through the incorporation of high-valent metal cations (e.g., Al^{3+} and Ti^{4+}) or more strongly binding organic ligands (e.g., pyrazolates and triazolates) is one approach by which this may be achieved. Furthermore, although most of the adsorption studies to date have evaluated the performance of materials through single-component CO_2 and N_2 adsorption isotherms or breakthrough experiments using a CO_2/N_2 mixed gas, the impact of the presence of water and other minor components in the flue gas is an aspect where a greater understanding is urgently needed. In addition to affecting the separation performance, the impurity components (O_2, CO, SO_x, NO_x) may have significant consequences in terms of the long-term stability of the materials, as well as the energy requirements for regeneration. Thus, the study of metal−organic frameworks under conditions that simulate realistic working conditions (gas composition, temperature, and pressure) is essential for fully evaluating the performance of a given material.

For pre-combustion CO_2 capture, metal−organic frameworks have recently been demonstrated to show enhanced CO_2/H_2 selectivities and working capacities over conventional materials, such as activated carbons and zeolites. Although only a small number of compounds have been experimentally studied to date, a significant body of theoretical work examining this separation in metal−organic frameworks now has emerged. Nevertheless, there remains a need for a broader range of frameworks to be examined in order to identify the materials that provide the best properties for application in a real-world capture process. Similar to post-combustion capture, there is a need for the effect of the minor components of the flue gas (predominantly CO and CH_4) to be fully elucidated, although these trace impurities are not expected to significantly interfere with the performance of the materials owing to their relatively weak interactions with the surfaces of metal−organic frameworks. Moreover, the practical aspects of employing a pressure swing adsorption process, such as the desorption of CO_2 by purge, have not yet been investigated in detail. More thorough investigations of the complete process under the conditions relevant for pre-combustion CO_2 will allow the prospects of employing these materials in an industrial setting to be more accurately evaluated.

Oxy-fuel combustion has emerged as an application in which the chemical tunability of metal−organic frameworks may allow high-performance materials to be prepared. The ability of the exposed electron-donating metal centers within Fe_2(dobdc) to bind O_2 preferentially via charge transfer interactions has led to a high O_2/N_2 selectivity, but the low temperatures at which the binding can be reversed is a significant drawback of the material. At room temperature, the O_2 adsorption is irreversible owing to a two-electron transfer process and the concomitant formation of a peroxide (O_2^{2-}) species bound to the metal centers. An enhanced control over the electronic properties of the exposed metal cation sites would allow the electron transfer to be limited to a one-electron process, which has been shown to permit the reversible binding of O_2 at high capacity. The generation of new metal−organic frameworks bearing exposed redox-active metals (such as Cr^{2+}, Mn^{2+}, Fe^{2+}, Co^{2+}, or Cu^{+}) and the fine-tuning of the electron density available at these adsorption sites through substitution of the organic backbone of the materials are expected to afford new materials that reversibly bind O_2 near ambient temperatures with high selectivity and working capacity.

The large-scale implementation of metal−organic frameworks for CO_2 capture will also inevitably require the consideration of a number of other aspects in addition to the adsorptive properties of the materials. The performance of the materials should be evaluated in the context of engineering process models that take performance parameters, such as the working capacity and selectivity, as input to allow optimized working conditions to be developed for each adsorbent. Life-cycle analyses should be performed in order to ascertain the feasibility of bulk preparations of the most promising metal−organic frameworks, taking into account the many practical considerations for large-scale synthesis, including the supply chain of the precursor materials, cost, environmental impact of waste products, and recycling following use of the adsorbent. Before such detailed analyses are performed, however, the synthetic challenge of preparing robust new materials that are truly well-suited to each capture scenario must be addressed. Owing to the large number of possible metal−organic framework structures that can be assembled, the use of computational and theoretical approaches may assist the synthetic efforts by identifying new target materials predicted to display the appropriate properties. The tremendous progress already made in improving the properties of metal−organic frameworks is indeed promising for real-world applications, and we remain optimistic that materials capable of serving as next-generation CO_2 capture

dx.doi.org/10.1021/cr2003272 |Chem. Rev. 2012, 112, 724–781

adsorbents will be discovered through continued investigations in the field.

AUTHOR INFORMATION

Corresponding Author
*E-mail: jrlong@berkeley.edu.

Author Contributions
†These authors contributed equally to this work.

BIOGRAPHIES

Kenji Sumida was born in 1982 in New Zealand and obtained his B.Sc. in Computer Science in 2002 and his M.Sc. degree in Chemistry in 2007 at the University of Auckland under the supervision of Prof. Penny J. Brothers. He joined Jeffrey Long's research group at the University of California, Berkeley, in 2007, where his work focuses on the development of high-throughput methodologies for the discovery of novel metal−organic frameworks for gas storage and molecular separation applications.

David L. Rogow was born in 1976 in Las Vegas, Nevada. He received his B.S. (2005) in Chemistry at Portland State University, Portland, Oregon, and earned his Ph.D. (2010) at the University of California, Santa Cruz, in Chemistry and Biochemistry under the supervision of Prof. Scott R. J. Oliver. He is currently a postdoctoral fellow (NSF) in Jeffrey Long's research group at the University of California, Berkeley. His research focuses on the synthesis of functionalized metal−organic frameworks for carbon dioxide capture.

Jarad A. Mason was born in 1987 in North Carolina. He received his B.A. (2009) and M.S. (2009) in Chemistry at the University of Pennsylvania, where he studied polymeric precursors to ultra-high-temperature ceramics under the supervision of Prof. Larry G. Sneddon. He is currently a graduate student in Jeffrey Long's research group at the University of California, Berkeley. His research focuses on the synthesis of highly robust metal−organic frameworks for gas storage and separation applications.

Thomas M. McDonald was born and raised in Denver, Colorado. In 2007, he received a B.A. in Chemistry from Northwestern University, where he worked under the guidance of Prof. Teri Odom and Prof. Ken Poeppelmeier. He joined the research laboratory of Jeffrey Long in 2008 and is currently researching novel porous materials for gas separations and storage.

Eric D. Bloch was born in 1983 in Wisconsin. He received his B.S. (2008) in Chemistry at the University of Wisconsin—Milwaukee and is currently a graduate student in Jeffrey Long's research group at the

University of California, Berkeley. His research focuses on the synthesis of metal−organic frameworks containing redox-active metal centers for gas separation applications.

Zoey R. Herm was born in 1984 in Chicago, Illinois. She received her B.A. (2007) in Chemistry at Macalester College in St. Paul, Minnesota, where she studied group VI organometallic carbonyl complexes under the supervision of Prof. Paul J. Fischer. She is currently a Ph.D. student in Jeffrey Long's research group at the University of California, Berkeley. Her research focuses on precombustion carbon dioxide capture in metal−organic frameworks.

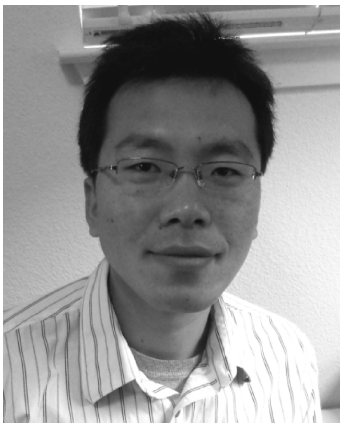

Tae-Hyun Bae was born in 1977 in South Korea and received his B.S. (1999), M.S. (2001), and Ph.D. (2006) degrees in natural fiber science at Seoul National University. He earned his second Ph.D. (2010) in chemical engineering at Georgia Institute of Technology under the supervision of Prof. Christopher W. Jones and Prof. Sankar Nair. Currently, he is a postdoctoral fellow in Jeffrey Long's research group, where he is working on CO_2 separation with metal−organic frameworks.

Jeffrey R. Long was born in Rolla, Missouri, USA, in 1969. He received his B.S. in Chemistry from Cornell University in 1991 and Ph.D. in Chemistry at Harvard University in 1995. Following postdoctoral work at Harvard and the University of California, Berkeley, he joined the faculty at Berkeley in 1997, where he is currently Professor of Chemistry. He is also a Faculty Senior Scientist in the Materials Sciences Division of Lawrence Berkeley National Laboratory. His research involves the synthesis of new inorganic clusters and solids, with emphasis on magnetic and microporous materials.

ACKNOWLEDGMENT

This research was funded through the Center for Gas Separations Relevant to Clean Energy Technologies, an Energy Frontier Research Center funded by the U.S. Department of Energy, Office of Science, Office of Basic Energy Sciences, under Award No. DE-SC0001015. We thank Fulbright New Zealand for partial support of K.S., the NSF ACC-F Award No. 1042021 for support of D.L.R., and NSF for fellowship support of J.A.M.

LIST OF ABBREVIATIONS

abtc	3,3′,5,5′-azobenzenetetracarboxylate
ACMP	acetylene-mediated conjugated microporous polymers
ADA	adamantanediacetate
ADC	4,4′-azobenzenedicarboxylate
ade	adenine
almeIm	4-methylimidazole-5-carbaldehyde
AZPY	4,4′-azo(bis)pyridine
atz	3-amino-1,2,4-triazole
BBC	4,4′,4″-(benzene-1,3,5-triyl-tris(benzene-4,1-diyl))-tribenzoate
bbIm	5-bromobenzimidazole
BBPDC	4′-*tert*-butyl-biphenyl-3,5-dicarboxylate
bcphfp	2,2′-bis(4-carboxyphenyl)hexafluoropropane
BDC	1,4-benzenedicarboxylate
bdcppi	*N*,*N*′-bis(3,5-dicarboxyphenyl)pyromellitic diimide
bdi	5,5′-(buta-1,3-diyne-1,4-diyl)diisophthalate
BDoborDC	1,4-bis(1,12-dicarbonyl-*closo*-dodecaborane)-benzene
benzDHP	1,4-benzenedihydrogenphosphonate
benzTB	*N*,*N*,*N*′,*N*′-benzidinetetrabenzoate
bIm	benzimidazole
BME-bdc	2,5-bis(2-methoxyethoxy)benzene-1,4-dicarboxylate
BPDC	biphenyl-4,4′-dicarboxylate
bpe	1,2-bis(4-pyridyl)ethane
bpee	1,2-bis(4-pyridyl)ethylene
bpetha	1,2-bis(4-pyridyl)ethane
BPnDC	benzophenone-4,4′-dicarboxylic acid
bpp	1,3-bis(4-pyridyl)propane
bpta	3,6-di(4-pyridyl)-1,2,4,5-tetrazine
bptb	2,2′-biphenol-3,3′,5,5′-tetrakis(4-benzoate)
BPTC	3,3′,5,5′-biphenyltetracarboxylic acid
bpy	4,4′-bipyridine
bpydc	2,2′-bipyridine-5,5′-dicarboxylate
BTB	4,4′,4″-benzene-1,3,5-triyl-tribenzoate
BTC	1,3,5-benzenetriscarboxylate
btdc	2,2′-bithiophene-5,5′-dicarboxylate
BTE	4,4′,4″-(benzene-1,3,5-triyl-tris(ethyne-2,1-diyl))-tribenzoate
btei	5,5′,5″-benzene-1,3,5-triyltris(1-ethynyl-2-isophthalate)
BTetB	4,4′,4″,4‴-benzene-1,2,4,5-tetrayltetrabenzoic acid

dx.doi.org/10.1021/cr2003272 |*Chem. Rev.* 2012, 112, 724–781

BTP	1,3,5-tris(1*H*-pyrazol-4-yl)benzene
bttb	4,4′,4″,4‴-benzene-1,2,4,5-tetrayl-tetrabenzoate
cbIm	5-chlorobenzimidazole
CDC	1,12-dihydroxydicarbonyl-1,12-dicarba-*closo*-dodecaborane
CEbnbpy	(*R*)-6,6′-dichloro-2,2′-diethoxy-1,1′-binaphthyl-4,4′bipyridine
cis-chdc	1,4-cyclohexanedicarboxylate
CNBPDC	2,2′-dicyano-4,4′-biphenyldicarboxylic acid
CNC	4-carboxycinnamate
cnIm	4-cyanoimidazole
CNT	carbon nanotubes
CPI	5-(4-carboxy-phenoxy)isophthalate
CPOM	[(4-carboxyphenyl)oxamethyl]methanoate
cyamIm	4-aminoimidazole-5-carbonitrile
DABCO	triethylenediamine (1,4-diazabicyclo[2.2.2]octane)
DBM	dibenzoylmethanato
DBNBVP	(*S*)-2,2′-diethoxy-1,1′-binaphthyl-6,6′-bis-(4-vinylpyridine)
DBS	4,4′-dibenzoate-2,2′-sulfone
dcIm	4,5-dichloroimidazole
dhbc	2,5-dihydroxybenzoate
dhbpc	4,4′-dihydroxybiphenyl-3-carboxylate
DHT	dihydroxyterephthalic acid
diazBDC	5,5′-(1*E*)-1,2-diazinediylbis(1,3-benzendicarboxylate)
DCTP	3,3″-dicarboxy-1,1′:4′,1″-terphenyl
dImb	1,4-di(1*H*-imidazol-4-yl)benzene
diPyNI	*N*,*N*′-di-(4-pyridyl)-1,4,5,8-naphthal-enetetracarboxy-diimide
DMA	*N*,*N*′-dimethylacetamide
dobdc	2,5-dioxido-1,4-benzenedicarboxylate
doborDC	1,12-dihydroxy-carbonyl-1,12-dicarba-*closo*-dodecaborane
dpa	1,1′-biphenyl-2,2′-dicarboxylate
dpe	1,2-di(4-pyridyl)ethylene
DPG	*meso*-1,2-bis(4-pyridyl)-1,2-ethanediol
DPNI	*N*,*N*′-di-(4-pyridyl)-1,4,5,8-naphthalenetetracarboxy-diimide
dpntcd	*N*,*N*-di(4-pyridyl)-1,4,5,8-naphthalenetetracarboxy-diimide
DPT	3,6-di-4-pyridyl-1,2,4,5-tetrazine
dpt24	3-(2-pyridyl)-5-(4-pyridyl)-1,2,4-triazolate
DSbpyDO	4,4′-disulfo-2,2′-bipyridine-*N*,*N*′-dioxide
dtp	2,3-di-1*H*-tetrazol-5-yl-pyrazine
EBTC	1,1′-ethynebenzene-3,3′,5,5′-tetracarboxylate
eIm	2-ethylimidazole
ELM	elastic layer-structured MOF
etz	2,5-diethyl-1,2,4-triazole
FMA	fumarate
F-pymo	5-fluoropyrimidin-2-olate
Gly-Ala	glycylalanine
hymeIm	4-hydroxymethyl-5-methylimidazole
H_4abtc	1,1′-azobenzene-3,3′,5,5′-tetracarboxylic acid
H_4bdi	5,5′-(buta-1,3-diyne-1,4-diyl)diisophthalic acid
H_3BPT	biphenyl-3,4′,5-tricarboxylate
H_2bpydc	2,2′-bipyridine-5,5′-dicarboxylic acid
H_2BPDC	4,4′-biphenyldicarboxylic acid
H_4DHBP	1,4-dihydroxy-2,5-benzenediphosphonic acid
H_2fipbb	4,4′-(hexafluoroisopropylidene)-bis(benzoic acid)
H_3idc	4,5-imidazoledicarboxylic acid
H_4MTB	methanetetrabenzoic acid
H_2obb	4,4′-oxybis(benzoic acid)
Hoxonic	4,6-dihydroxy-1,2,3-triazine-2-carboxylic acid
H_2ppt	3-(2-phenol)-5-(4-pyridyl)-1,2,4-triazole
H_3pzdc	3,5-pyrazoledicarboxylic acid
IBPDC	dimethyl-2,2′-diiodo-4,4′-biphenyldicarboxylate
IDC	2-methylimidazolate-4-amide-5-imidate
Im	imidazole
IN	isonicotinate
MAF	metal azolate framework
MAMS	mesh-adjustable molecular sieves
mbIm	5-methylbenzimidazole
mdpt24	3-(3-methyl-2-pyridyl)-5-(4-pyridyl)-1,2,4-triazolate
Me_4bpz	3,3′,5,5′-tetramethyl-4,4′-bis(pyrazolate)
mIm	2-methylimidazole
m-TATB	3,3′,3″-*s*-triazine-2,4,6-triyltribenzoate
nbIm	5-nitrobenzimidazole
NDC	2,6-naphthalenedicarboxylate
ndc	naphthalene-2,6-dicarboxylic acid
nIm	2-nitroimidazole
NTC	naphthalene-1,4,5,8-tetracarboxylate
ntei	5,5′,5″-(4,4′,4″-nitrilotris(benzene-4,1-diyl)-tris(ethyne-2,1-diyl))triisophthalate
pba	4-(pyridin-4-yl)benzoate
pbmp	*N*,*N*-piperazinebismethylenephosphonate
p-CDC	1,12-dihydroxycarbonyl-1,12-dicarba-*closo*-dodecaborane
PCN	porous coordination network
PDA	phenylenediacetate
pdc	3,5-pyridinedicarboxylate
PDC	pyrenedicarboxylic acid
pegBTB	2,2′-penta(ethylene glycol)biphenyl-3,3′,5,5′-tetrakis-(4-benzoate)
phen	1,10-phenanthroline
pmc	pyrimidine-5-carboxylate
pmdc	pyrimidine-4,6-dicarboxylate
ptei	5,5′-((5′-(4-((3,5-dicarboxyphenyl)ethynyl)phenyl)-[1,1′:3′,1″-terphenyl]-4,4″-diyl)-bis(ethyne-2,1-diyl))diisophthalate
Pur	purine
py	pyridine
pydc	3,5-pyridinedicarboxylate
pymo	pyrimidinolate
pyrdc	pyridine-2,3-dicarboxylate
pyz	pyrazine
pzdc	2,3-pyrazinedicarboxylate
SCA	sulfonatocalix[4]arene
TATB	4,4′,4″-s-triazine-2,4,6-triyl-tribenzoate
TBA	tetrabutylammonium
TCEPEB	1,3,5-tris[(1,3-carboxylic acid-5-(4-ethynyl)phenyl))-ethynyl]benzene
TCM	tetrakis[4-(carboxyphenyl)-oxamethyl]methane
TCMO	tetrakis[4-(carboxyphenyl)-oxamethyl]methanoate
TCPB	1,2,4,5-tetrakis(4-carboxyphenyl)benzene
TCPBDA	*N*,*N*,*N*′,*N*′-tetrakis(4-carboxyphenyl)-biphenyl-4,-4′-diamine
TDCPTM	4,4′,4″,4‴-tetrakis[3,5-di(carboxylate)-1-phenyl]-tetraphenyl methane
TEA	tetraethylammonium
TED	triethylenediamine
tImb	1,3,5-tris(1*H*-imidazol-4-yl)benzene
TMA	tetramethylammonium
Tp	hydrotris(pyrazolyl)borate
TPBTM	*N*,*N*′,*N*″-tris(isophthalyl)-1,3,5-benzenetricarboxamide

dx.doi.org/10.1021/cr2003272 |*Chem. Rev.* 2012, 112, 724–781

tpom	tetrakis(4-pyridyloxymethylene)methane
TP	2-tetrazolepyrimidine
TZI	tetrazolylisophthalate
2,7-ndc	naphthalene-2,7-dicarboxylate
2-stp	2-sulfonylterephthalate
3-mepy	3-methylpyridine
4-bcba-H3	bis(4-carboxy-benzyl)amine
4,4′-bpe	*trans*-bis(4-pyridyl)ethylene
4-mIm	4-methylimidazolate
5-MeO-ip	5-methoxyisophthalate
5-NO-ip	5-nitro-isophthalate

REFERENCES

(1) Quadrelli, R.; Peterson, S. *Energy Policy* **2007**, *35*, 5938.
(2) Pachauri, R. K.; Reisinger, A. *IPCC Fourth Assessment Report*, Intergovernmental Panel on Climate Change, 2007.
(3) U.S. Environmental Protection Agency: http://www.epa.gov/climatechange/emissions/co2_human.html.
(4) Carbon Capture and Storage, Full-Scale Demonstration Progress Update: www.iea.org/G8/docs/ccs_g8july09.pdf, OECD/IEA, 2009.
(5) International Energy Agency (IEA): http://www.iea.org/index_info.asp?id=1959, 2011.
(6) Ritter, S. K. *Chem. Eng. News* **2007**, *85*, 7.
(7) Kumar, B.; Smieja, J. M.; Kubiak, C. P. *J. Phys. Chem. C* **2010**, *114*, 14220.
(8) Haszeldine, R. S. *Science* **2009**, *325*, 1644.
(9) Choi, S.; Drese, J. H.; Jones, C. W. *ChemSusChem* **2009**, *2*, 796.
(10) Li, J.-R.; Kuppler, R. J.; Zhou, H.-C. *Chem. Soc. Rev.* **2009**, *38*, 1477.
(11) Keskin, S.; van Heest, T. M.; Sholl, D. S. *ChemSusChem* **2010**, *3*, 879.
(12) D'Alessandro, D. M.; Smit, B.; Long, J. R. *Angew. Chem., Int. Ed.* **2010**, *49*, 6058.
(13) Ma, S.; Zhou, H.-C. *Chem. Commun.* **2010**, *46*, 44.
(14) Willis, R. R.; Benin, A. I.; Snurr, R. Q.; Yazaydin, A. O. *Nanotechnology for Carbon Dioxide Capture*; Wiley-VCH Verlag GmbH & Co.: Weinheim, Germany, 2010.
(15) Li, J.-R.; Ma, Y.; McCarthy, M. C.; Sculley, J.; Yu, J.; Jeong, H.-K.; Balbuena, P. B.; Zhou, H.-C. *Coord. Chem. Rev.* **2011**, *255*, 1791.
(16) Férey, G.; Serre, C.; Devic, T.; Maurin, G.; Jobic, H.; Llewellyn, P. L.; De Weireld, G.; Vimont, A.; Daturi, M.; Chang, J.-S. *Chem. Soc. Rev.* **2011**, *40*, 550.
(17) Morris, R. E.; Wheatley, P. S. *Angew. Chem., Int. Ed.* **2008**, *47*, 4966.
(18) Phan, A.; Doonan, C. J.; Uribe-Romo, F. J.; Knobler, C. B.; O'Keefe, M.; Yaghi, O. M. *Acc. Chem. Res.* **2010**, *43*, 58.
(19) Simmons, J. M.; Wu, H.; Zhou, W.; Yildirim, T. *Energy Environ. Sci.* **2011**, *4*, 2177.
(20) Earth System Research Laboratory: http://www.esrl.noaa.gov/gmd/ccgg/trends/index.html, 2011.
(21) Fischer, H.; Wahlen, M.; Smith, J.; Mastroianni, D.; Deck, B. *Science* **1999**, *283*, 1712.
(22) Demicco, R. V.; Lowenstein, T. K.; Hardie, L. A. *Geology* **2003**, *31*, 793.
(23) Najam, A.; Rahman, A. A.; Huq, S.; Sokona, Y. *Clim. Policy* **2003**, *3*, S9.
(24) Demirbas, A. *Energy Sources, Part A* **2008**, *30*, 70.
(25) Petron, G.; Tans, P.; Frost, G.; Chao, D.; Trainer, M. *J. Geophys. Res.* **2008**, *113*, 1.
(26) U.S. Energy Information Administration: http://www.eia.gov/electricity/monthly/index.cfm, 2011.
(27) Shafiee, S.; Topal, E. *Energy Policy* **2009**, *37*, 181.
(28) International Energy Outlook: DOE/EIA-0484, U.S. Energy Information Administration, 2010 http://www.eia.gov/forecasts/ieo/index.cfm (Accessed March 2010).
(29) Botzen, W. J. W.; Gowdy, J. M.; Van Den Bergh, J. C. J. M. *Clim. Policy* **2008**, *8*, 569.
(30) Rochelle, G. T. *Science* **2009**, *325*, 1652.
(31) Granite, E. J.; Pennline, H. W. *Ind. Eng. Chem. Res.* **2002**, *41*, 5470.
(32) Lide, D. R. *CRC Handbook of Chemistry and Physics*; CRC Press: Boca Raton, FL, 2004.
(33) Yamposkii, Y.; Pinnau, I.; Freeman, B. D. *Materials Science of Membranes for Gas and Vapor Separation*; John Wiley & Sons Ltd.: West Sussex, England, 2006.
(34) Benson, S. M.; Surles, T. *Proc. IEEE* **2006**, *94*, 1795.
(35) Aydin, G.; Karakurt, I.; Aydiner, K. *Energy Policy* **2010**, *38*, 5072.
(36) Khoo, H. H.; Tan, R. B. H. *Energy Fuels* **2006**, *20*, 1914.
(37) Service, R. F. *Science* **2009**, *325*, 1644.
(38) Metz, B.; Davidson, O.; de Coninck, H.; Loos, M.; Meyer, L. *Special Report on Carbon Dioxide Capture and Storage*; Cambridge Univ. Press: Cambridge, U.K., 2006.
(39) Klara, S. M.; Srivastava, R. D. *Environ. Prog.* **2002**, *21*, 247.
(40) da Silva, E. F.; Svendsen, H. F. *Int. J. Greenhouse Gas Control* **2007**, *1*, 151.
(41) le Bouhelec, E. B.; Mougin, P.; Barreau, A.; Solimando, R. *Energy Fuels* **2007**, *21*, 2044.
(42) Peeters, A. N. M.; Faaij, A. P. C; Turkenburg, W. C. *Int. J. Greenhouse Gas Control* **2007**, *1*, 396.
(43) Oyenekan, B. A.; Rochelle, G. T. *AIChE J.* **2007**, *53*, 3144.
(44) Freeman, S. A.; Dugas, R.; Van Wagener, D. H.; Nguyen, T.; Rochelle, G. T. *Int. J. Greenhouse Gas Control* **2010**, *4*, 119.
(45) Karadas, F.; Atilhan, M.; Aparicio, S. *Energy Fuels* **2010**, *24*, 5817.
(46) Idem, R.; Wilson, M.; Tontiwachwithikul, P.; Chakma, A.; Veawab, A.; Aroonwilas, A.; Gelowitz, D. *Ind. Eng. Chem. Res.* **2006**, *45*, 3414.
(47) Weiland, R. H.; Dingman, J. C.; Cronin, D. B. *J. Chem. Eng. Data* **1997**, *42*, 1004.
(48) Mason, J. A.; Sumida, K.; Herm, Z. R.; Krishna, R.; Long, J. R. *Energy Environ. Sci.* **2011**, *4*, 3030.
(49) Čejka, J.; Corma, A.; Zones, S. *Zeolites and Catalysis: Synthesis, Reactions and Applications*; Wiley-VCH: Weinheim, Germany, 2010.
(50) Kusakabe, K.; Kuroda, T.; Murata, A.; Morooka, S. *Ind. Eng. Chem. Res.* **1997**, *36*, 649.
(51) Cavenati, S.; Grande, C. A.; Rodrigues, A. E. *J. Chem. Eng. Data* **2004**, *49*, 1095.
(52) Cavenati, S.; Grande, C. A.; Rodrigues, A. E. *Chem. Eng. Sci.* **2006**, *61*, 3893.
(53) Himeno, S.; Tomita, T.; Suzuki, K.; Yoshida, S. *Microporous Mesoporous Mater.* **2007**, *98*, 62.
(54) Ghoufi, A.; Gaberova, L.; Rouquerol, J.; Vincent, D.; Llewellyn, P. L.; Maurin, G. *Microporous Mesoporous Mater.* **2009**, *119*, 117.
(55) Lee, J.-S.; Kim, J.-H.; Kim, J.-T.; Suh, J.-K.; Lee, J.-M.; Lee, C.-H. *J. Chem. Eng. Data* **2002**, *47*, 1237.
(56) Wang, Y.; LeVan, M. D. *J. Chem. Eng. Data* **2009**, *54*, 2839.
(57) O'Keefe, M.; Peskov, M. A.; Ramsden, S. J.; Yaghi, O. M. *Acc. Chem. Res.* **2008**, *41*, 1782.
(58) Jiang, J.; Yu, J.; Corma, A. *Angew. Chem., Int. Ed.* **2010**, *49*, 3120.
(59) Palomino, M.; Corma, A.; Rey, F.; Valencia, S. *Langmuir* **2010**, *26*, 1910.
(60) Zhang, J.; Webley, P. A.; Xiao, P. *Energy Convers. Manage.* **2008**, *49*, 346.
(61) Li, G.; Xiao, P.; Webley, P.; Zhang, J.; Singh, R.; Marshall, M. *Adsorption* **2008**, *14*, 415.
(62) Li, G.; Xiao, P.; Webley, P.; Zhang, J.; Singh, R. *Energy Procedia* **2009**, *1*, 1123.
(63) Konduru, N.; Linder, P.; Assaf-Anid, N. M. *AIChE J.* **2007**, *53*, 3137.
(64) Jadhav, P. D.; Chatti, R. V.; Biniwale, R. B.; Labhsetwar, N. K.; Devotta, S.; Rayalu, S. S. *Energy Fuels* **2007**, *21*, 3555.
(65) Zhang, J.; Singh, R.; Webley, P. A. *Microporous Mesoporous Mater.* **2008**, *111*, 478.

(66) Martin, C. F.; Plaza, M. G.; Pis, J. J.; Rubiera, F.; Pevida, C.; Centeno, T. A. *Sep. Purif. Technol.* **2010**, *74*, 225.
(67) Silvestre-Albero, J.; Wahby, A.; Sepúlveda, E.; Martínez-Escandell, M.; Kaneko, K.; Rodríguez-Reinoso, F. *Chem. Commun.* **2011**, *47*, 6840.
(68) Plaza, M. G.; García, S.; Rubiera, F.; Pis, J. J.; Pevida, C. *Chem. Eng. J.* **2010**, *163*, 41.
(69) Plaza, M. G.; Pevida, C.; Arenillas, A.; Rubiera, F.; Pis, J. J. *Fuel* **2007**, *86*, 2204.
(70) Plaza, M. G.; Pevida, C.; Arias, B.; Casal, M. D.; Martín, C. F.; Fermosa, J.; Rubiera, F.; Pis, J. J. *J. Environ. Eng.* **2009**, *135*, 426.
(71) Bezerra, D. P.; Oliviera, R. S.; Vieira, R. S.; Cavalcante, C. L., Jr.; Azevedo, D. C. S. *Adsorption* **2011**, *17*, 235.
(72) El-Kaderi, H. M.; Hunt, J. R.; Medoza-Cortéz, J. L.; Côte, A. P.; Taylor, R. E.; O'Keefe, M.; Yaghi, O. M. *Science* **2007**, *316*, 268.
(73) Côte, A. P.; El-Kaderi, H. M.; Furukawa, H.; Hunt, J. R.; Yaghi, O. M. *J. Am. Chem. Soc.* **2007**, *129*, 12914.
(74) Han, S. S.; Furukawa, H.; Yaghi, O. M.; Goddard, W. A. *J. Am. Chem. Soc.* **2008**, *130*, 11580.
(75) Glover, T. G.; Hunt, J. R.; Yaghi, O. M. *Nature* **2010**, *2*, 235.
(76) Dogru, M.; Sonnauer, A.; Gavryushin, A.; Knochel, P.; Bein, T. *Chem. Commun.* **2011**, *47*, 1707.
(77) Choi, Y. J.; Choi, J. H.; Choi, K. M.; Kang, J. K. *J. Mater. Chem.* **2011**, *21*, 1073.
(78) Hicks, J. C.; Drese, J. H.; Fauth, D. J.; Gray, M. L.; Qi, G.; Jones, C. W. *Microporous Mesoporous Mater.* **2003**, *62*, 29.
(79) Xu, X.; Song, C.; Andresen, J. M.; Miller, B. G.; Scaroni, A. W. *Microporous Mesoporous Mater.* **2003**, *62*, 29.
(80) Jones, J. *J. Am. Chem. Soc.* **2008**, *130*, 2902.
(81) Jiang, J.-X.; Su, F.; Trewin, A.; Wood, C. D.; Campbell, N. L.; Niu, H.; Dickinson, C.; Ganin, A. Y.; Rosseinsky, M. J.; Khimyak, Y. Z.; Cooper, A. I. *Angew. Chem., Int. Ed.* **2007**, *46*, 8574.
(82) Cooper, A. I. *Adv. Mater.* **2009**, *21*, 1291.
(83) Du, N.; Park, H. B.; Robertson, G. P.; Dal-Cin, M. M.; Visser, T.; Scoles, L.; Guiver, M. D. *Nat. Mater.* **2011**, *10*, 372.
(84) Martin, C. F.; Stockel, E.; Clowes, R. A.; Adams, D. J.; Cooper, A. I.; Pis, J. J.; Rubiera, F.; Pevida, C. *J. Mater. Chem.* **2011**, *21*, 5475.
(85) Merel, J.; Marc, C.; Francis, M. *Ind. Eng. Chem. Res.* **2008**, *47*, 209.
(86) Berger, A. H.; Bhown, A. S. *Energy Procedia* **2011**, *4*, 562.
(87) Herm, Z. R.; Swisher, J. A.; Smit, B.; Krishna, R.; Long, J. R. *J. Am. Chem. Soc.* **2011**, *133*, 5664.
(88) Ishibashi, M.; Ota, H.; Akutsu, N.; Umeda, S.; Tajika, M.; Izumi, J.; Yasutake, A.; Kabata, T.; Kageyama, Y. *Energy Convers. Manage.* **1996**, *37*, 929.
(89) Mulgundmath, V.; Tezel, F. H. *Adsorption* **2010**, *16*, 587.
(90) Rubin, E. S.; Chao, C.; Rao, A. B. *Energy Policy* **2007**, *35*, 4444.
(91) House, K. Z.; Harvey, C. F.; Aziz, M. J.; Schrag, D. P. *Energy Environ. Sci.* **2009**, *2*, 193.
(92) Kitagawa, S.; Kitaura, R.; Noro, S.-I. *Angew. Chem., Int. Ed.* **2004**, *43*, 2334.
(93) Férey, G. *Chem. Soc. Rev.* **2008**, *37*, 191.
(94) Lee, J. Y.; Farha, O. K.; Roberts, J.; Scheidt, K. A.; Nguyen, S. T.; Hupp, J. T. *Chem. Soc. Rev.* **2009**, *38*, 1450.
(95) Murray, L. J.; Dincă, M.; Long, J. R. *Chem. Soc. Rev.* **2009**, *38*, 1294.
(96) Kuppler, R. J.; Timmons, D. J.; Fang, Q.-R.; Li, J.-R. M.; T., A.; Young, M. D.; Yuan, D.; Zhao, D.; Zhuang, W.; Zhou, H.-C. *Coord. Chem. Rev.* **2009**, *253*, 3042.
(97) Farrusseng, D.; Aguado, S.; Pinel, C. *Angew. Chem., Int. Ed.* **2009**, *48*, 7502.
(98) Corma, A.; García, H.; Llabrés, i; Xamena, F. X. *Chem. Rev.* **2010**, *110*, 4606.
(99) Furukawa, H.; Ko, N.; Go, Y. B.; Aratani, N.; Choi, S. B.; Choi, E.; Yazaydin, A. O.; Snurr, R. Q.; O'Keefe, M.; Kim, J.; Yaghi, O. M. *Science* **2010**, *329*, 424.
(100) Rowsell, J. L. C.; Yaghi, O. M. *J. Am. Chem. Soc.* **2006**, *128*, 1304.
(101) Furukawa, H.; Kim, J.; Ockwig, N. W.; O'Keefe, M.; Yaghi, O. M. *J. Am. Chem. Soc.* **2008**, *130*, 11650.
(102) Wang, Z.; Cohen, S. M. *Chem. Soc. Rev.* **2009**, *38*, 1315.
(103) Tanabe, K. K.; Cohen, S. M. *Chem. Soc. Rev.* **2011**, *40*, 498.
(104) Czaja, A. U.; Trukhan, N.; Müller, U. *Chem. Soc. Rev.* **2009**, *38*, 1284.
(105) Férey, G.; Mellot-Draznieks, C.; Serre, C.; Millange, F. *Acc. Chem. Res.* **2005**, *38*, 217.
(106) Kitagawa, S.; Matsuda, R. *Coord. Chem. Rev.* **2007**, *251*, 2490.
(107) Klinowski, J.; Paz, F. A. A.; Silva, P.; Rocha, J. *Dalton Trans.* **2011**, *40*, 321.
(108) Jung, D.-W.; Yang, D.-A.; Kim, J.; Kim, J.; Ahn, W.-S. *Dalton Trans.* **2010**, *39*, 2883.
(109) Cantwell, C. G.; Brown, A. J.; Sholl, D. S.; Nair, S. *Cryst. Growth Des.* **2011**, *11*, 4505.
(110) Pichon, A.; James, S. L. *CrystEngComm* **2008**, *10*, 1839.
(111) Klimakow, M.; Klobes, P.; Thuenemann, A. F.; Rademann, K.; Emmerling, F. *Chem. Mater.* **2010**, *22*, 5216.
(112) Li, M.; Dincă, M. *J. Am. Chem. Soc.* **2011**, *133*, 12926.
(113) Li, H.; Eddaoudi, M.; O'Keefe, M.; Yaghi, O. M. *Nature* **1999**, *402*, 276.
(114) Eddaoudi, M.; Li, H.; Yaghi, O. M. *J. Am. Chem. Soc.* **2000**, *122*, 1391.
(115) Kaye, S. S.; Dailly, A.; Yaghi, O. M.; Long, J. R. *J. Am. Chem. Soc.* **2007**, *129*, 14176.
(116) Eddaoudi, M.; Kim, J.; Rosi, N.; Vodak, D.; Wachter, J.; O'Keefe, M.; Yaghi, O. M. *Science* **2002**, *295*, 469.
(117) Cavka, J. H.; Jakobsen, S.; Olsbye, U.; Guillou, N.; Lamberti, C.; Bordiga, S.; Lillerud, K. P. *J. Am. Chem. Soc.* **2008**, *130*, 13850.
(118) Garibay, S. J.; Cohen, S. M. *Chem. Commun.* **2010**, *46*, 7700.
(119) Serre, C.; Millange, F.; Thouvenot, C.; Noguès, M.; Marsolier, G.; Louër, D.; Férey, G. *J. Am. Chem. Soc.* **2002**, *124*, 13519.
(120) Biswas, S.; Ahnfeldt, T.; Stock, N. *Inorg. Chem.* **2011**, *50*, 9518.
(121) Lin, X.; Telepeni, I.; Blake, A. J.; Dailly, A.; Brown, C. M.; Simmons, J. M.; Zoppi, M.; Walker, G. S.; Thomas, M.; Mays, T. J.; Hubberstey, P.; Champness, N. R.; Schröder, M. *J. Am. Chem. Soc.* **2009**, *131*, 2159.
(122) Férey, G.; Serre, C. *Chem. Soc. Rev.* **2009**, *38*, 1380.
(123) Horike, S.; Shimomura, S.; Kitagawa, S. *Nat. Chem.* **2009**, *1*, 695.
(124) Wang, Z.; Cohen, S. M. *J. Am. Chem. Soc.* **2007**, *129*, 12368.
(125) Wang, Z.; Cohen, S. M. *J. Am. Chem. Soc.* **2009**, *131*, 16675.
(126) Savonnet, M.; Baser-Bachi, D.; Bats, N.; Perez-Pellitero, J.; Jeanneau, E.; Lecocq, V.; Pine, C.; Farrusseng, D. *J. Am. Chem. Soc.* **2010**, *132*, 4518.
(127) Bernt, S.; Guillerm, V.; Serre, C.; Stock, N. *Chem. Commun.* **2011**, *47*, 2838.
(128) Vimont, A.; Goupil, J.-M.; Lavalley, J.-C.; Daturi, M.; Surblé, S.; Serre, C.; Millange, F.; Férey, G.; Audebrand, N. *J. Am. Chem. Soc.* **2006**, *128*, 3218.
(129) Dincă, M.; Long, J. R. *Angew. Chem., Int. Ed.* **2008**, *47*, 6766.
(130) Zhou, W.; Wu, H.; Yildirim, T. *J. Am. Chem. Soc.* **2008**, *130*, 15268.
(131) Dietzel, P. D. C.; Besikiotis, V.; Blom, R. *J. Mater. Chem.* **2009**, *19*, 7362.
(132) Chen, B.; Xiang, S.; Qian, G. *Acc. Chem. Res.* **2010**, *43*, 1115.
(133) Chui, S. S.-Y.; Lo, S. M.-F.; Charmant, J; Orpen, A. G.; Williams, I. D. *Science* **1999**, *283*, 1148.
(134) Murray, L. J.; Dincă, M.; Yano, J.; Chavan, S.; Bordiga, S.; Brown, C. M.; Long, J. R. *J. Am. Chem. Soc.* **2010**, *132*, 7856.
(135) Xie, L.; Liu, S.; Gao, C.; Cao, R.; Cao, J.; Sun, C.; Su, Z. *Inorg. Chem.* **2007**, *46*, 7782.
(136) Feldblyum, J. I.; Liu, M.; Gidley, D. W.; Matzger, A. J. *J. Am. Chem. Soc.* **2011**, *133*, 18257.
(137) Kramer, M.; Schwarz, U.; Kaskel, S. *J. Mater. Chem.* **2006**, *16*, 2245.
(138) Dincă, M.; Long, J. R. *J. Am. Chem. Soc.* **2007**, *129*, 11172.
(139) Dincă, M.; Han, W. S.; Liu, Y.; Dailly, A.; Brown, C. M.; Long, J. R. *Angew. Chem., Int. Ed.* **2007**, *46*, 1419.

(140) Sumida, K.; Horike, S.; Kaye, S. S.; Herm, Z. R.; Queen, W. L.; Brown, C. M.; Grandjean, F.; Long, G. J.; Dailly, A.; Long, J. R. *Chem. Sci.* **2010**, *1*, 184.
(141) Barthelet, K.; Marrot, J.; Riou, D.; Feréy, G. *Angew. Chem., Int. Ed.* **2002**, *41*, 281.
(142) Férey, G.; Latroche, M.; Serre, C.; Millange, F.; Loiseau, T.; Percheron-Guégan, A. *Chem. Commun.* **2003**, 2976.
(143) Miller, S. R.; Wright, P. A.; Serre, C.; Loiseau, T.; Marrot, J.; Férey, G. *Chem. Commun.* **2005**, 3850.
(144) Whitfield, T. R.; Wang, X.; Liu, L.; Jacobson, A. J. *Solid State Sci.* **2005**, *7*, 1096.
(145) Anokhina, E. V.; Vougo-Zanda, M.; Wang, X.; Jacobson, A. J. *J. Am. Chem. Soc.* **2005**, *127*, 15000.
(146) Arstad, B.; Fjellvåg, H.; Kongshaug, K. O.; Swang, O.; Blom, R. *Adsorption* **2008**, *14*, 755.
(147) Couck, S.; Denayer, J. F. M.; Baron, G. V.; Rémy, T.; Gascon, J.; Kapteijn, F. *J. Am. Chem. Soc.* **2009**, *131*, 6326.
(148) Surblé, S.; Serre, C.; Mellot-Draznieks, C.; Millange, F.; Férey, G. *Chem. Commun.* **2006**, 284.
(149) Britt, D.; Tranchemontagne, D.; Yaghi, O. M. *Proc. Natl. Acad. Sci. U.S.A.* **2008**, *105*, 11623.
(150) Caskey, S. R.; Wong-Foy, A. G.; Matzger, A. J. *J. Am. Chem. Soc.* **2008**, *130*, 10870.
(151) Bauer, S.; Serre, C.; Devic, T.; Horcajada, P.; Marrot, J.; Férey, G.; Stock, N. *Inorg. Chem.* **2008**, *47*, 7568.
(152) Biemmi, E.; Christian, S.; Stock, N.; Bein, T. *Microporous Mesoporous Mater.* **2009**, *117*, 111.
(153) Ahnfeldt, T.; Guillou, N.; Gunzelmann, D.; Margiolaki, I.; Loiseau, T.; Férey, G.; Senker, J.; Stock, N. *Angew. Chem., Int. Ed.* **2009**, *48*, 5163.
(154) Palanikumar, M.; Stock, N. *Inorg. Chem.* **2011**, *50*, 5085.
(155) Low, J. J.; Benin, A. I.; Jakubczak, P.; Abrahamian, J. F.; Faheem, S. A.; Willis, R. R. *J. Am. Chem. Soc.* **2009**, *131*, 15834.
(156) Tan, J. C.; Cheetham, A. K. *Chem. Soc. Rev.* **2011**, *40*, 1059.
(157) Chapman, K. W.; Halder, G. J.; Chupas, P. J. *J. Am. Chem. Soc.* **2008**, *130*, 10524.
(158) Huang, B. L.; Ni, Z.; Millward, A. R.; McGaughey, A. J. H.; Uher, C.; Kaviany, M.; Yaghi, O. M. *Mass Transfer* **2007**, *50*, 405.
(159) Jakubinek, M. B.; Zhan, B.-Z.; White, M. A. *Microporous Mesoporous Mater.* **2007**, *103*, 108.
(160) Millward, A. R.; Yaghi, O. M. *J. Am. Chem. Soc.* **2005**, *127*, 17998.
(161) Farha, O. K.; Yazaydin, A. O.; Eryazici, I.; Malliakas, C. D.; Hauser, B. G.; Kanatzidis, M. G.; Nguyen, S. T.; Snurr, R. Q.; Hupp, J. T. *Nat. Chem.* **2010**, *2*, 944.
(162) Xue, M.; Liu, Y.; Schaffino, R. M.; Xiang, S.; Zhao, X.; Zhu, G.-S.; Qiu, S.-L.; Chen, B. *Inorg. Chem.* **2009**, *48*, 4649.
(163) Botas, J. A.; Calleja, G.; Sánchez-Sánchez, M.; Orcajo, M. G. *Langmuir* **2010**, *26*, 5300.
(164) Choi, J.-S.; Son, W.-J.; Kim, J.; Ahn, W.-S. *Microporous Mesoporous Mater.* **2008**, *116*, 727.
(165) Gedrich, K.; Senkovska, I.; Klein, N.; Stoeck, U.; Henshcel, A.; Lohe, M. R.; Baburin, I. A.; Mueller, U.; Kaskel, S. *Angew. Chem., Int. Ed.* **2010**, *49*, 8489.
(166) Yuan, D.; Zhao, D.; Sun, D.; Zhou, H.-C. *Angew. Chem., Int. Ed.* **2010**, *49*, 5357.
(167) Llewellyn, P. L.; Bourrelly, S.; Serre, C.; Vimont, A.; Daturi, M.; Hamon, L.; Weireld, G. D.; Chang, J.-S.; Hong, D.-Y.; Hwang, Y. K.; Jhung, S. H.; Férey, G. *Langmuir* **2008**, *24*, 7245.
(168) Zhang, Z.; Huang, S.; Xian, S.; Xi, H.; Li, Z. *Energy Fuels* **2011**, *25*, 835.
(169) Mu, B.; Schoenecker, P. M.; Walton, K. S. *J. Phys. Chem. C* **2010**, *114*, 6464.
(170) Tan, C.; Yang, S.; Champness, N. R.; Lin, X.; Blake, A. J.; Lewis, W.; Schröder, M. *Chem. Commun.* **2011**, *47*, 4487.
(171) Park, Y. K.; Choi, S. B.; Kim, H.; Kim, K.; Won, B.-H.; Choi, K.; Choi, J.-S.; Ahn, W.-S.; Won, N.; Kim, S.; Jung, D. H.; Choi, S.-H.; Kim, G.-H.; Cha, S.-S.; Jhon, Y. H.; Yang, J. K.; Kim, J. *Angew. Chem., Int. Ed.* **2007**, *46*, 8230.
(172) Moellmer, J.; Moeller, A.; Driesbach, F.; Glaeser, R.; Staudt, R. *Microporous Mesoporous Mater.* **2011**, *138*, 140.
(173) Hamon, L.; Jolimaître, E.; Pirngruber, G. D. *Ind. Eng. Chem. Res.* **2010**, *49*, 7497.
(174) Liang, Z.; Marshall, M.; Chaffee, A. L. *Energy Procedia* **2009**, *1*, 1265.
(175) Liang, Z.; Marshall, M.; Chaffee, A. L. *Energy Fuels* **2009**, *23*, 2785.
(176) Liang, Z.; Marshall, M.; Chaffee, A. L. *Microporous Mesoporous Mater.* **2010**, *132*, 305.
(177) Nune, S. K.; Thallapally, P. K.; Dohnalkova, A.; Wang, C.; Liu, J.; Exarhos, G. J. *Chem. Commun.* **2010**, *46*, 4878.
(178) Bourrelly, S.; Llewellyn, P. L.; Serre, C.; Millange, F.; Loiseau, T.; Férey, G. *J. Am. Chem. Soc.* **2005**, *127*, 13519.
(179) Park, H. J.; Suh, M. P. *Chem. Commun.* **2010**, *46*, 610.
(180) Senkovska, I.; Hoffmann, F.; Fröba, M.; Getzschmann, J.; Böhlmann, W.; Kaskel, S. *Microporous Mesoporous Mater.* **2009**, *122*, 93.
(181) Chowdhury, P.; Bikkina, C.; Gumma, S. *J. Phys. Chem. C* **2009**, *113*, 6616.
(182) Galli, S.; Masciocchi, N.; Tagliabue, G.; Sironi, A.; Navarro, J. A. R.; Salas, J. M.; Mendez-Liñan, L.; Domingo, M.; Pérez-Mendoza, M.; Barea, E. *Chem.—Eur. J.* **2008**, *14*, 9890.
(183) Zhang, J.; Xue, Y.-S.; Liang, L.-L.; Ren, S.-B.; Li, Y.-Z.; Du, H.-B.; You, X.-Z. *Inorg. Chem.* **2010**, *49*, 7685.
(184) Weirsum, A. D.; Soubeyrand-Lenoir, E.; Yang, Q.; Moulin, B.; Guillerm, V.; Yahia, M. B.; Bourrelly, S.; Vimont, A.; Miller, S.; Vagner, C.; Daturi, M.; Guillaume, C.; Serre, C.; Maurin, G.; Llewellyn, P. L. *Chem.—Asian J.* **2011**, DOI: 10.1002/asia.201100201.
(185) Rabone, J.; Yue, Y.-F.; Chong, S. Y.; Stylianou, K. C.; Basca, J.; Bradshaw, D.; Darling, G. R.; Berry, N. G.; Khimyak, Y. Z.; Ganin, A. Y.; Wiper, P.; Claridge, J. B.; Rosseinsky, M. J. *Science* **2010**, *329*, 1053.
(186) Loiseau, T.; Lecroq, L.; Volkringer, C.; Marrot, J.; Férey, G.; Haouas, M.; Taulelle, F.; Bourrelly, S.; Llewellyn, P. L.; Latroche, M. *J. Am. Chem. Soc.* **2006**, *128*, 10223.
(187) Surblé, S.; Millange, F.; Serre, C.; Duren, T.; Latroche, M.; Bourrelly, S.; Llewellyn, P. L.; Férey, G. *J. Am. Chem. Soc.* **2006**, *128*, 14889.
(188) Bao, Z.; Yu, L.; Ren, Q.; Lu, X.; Deng, S. *J. Colloid Interface Sci.* **2011**, *353*, 549.
(189) Yazaydin, A. Ö.; Snurr, R. Q.; Park, T.-H.; Koh, K.; Liu, J.; LeVan, M. D.; Benin, A. I.; Jakubczak, P.; Lanuza, M.; Galloway, D. B.; Low, J. L.; Willis, R. R. *J. Am. Chem. Soc.* **2009**, *131*, 18198.
(190) Britt, D.; Furukawa, H.; Wang, B.; Glover, T. G.; Yaghi, O. M. *Proc. Natl. Acad. Sci. U.S.A.* **2009**, *106*, 20637.
(191) Yazaydin, A. Ö.; Benin, A. I.; Faheem, S. A.; Jakubczak, P.; Low, J. L.; Willis, R. R.; Snurr, R. Q. *Chem. Mater.* **2009**, *21*, 1425.
(192) Liu, J.; Wang, Y.; Benin, A. I.; Jakubczak, P.; Willis, R. R.; LeVan, M. D. *Langmuir* **2010**, *26*, 14301.
(193) Dietzel, P. D. C.; Johnsen, R. E.; Fjellvag, H.; Bordiga, S.; Groppo, E.; Chavan, S.; Blom, R. *Chem. Commun.* **2008**, 5125.
(194) Aprea, P.; Caputo, D.; Gargiulo, N.; Iucolano, F.; Pepe, F. *J. Chem. Eng. Data* **2010**, *55*, 3655.
(195) Chowdhury, P.; Bikkina, C.; Meister, D.; Dreisbach, F.; Gumma, S. *Microporous Mesoporous Mater.* **2009**, *117*, 406.
(196) Farrusseng, D.; Daniel, C.; Gaudillère, C.; Ravon, U.; Schuurman, Y.; Mirodatos, C.; Dubbeldam, D.; Frost, H.; Snurr, R. Q. *Langmuir* **2009**, *25*, 7383.
(197) Kim, J.; Yang, S.-T.; Choi, S. B.; Sim, J.; Kim, J.; Ahn, W.-S. *J. Mater. Chem.* **2011**, *21*, 3070.
(198) McDonald, T. M.; D'Alessandro, D. M.; Krishna, R.; Long, J. R. *Chem. Sci.* **2011**, *2*, 2022.
(199) An, J.; Geib, S. J.; Rosi, N. *J. Am. Chem. Soc.* **2009**, *132*, 38.
(200) Demessence, A.; D'Alessandro, D. M.; Foo, M. L.; Long, J. R. *J. Am. Chem. Soc.* **2009**, *131*, 8784.
(201) Vaidhyanathan, R.; Iremonger, S. S.; Dawson, K. W.; Shimizu, G. K. H. *Chem. Commun.* **2009**, 5230.
(202) Prasad, T. K.; Hong, D. H.; Suh, M. P. *Chem.—Eur. J.* **2010**, *16*, 14043.

(203) Kanoh, H.; Kondo, A.; Noguchi, H.; Kajiro, H.; Tohdoh, A.; Hattori, Y.; Xu, W.-C.; Inoue, M.; Sugiura, T.; Morita, K.; Tanaka, H.; Ohba, T.; Kaneko, K. *J. Colloid Interface Sci.* **2009**, *334*, 1.
(204) Bloch, E. D.; Britt, D.; Lee, C.; Doonan, C. J.; Uribe-Romo, F. J.; Furukawa, H.; Long, J. R.; Yaghi, O. M. *J. Am. Chem. Soc.* **2010**, *132*, 14382.
(205) Chen, S.-S.; Chen, M.; Takamizawa, S.; Wang, P.; Lv, G.-C.; Sun, W.-Y. *Chem. Commun.* **2011**, *47*, 4902.
(206) Kim, T. K.; Suh, M. P. *Chem. Commun.* **2011**, *47*, 4258.
(207) Navarro, J. A. R.; Barea, E.; Salas, J. M.; Masciocchi, N.; Galli, S.; Sironi, A.; Ania, C. O.; Parra, J. B. *J. Mater. Chem.* **2007**, *17*, 1939.
(208) Rallapalli, P.; Prasanth, K. P.; Patil, D.; Somani, R. S.; Jasra, R. V.; Bajaj, H. C. *J. Porous Mater.* **2011**, *18*, 205.
(209) Miller, S. R.; Pearce, G. M.; Wright, P. A.; Bonino, F.; Chavan, S.; Bordiga, S.; Margiolaki, I.; Guillou, N.; Férey, G.; Bourrelly, S.; Llewellyn, P. L. *J. Am. Chem. Soc.* **2008**, *130*, 15967.
(210) Stylianou, K. C.; Warren, J. E.; Chong, S. Y.; Rabone, J.; Basca, J.; Bradshaw, D.; Rosseinsky, M. J. *Chem. Commun.* **2011**, *47*, 3389.
(211) Chen, Z.; Xiang, S.; Arman, H. D.; Li, P.; Tidrow, S.; Zhao, D.; Chen, B. *Eur. J. Inorg. Chem.* **2010**, *24*, 3745.
(212) Southon, P. D.; Liu, L.; Fellows, E. A.; Price, D. J.; Halder, G. J.; Chapman, K. W.; Moubaraki, B.; Murray, K. S.; Létard, J.-F.; Kepert, C. J. *J. Am. Chem. Soc.* **2009**, *131*, 10998.
(213) Banerjee, R.; Furukawa, H.; Britt, D.; Knobler, C.; O'Keefe, M.; Yaghi, O. M. *J. Am. Chem. Soc.* **2009**, *131*, 3875.
(214) Morris, W.; Leung, B.; Furukawa, H.; Yaghi, O. K.; He, N.; Hayashi, H.; Houndonougbo, Y.; Asta, M.; Laird, B. B.; Yaghi, O. M. *J. Am. Chem. Soc.* **2010**, *132*, 11006.
(215) Debatin, F.; Thomas, A.; Kelling, A.; Hedin, N.; Bacsik, Z.; Senkovska, I.; Kaskel, S.; Junginger, M.; Muller, H.; Schilde, U.; Jager, C.; Friedrich, A.; Holdt, H.-J. *Angew. Chem., Int. Ed.* **2010**, *49*, 1258.
(216) Zhao, Z.; Li, Z.; Lin, Y. S. *Ind. Eng. Chem. Res.* **2009**, *48*, 10015.
(217) Saha, D.; Bao, Z.; Jia, F.; Deng, S. *Environ. Sci. Technol.* **2010**, *44*, 1820.
(218) Lu, C.-M.; Liu, J.; Xiao, K.; Harris, A. T. *Chem. Eng. J.* **2010**, *156*, 465.
(219) Deng, H.; Doonan, C. J.; Furukawa, H.; Ferriera, R. B.; Towne, J.; Knobler, C. B.; Wang, B.; Yaghi, O. M. *Science* **2010**, *327*, 846.
(220) Llewellyn, P. L.; Bourrelly, S.; Serre, C.; Filinchuk, Y.; Férey, G. *Angew. Chem., Int. Ed.* **2006**, *45*, 7751.
(221) Chen, Z.; Liu, X.; Zhang, C.; Zhang, Z.; Liang, F. *Dalton Trans.* **2010**, *40*, 1911.
(222) Chen, Z.; Xiang, S.; Zhao, D.; Chen, B. *Cryst. Growth Des.* **2009**, *9*, 5293.
(223) Zhang, Z.; Xiang, S.; Rao, X.; Zheng, Q.; Fronczek, F. R.; Qian, G.; Chen, B. *Chem. Commun.* **2010**, *46*, 7205.
(224) Beobide, G.; Wang, W.-G.; Castillo, O.; Luque, A.; Román, P.; Tagliabue, G.; Galli, S.; Navarro, J. A. R. *Inorg. Chem.* **2008**, *47*, 5267.
(225) Navarro, J. A. R.; Barea, E.; Salas, J. M.; Masciocchi, N.; Galli, S.; Sironi, A.; Ania, C. O.; Parra, J. B. *Inorg. Chem.* **2006**, *45*, 2397.
(226) Banerjee, R.; Phan, A.; Wang, B.; Knobler, C.; Furukawa, H.; O'Keefe, M.; Yaghi, O. M. *Science* **2008**, *319*, 939.
(227) An, J.; Rosi, N. L. *J. Am. Chem. Soc.* **2010**, *132*, 5578.
(228) García-Ricard, O. J.; Hernández-Maldonado, A. J. *J. Phys. Chem. C* **2010**, *114*, 1827.
(229) Mulfort, K. L.; Farha, O. K.; Malliakas, C. D.; Kanatzidis, M. G.; Hupp, J. T. *Chem.—Eur. J.* **2010**, *16*, 276.
(230) Kitaura, R.; Matsuda, R.; Kubota, Y.; Kitagawa, S.; Takata, M.; Kobayashi, T. C.; Suzuki, M. *J. Phys. Chem. B* **2005**, *109*, 23378.
(231) Bae, Y.-S.; Hauser, B. G.; Farha, O. K.; Hupp, J. T.; Snurr, R. Q. *Microporous Mesoporous Mater.* **2011**, *141*, 231.
(232) Lincke, J.; Lässig, D.; Moellmer, J.; Reichenbach, C.; Puls, A.; Moeller, A.; Gläser, R.; Kalies, G.; Staudt, R.; Krautscheid, H. *Microporous Mesoporous Mater.* **2011**, *142*, 62.
(233) Tian, J.; Motkuri, R. K.; Thallapally, P. K.; McGrail, B. P. *Cryst. Growth Des* **2010**, *10*, 5327.
(234) Bae, Y.-S.; Dubbeldam, D.; Nelson, A.; Walton, K. S.; Hupp, J. T.; Snurr, R. Q. *Chem. Mater.* **2009**, *21*, 4768.
(235) Pachfule, P.; Das, R.; Poddar, P.; Banerjee, R. *Cryst. Growth Des.* **2011**, *11*, 1215.
(236) Zhang, J.; Wu, H.; Emge, T. J.; Li, J. *Chem. Commun.* **2010**, *46*, 9152.
(237) Thétiot, F.; Duhayon, C.; Venkatakrishnan, T. S.; Sutter, J.-P. *Cryst. Growth Des.* **2008**, *8*, 1870.
(238) Thallapally, P. K.; Tian, J.; Kishan, M. R.; Fernandez, C. A.; Dalgarno, S. J.; McGrail, P. B.; Warren, J. E.; Atwood, J. L. *J. Am. Chem. Soc.* **2008**, *130*, 16842.
(239) Kishan, M. R.; Tian, J.; Thallapally, P. K.; Fernandez, C. A.; Dalgarno, S. J.; Warren, J. E.; McGrail, B. P.; Atwood, J. L. *Chem. Commun.* **2010**, *46*, 538.
(240) Pachfule, P.; Das, R.; Poddar, P.; Banerjee, R. *Cryst. Growth Des.* **2010**, *10*, 2475.
(241) Park, H. J.; Cheon, Y. E.; Suh, M. P. *Chem.—Eur. J.* **2010**, *16*, 11662.
(242) Chen, S.-S.; Chen, M.; Takamizawa, S.; Chen, M.-S.; Su, Z.; Sun, W.-Y. *Chem. Commun.* **2011**, *47*, 752.
(243) Wu, H.; Reali, R. S.; Smith, D. A.; Trachtenberg, M. C.; Li, J. *Chem.—Eur. J.* **2010**, *16*, 13951.
(244) Fernandez, C. A.; Thallapally, P. K.; Motkuri, R. K.; Nune, S. K.; Sumrak, J. C.; Tian, J.; Liu, J. *Cryst. Growth Des.* **2010**, *10*, 1037.
(245) Farha, O. K.; Spokoyny, A. M.; Mulfort, K. L.; Hawthorne, M. F.; Mirkin, C. A.; Hupp, J. T. *J. Am. Chem. Soc.* **2007**, *129*, 12680.
(246) Bae, Y.-S.; Farha, O. K.; Spokoyny, A. M.; Mirkin, C. A.; Hupp, J. T.; Snurr, R. Q. *Chem. Commun.* **2008**, 4135.
(247) Wang, B.; Côte, A. P.; Furukawa, H.; O'Keefe, M.; Yaghi, O. M. *Nature* **2008**, *453*, 207.
(248) Zhang, J.-P.; Chen, X.-M. *J. Am. Chem. Soc.* **2009**, *131*, 5516.
(249) Pachfule, P.; Panda, T.; Dey, C.; Banerjee, R. *CrystEngComm* **2010**, *12*, 2381.
(250) Miller, S. R.; Wright, P. A.; Devic, T.; Serre, C.; Férey, G.; Llewellyn, P. L.; Denoyel, R.; Gaberova, L.; Filinchuk, Y. *Langmuir* **2009**, *25*, 3618.
(251) Zhang, Y.-J.; Liu, T.; Kanegawa, S.; Sato, O. *J. Am. Chem. Soc.* **2010**, *132*, 912.
(252) Mallick, A.; Saha, S.; Pachfule, P.; Roy, S.; Banerjee, R. *J. Mater. Chem.* **2010**, *20*, 9073.
(253) Bao, Z.; Alnemrat, S.; Yu, L.; Vasiliev, I.; Ren, Q.; Lu, X.; Deng, S. *J. Colloid Interface Sci.* **2011**, *357*, 504.
(254) Bae, Y.-S.; Spokoyny, A. M.; Farha, O. K.; Snurr, R. Q.; Hupp, J. T.; Mirkin, C. A. *Chem. Commun.* **2010**, *46*, 3478.
(255) Gándara, F.; Gutiérrez-Puebla, E.; Iglesias, M.; Snejko, N.; Monge, M. A. *Cryst. Growth Des.* **2010**, *10*, 128.
(256) Culp, J. T.; Goodman, A. L.; Chirdon, D.; Sankar, S. G.; Matranga, C. *J. Phys. Chem. C* **2010**, *114*, 2184.
(257) Lambert, J. B.; Liu, Z.; Liu, C. *Organometallics* **2008**, *27*, 1464.
(258) Lee, Y.-G.; Moon, H. R.; Cheon, Y. E.; Suh, M. P. *Angew. Chem., Int. Ed.* **2008**, *47*, 7741.
(259) Guo, X.; Zhu, G.; Li, Z.; Sun, F.; Yang, Z.; Qiu, S. *Chem. Commun.* **2006**, 3172.
(260) Hu, Y.; Xiang, S.; Zhang, W.; Zhang, Z.; Wang, L.; Bai, J.; Chen, B. *Chem. Commun.* **2009**, 7551.
(261) Si, X.; Jiao, C.; Li, F.; Zhang, J.; Wang, S.; Liu, S.; Li, Z.; Sun, L.; Xu, F.; Gabelica, Z.; Schick, C. *Energy Environ. Sci.* **2011**, *4*, 4522.
(262) Bae, Y.-S.; Farha, O. K.; Hupp, J. T.; Snurr, R. Q. *J. Mater. Chem.* **2009**, *19*, 2131.
(263) Moellmer, J.; Celer, E. B.; Luebke, R.; Cairns, A. J.; Staudt, R.; Eddaoudi, M.; Thommes, M. *Microporous Mesoporous Mater.* **2010**, *129*, 345.
(264) Farha, O. K.; Spokoyny, A. M.; Mulfort, K. L.; Galli, S.; Hupp, J. T.; Mirkin, C. A. *Small* **2009**, *15*, 1727.
(265) Kondo, A.; Chinen, A.; Kajiro, H.; Nakagawa, T.; Kato, K.; Takata, M.; Hattori, Y.; Okino, F.; Ohba, T.; Kaneko, K.; Kanoh, H. *Chem.—Eur. J.* **2009**, *15*, 7549.
(266) Cheng, Y.; Kondo, A.; Noguchi, H.; Kajiro, H.; Urita, K.; Ohba, T.; Kaneko, K.; Kanoh, H. *Langmuir* **2009**, *25*, 4510.
(267) Wu, S.; Ma, L.; Long, L.-S.; Zheng, L.-S.; Lin, W. *Inorg. Chem.* **2009**, *48*, 2436.

(268) Hayashi, H.; Côte, A. P.; Furukawa, H.; O'Keefe, M.; Yaghi, O. M. *Nat. Mater.* **2007**, *6*, 501.
(269) Chandler, B. D.; Cramb, D. T.; Shimizu, G. K. H. *J. Am. Chem. Soc.* **2006**, *128*, 10403.
(270) Wu, C.-D.; Lin, W. *Angew. Chem., Int. Ed.* **2005**, *44*, 1958.
(271) Spokoyny, A. M.; Farha, O. K.; Mulfort, K. L.; Hupp, J. T.; Mirkin, C. A. *Inorg. Chim. Acta* **2010**, *364*, 266.
(272) Gadzikwa, T.; Farha, O. K.; Mulfort, K. L.; Hupp, J. T.; Nguyen, S. T. *Chem. Commun.* **2009**, 3720.
(273) Inubushi, Y.; Horike, S.; Fukushima, T.; Akiyama, G.; Matsuda, R.; Kitagawa, S. *Chem. Commun.* **2010**, *46*, 9229.
(274) Fletcher, A. J.; Cussen, E. J.; Bradshaw, D.; Rosseinsky, M. J.; Thomas, K. M. *J. Am. Chem. Soc.* **2004**, *126*, 9750.
(275) Park, H. J.; Suh, M. P. *Chem.—Eur. J.* **2008**, *14*, 8812.
(276) Tian, Y.-Q.; Yao, S.-Y.; Gu, D.; Cui, K.-H.; Guo, D.-W.; Zhang, G.; Chen, Z.-X.; Zhao, D.-Y. *Chem.—Eur. J.* **2010**, *16*, 1137.
(277) Zheng, S.-T.; Li, Y.; Wu, T.; Nieto, R. A.; Feng, P.; Bu, X. *Chem.—Eur. J.* **2010**, *16*, 13035.
(278) Wu, C.-D.; Lin, W. *Dalton Trans.* **2006**, 4563.
(279) Neofotistou, E.; Malliakas, C. D.; Trikalitis, P. N. *Chem.—Eur. J.* **2009**, *15*, 4523.
(280) Tan, Y.-X.; Wang, F.; Kang, Y.; Zhang, J. *Chem. Commun.* **2011**, *47*, 770.
(281) Cheon, Y. E.; Suh, M. P. *Chem. Commun.* **2009**, 2296.
(282) Chun, H.; Seo, J. *Inorg. Chem.* **2009**, *48*, 9980.
(283) Wu, T.; Zhang, J.; Zhou, C.; Wang, L.; Bu, X.; Feng, P. *J. Am. Chem. Soc.* **2009**, *131*, 6111.
(284) Moon, H. R.; Kobayashi, N.; Suh, M. P. *Inorg. Chem.* **2006**, *45*, 8672.
(285) Walton, K. S.; Millward, A. R.; Dubbeldam, D.; Frost, H.; Low, J. L.; Yaghi, O. K.; Snurr, R. Q. *J. Am. Chem. Soc.* **2008**, *130*, 406.
(286) Lama, P.; Aijaz, A.; Neogi, S.; Barbour, L. J.; Bharadwaj, P. K. *Cryst. Growth Des.* **2010**, *10*, 3410.
(287) Wu, C.-D.; Lin, W. *Chem. Commun.* **2005**, 3673.
(288) Chandler, B. D.; Yu, J. O.; Cramb, D. T.; Shimizu, G. K. H. *Chem. Mater.* **2007**, *19*, 4467.
(289) Pan, L.; Adams, K. M.; Hernandez, H. E.; Wang, X.; Zheng, C.; Hattori, Y.; Kaneko, K. *J. Am. Chem. Soc.* **2003**, *125*, 3062.
(290) Vaidhyanathan, R.; Liang, J.; Iremonger, S. S.; Shimizu, G. K. H. *Supramol. Chem.* **2011**, *23*, 278.
(291) Alsobrook, A. N.; Hauser, B. G.; Hupp, J. T.; Alekseev, E. V.; Depmeier, W.; Albrecht-Schmitt, T. E. *Chem. Commun.* **2010**, *46*, 9167.
(292) Liang, J.; Shimizu, G. K. H. *Inorg. Chem.* **2007**, *46*, 10449.
(293) Pan, H.; Ritter, J. A.; Balbuena, P. B. *Langmuir* **1998**, *14*, 6323.
(294) Czepirsky, L.; Jagiello, J. *Chem. Eng. Sci.* **1989**, *44*, 797.
(295) Gu, J.-M.; Kwon, T.-H.; Park, J.-H.; Huh, S. *Dalton Trans.* **2010**, *39*, 5608.
(296) Volkringer, C.; Loiseau, T.; Haouas, M.; Taulelle, F.; Popov, D.; Burghammer, M.; Riekel, C.; Zlotea, C.; Cuevas, F.; Latroche, M.; Phanon, D.; Knofelv, C.; Llewellyn, P. L.; Férey, G. *Chem. Mater.* **2009**, *21*, 5783.
(297) Xiang, Z.; Hu, Z.; Cao, D.; Yang, W.; Jianmin, L.; Han, B.; Wang, W. *Angew. Chem., Int. Ed.* **2011**, *50*, 491.
(298) Wang, Q. M.; Shen, D.; Bülow, M.; Lau, M. L.; Deng, S.; Fitch, F. R.; Lemcoff, N. O.; Semanscin, J. *Microporous Mesoporous Mater.* **2002**, *55*, 217.
(299) Choi, S. B.; Seo, M. J.; Cho, M.; Kim, Y.; Jin, M. K.; Jung, D.-Y.; Choi, J.-S.; Ahn, W.-S.; Rowsell, J. L. C.; Kim, J. *Cryst. Growth Des.* **2007**, *7*, 2290.
(300) Lin, J.-B.; Zhang, J.-P.; Chen, X.-M. *J. Am. Chem. Soc.* **2010**, *132*, 6654.
(301) Culp, J. T.; Smith, M. R.; Bittner, E.; Bockrath, B. *J. Am. Chem. Soc.* **2008**, *130*, 12427.
(302) Procopio, E. Q.; Linares, F.; Montoro, C.; Colombo, V.; Maspero, A.; Barea, E.; Navarro, J. A. R. *Angew. Chem., Int. Ed.* **2010**, *49*, 7308.
(303) Bárcia, P. S.; Bastin, L.; Hurtado, E. J.; Silva, J. A. C.; Rodrigues, A. E.; Chen, B. *Sep. Sci. Technol.* **2008**, *43*, 3494.
(304) Bastin, L.; Bárcia, P. S.; Hurtado, E. J.; Silva, J. A. C.; Rodrigues, A. E.; Chen, B. *J. Phys. Chem. C* **2008**, *112*, 1575.
(305) Dincă, M.; Long, J. R. *J. Am. Chem. Soc.* **2005**, *127*, 9376.
(306) Bae, Y.-S.; Lee, C.-H. *Carbon* **2005**, *43*, 95.
(307) Myers, A. L.; Prausnitz, J. M. *AIChE J.* **1965**, *11*, 121.
(308) Keskin, S. *J. Phys. Chem. C* **2011**, *115*, 800.
(309) Coudert, F.-X.; Mellot-Draznieks, C.; Fuchs, A. J.; Boutin, A. *J. Am. Chem. Soc.* **2009**, *131*, 11329.
(310) Coudert, F.-X. *Phys. Chem. Chem. Phys.* **2010**, *12*, 10904.
(311) Zheng, B.; Bai, J.; Duan, J.; Wojtas, L.; Zaworotko, M. J. *J. Am. Chem. Soc.* **2011**, *133*, 748.
(312) Keskin, S. *Ind. Eng. Chem. Res.* **2011**, *50*, 8230.
(313) Keskin, S.; Sholl, D. S. *Ind. Eng. Chem. Res.* **2009**, *48*, 914.
(314) Liu, Y.; Liu, D.; Yang, Q.; Zhong, C.; Mi, J. *Ind. Eng. Chem. Res.* **2010**, *49*, 2902.
(315) Chen, Y. F.; Jiang, J. W. *ChemSusChem* **2010**, *3*, 982.
(316) Yang, Q.; Zhong, C. *J. Phys. Chem. B* **2006**, *110*, 17776.
(317) Krishna, R.; van Baten, J. M. *Phys. Chem. Chem. Phys.* **2011**, *13*, 10593.
(318) Keskin, S.; Liu, J.; Johnson, J. K.; Sholl, D. S. *Langmuir* **2008**, *24*, 8254.
(319) Keskin, S. *Ind. Eng. Chem. Res.* **2010**, *49*, 11689.
(320) Liu, B.; Yang, Q.; Xue, C.; Zhong, C.; Chen, B.; Smit, B. *J. Phys. Chem. C* **2008**, *112*, 9854.
(321) Liu, B.; Smit, B. *Langmuir* **2009**, *25*, 5918.
(322) Yang, Q.; Xue, C.; Zhong, C.; Chen, J.-F. *AIChE J.* **2007**, *53*, 2832.
(323) Richter, E.; Schütz, W.; Myers, A. L. *Chem. Eng. Sci.* **1989**, *44*, 1609.
(324) Chen, H.; Sholl, D. S. *Langmuir* **2007**, *23*, 6431.
(325) Keskin, S.; Liu, J.; Rankin, R. B.; Johnson, J. K.; Sholl, D. S. *Ind. Eng. Chem. Res.* **2009**, *48*, 2355.
(326) Kizzie, A. C.; Wong-Foy, A. G.; Matzger, A. J. *Langmuir* **2011**, *27*, 6368.
(327) Hamon, L.; Llewellyn, P. L.; Devic, T.; Ghoufi, A.; Clet, G.; Guillerm, V.; Pirngruber, G. D.; Maurin, G.; Serre, C.; Driver, G.; van Beek, W.; Jolimaître, E.; Vimont, A.; Daturi, M.; Férey, G. *J. Am. Chem. Soc.* **2009**, *131*, 17490.
(328) Finsy, V.; Ma, L.; Alaerts, L.; De Vos, D. E.; Baron, G. V.; Denayer, J. F. M. *Microporous Mesoporous Mater.* **2009**, *120*, 221.
(329) Barea, E.; Tagliabue, G.; Wang, W.-G.; Pérez-Mendoza, M.; Mendez-Liñan, L.; López-Garzon, F. J.; Galli, S.; Masciocchi, N.; Navarro, J. A. R. *Chem.—Eur. J.* **2010**, *16*, 931.
(330) Nakagawa, K.; Tanaka, D.; Horike, S.; Shimomura, S.; Higuchi, M.; Kitagawa, S. *Chem. Commun.* **2010**, *46*, 4258.
(331) Warren, J. E.; Pritchard, R. G.; Abram, D.; Davies, H. M.; Savarese, T. L.; Cash, R. J.; Raithby, P. R.; Morris, R.; Jones, R. H.; Teat, S. J. *J. Appl. Crystallogr.* **2009**, *42*, 457.
(332) Xie, L.-H.; Lin, J.-B.; Liu, X.-M.; Wang, Y.; Zhang, W.-X.; Zhang, J.-P.; Chen, X.-M. *Inorg. Chem.* **2010**, *49*, 1158.
(333) Lin, J.-B.; Xue, W.; Zhang, J.-P.; Chen, X.-M. *Chem. Commun.* **2011**, *47*, 926.
(334) Serre, C.; Bourrelly, S.; Vimont, A.; Ramsahye, N. A.; Maurin, G.; Llewellyn, P. L.; Daturi, M.; Filinchuk, Y.; Leynaud, O.; Barnes, P.; Férey, G. *Adv. Mater.* **2007**, *19*, 2246.
(335) Loiseau, T.; Serre, C.; Huguenard, C.; Fink, G.; Taulelle, F.; Henry, M.; Bataille, T.; Férey, G. *Chem.—Eur. J.* **2004**, *10*, 1373.
(336) Vaidhyanathan, R.; Iremonger, S. S.; Shimizu, G. K. H.; Boyd, P. G.; Alavi, S.; Woo, T. K. *Science* **2010**, *330*, 650.
(337) Bordiga, S.; Regli, L.; Bonino, F.; Groppo, E.; Lamberti, C.; Xiao, B.; Wheatley, P. S.; Morris, R. E.; Zecchina, A. *Phys. Chem. Chem. Phys.* **2007**, *9*, 2676.
(338) Vimont, A.; Travert, A.; Bazin, P.; Lavalley, J.-C.; Daturi, M.; Serre, C.; Férey, G.; Bourrelly, S.; Llewellyn, P. L. *Chem. Commun.* **2007**, *31*, 3291.
(339) Valenzano, L.; Civalleri, B.; Chavan, S.; Palomino, G. T.; Areán, C. O.; Bordiga, S. *J. Phys. Chem. C* **2010**, *114*, 11185.
(340) Zhao, Y.; Wu, H.; Emge, T. J.; Gong, Q.; Nijem, N.; Chabal, Y. J.; Kong, L.; Langreth, D. C.; Liu, H.; Zeng, H.; Li, J. *Chem.—Eur. J.* **2011**, *17*, 5101.

(341) Kauffman, K. L.; Culp, J. T.; Goodman, A.; Matranga, C. *J. Phys. Chem. C* **2011**, *115*, 1857.
(342) Taylor, J. H.; Benedict, W. S.; Strong, J. *J. Chem. Phys.* **1952**, *20*, 1884.
(343) Yoon, J. W.; Seo, Y.-K.; Hwang, Y. K.; Chang, J.-S.; Leclerc, H.; Wuttke, S.; Bazin, P.; Vimont, A.; Daturi, M.; Bloch, E.; Llewellyn, P. L.; Serre, C.; Horcajada, P.; Grenéche, J.-M.; Rodrigues, A. E.; Férey, G. *Angew. Chem., Int. Ed.* **2010**, *49*, 5949.
(344) Windisch, C. F., Jr.; Thallapally, P. K.; McGrail, B. P. *Spectrochim. Acta A* **2009**, *74*, 629.
(345) Gascon, J.; Aktay, U.; Hernandez-Alonso, M. D.; van Klink, G. P. M; Kapteijn, F. *J. Catal.* **2009**, *261*, 75.
(346) Stavitski, E.; Pidko, E. A.; Couck, S.; Remy, T.; Hensen, E. J. M.; Weckhuysen, B. M.; Denayer, J.; Gascon, J.; Kapteijn, F. *Langmuir* **2011**, *27*, 3970.
(347) Dubbeldam, D.; Frost, H.; Walton, K. S.; Snurr, R. Q. *Fluid Phase Equilib.* **2007**, *261*, 152.
(348) Torrisi, A.; Bell, R. G.; Mellot-Draznieks, C. *Cryst. Growth Des.* **2010**, *10*, 2839.
(349) Babarao, R.; Jiang, J.; Sandler, S. I. *Langmuir* **2010**, *25*, 5239.
(350) Wu, D.; Xu, Q.; Liu, D.; Zhong, C. *J. Phys. Chem. C* **2010**, *114*, 16611.
(351) Wells, B. A.; Chaffee, A. L. *Adsorption* **2011**, *17*, 255.
(352) Walton, K. S.; Millward, A. R.; Dubbeldam, D.; Frost, H.; Low, J. J.; Yaghi, O. M.; Snurr, R. Q. *J. Am. Chem. Soc.* **2008**, 130.
(353) Ghoufi, A.; Maurin, G. *J. Phys. Chem. C* **2010**, *114*, 6496.
(354) Liu, B.; Smit, B. *J. Phys. Chem. C* **2010**, *114*, 8515.
(355) Valenzano, L.; Civalleri, B.; Chavan, S.; Bordiga, S.; Nilsen, M. H.; Jakobsen, S.; Lillerud, K. P.; Lamberti, C. *Chem. Mater.* **2011**, *23*, 1700.
(356) Grajciar, L.; Wiersum, A. D.; Llewellyn, P. L.; Chang, J.-S.; Nachtigall, P. *J. Phys. Chem. C* **2011**, *115*, 17925.
(357) Valenzano, L.; Civalleri, B.; Sillar, K.; Sauer, J. *J. Phys. Chem. C* **2011**, *115*, 21777.
(358) Wilmer, C. E.; Snurr, R. Q. *Chem. Eng. J.* **2011**, *171*, 775.
(359) Babarao, R.; Dai, S.; Jiang, D.-E. *Langmuir* **2011**, *27*, 3451.
(360) Torrisi, A.; Mellot-Draznieks, C.; Bell, R. G. *J. Chem. Phys.* **2009**, *130*, No. 194703.
(361) Torrisi, A.; Mellot-Draznieks, C.; Bell, R. G. *J. Chem. Phys.* **2010**, *132*, No. 044705.
(362) Ramsahye, N. A.; Maurin, G.; Bourrelly, S.; Llewellyn, P. L.; Devic, T.; Serre, C.; Loiseau, T.; Férey, G. *Adsorption* **2007**, *13*, 461.
(363) Babarao, R.; Jiang, J. *J. Phys. Chem. C* **2009**, *113*, 18287.
(364) Salles, F.; Ghoufi, A.; Maurin, G.; Bell, R. G.; Mellot-Draznieks, C.; Férey, G. *Angew. Chem., Int. Ed.* **2008**, *47*, 8487.
(365) Dubbeldam, D.; Krishna, R.; Snurr, R. Q. *J. Phys. Chem. C* **2009**, *113*, 19317.
(366) Jassim, M. S.; Rochelle, G. T. *Ind. Eng. Chem. Res.* **2006**, *45*, 2465.
(367) Lee, K. B.; Sircar, S. *AIChE J.* **2008**, *54*, 2293.
(368) An, J.; Geib, S. J.; Rosi, N. L. *J. Am. Chem. Soc.* **2010**, *132*, 38.
(369) Park, T.-H.; Cychosz, K. A.; Wong-Foy, A. G.; Dailly, A.; Matzger, A. J. *Chem. Commun.* **2011**, *47*, 1452.
(370) Henke, S.; Fischer, R. A. *J. Am. Chem. Soc.* **2011**, *133*, 2064.
(371) Cheon, Y. E.; Park, J.; Suh, M. P. *Chem. Commun.* **2009**, 5436.
(372) Zeleňák, V.; Vargová, Z.; Almáši, M.; Zeleňákova, A.; Kuchár, J. *Microporous Mesoporous Mater.* **2010**, *129*, 354.
(373) Perrin, D. D. *Dissociation Constants of Organic Bases in Aqueous Solution: Supplement*; Butterworths: London, 1972.
(374) Hwang, Y. K.; Hong, D.-Y.; Chang, J.-S.; Jhung, S. H.; Seo, Y.-K.; Kim, J.; Vimont, A.; Daturi, M.; Serre, C.; Férey, G. *Angew. Chem., Int. Ed.* **2008**, *47*, 4144.
(375) Yang, Q.; Wiersum, A. D.; Llewellyn, P. L.; Guillerm, V.; Serre, C.; Maurin, G. *Chem. Commun.* **2011**, *47*, 9603.
(376) Zhao, D.; Yuan, D.; Zhou, H.-C. *Energy Environ. Sci.* **2008**, *1*, 222.
(377) Sculley, J.; Yuan, D.; Zhou, H.-C. *Energy Environ. Sci.* **2011**, *4*, 2721.
(378) Horike, S.; Dincă, M.; Tamaki, K.; Long, J. R. *J. Am. Chem. Soc.* **2008**, *130*, 5854.
(379) Vishnayakov, A.; Ravikovitch, P. I.; Neimark, A. V.; Bülow, M.; Wang, Q. M. *Nano Lett.* **2003**, *3*, 713.
(380) Dietzel, P. D. C.; Morita, Y.; Blom, R.; Fjellvåg, H. *Angew. Chem., Int. Ed.* **2005**, *44*, 6354.
(381) Rosi, N. L.; Kim, J.; Eddaoudi, M.; Chen, B.; O'Keefe, M.; Yaghi, O. M. *J. Am. Chem. Soc.* **2005**, *127*, 1504.
(382) Dietzel, P. D. C.; Panella, B.; Hirscher, M.; Blom, R.; Fjellvåg, H. *Chem. Commun.* **2006**, 959.
(383) Dietzel, P. D. C.; Blom, R.; Fjellvåg, H. *Eur. J. Inorg. Chem.* **2008**, 3624.
(384) Sumida, K.; Brown, C. M.; Herm, Z. R.; Chavan, S.; Bordiga, S.; Long, J. R. *Chem. Commun.* **2011**, *47*, 1157.
(385) Huang, L.; Wang, H.; Chen, J.; Wang, Z.; Sun, J.; Zhao, D.; Yan, Y. *Microporous Mesoporous Mater.* **2003**, *58*, 105.
(386) Schröck, K.; Schröder, F.; Heyden, M.; Fischer, R. A.; Havenith, M. *Phys. Chem. Chem. Phys.* **2008**, *10*, 4732.
(387) Hausdorf, S.; Wagler, J.; Mossig, R.; Mertens, F. O. R. L. *J. Phys. Chem. A* **2008**, *112*, 7567.
(388) Greathouse, J. A.; Allendorf, M. D. *J. Am. Chem. Soc.* **2006**, *128*, 10678.
(389) Cychosz, K. A.; Matzger, A. J. *Langmuir* **2010**, *26*, 17198.
(390) Li, Y.; Yang, R. T. *Langmuir* **2007**, *23*, 12937.
(391) Park, K. S.; Ni, Z.; Côte, A. P.; Choi, J. Y.; Huang, R.; Uribe-Romo, F. J.; Chae, H. K.; O'Keefe, M.; Yaghi, O. M. *Proc. Natl. Acad. Sci. U.S.A.* **2006**, *103*, 10186.
(392) Huang, X.-C.; Lin, Y.-Y.; Zhang, J.-P.; Chen, X.-M. *Angew. Chem., Int. Ed.* **2006**, *45*, 1557.
(393) Gu, J.-Z.; Lu, W.-G.; Jiang, L.; Zhou, H.-C.; Lu, T.-B. *Inorg. Chem.* **2007**, *46*, 5835.
(394) Biswas, S.; Gryzwa, M.; Nayek, H. P.; Dehnen, S.; Senkovska, I.; Kaskel, S.; Volkmer, D. *Dalton Trans.* **2009**, 6487.
(395) Choi, H. J.; Dincă, M.; Dailly, A.; Long, J. R. *Energy Environ. Sci.* **2010**, *3*, 117.
(396) Galli, S.; Masciocchi, N.; Colombo, V.; Maspero, A.; Palmisiano, G.; López-Garzón, F. J.; Domingo-Garciá, M.; Fernández-Morales, I.; Barea, E.; Navarro, J. A. R. *Chem. Mater.* **2010**, *22*, 1664.
(397) Colombo, V.; Galli, S.; Choi, H.-J.; Han, G. D.; Maspero, A.; Palmisiano, G.; Masciocchi, N.; Long, J. R. *Chem. Sci.* **2011**, *2*, 1311.
(398) Catalán, J.; Abboud, J. L. M.; Elguero, J. *Adv. Heterocycl. Chem.* **1987**, *41*, 187.
(399) Ebert, C.; Elguero, J.; Musumarra, G. *J. Phys. Org. Chem.* **1990**, *3*, 651.
(400) Férey, G.; Serre, C.; Mellot-Draznieks, C.; Millange, F.; Surblé, S.; Dutour, J.; Margiolaki, I. *Angew. Chem., Int. Ed.* **2004**, *43*, 6296.
(401) Férey, G.; Mellot-Draznieks, C.; Serre, C.; Millange, F.; Dutour, J.; Surblé, S.; Margiolaki, I. *Science* **2005**, *309*, 2040.
(402) Volkringer, C.; Popov, D.; Loiseau, T.; Guillou, N.; Férey, G.; Haouas, M.; Taulelle, F.; Mellot-Draznieks, C.; Burghammer, M.; Riekel, C. *Nat. Mater.* **2007**, *6*, 760.
(403) Küsgens, P.; Rose, M.; Senkovska, I.; Fröde, H.; Henshcel, A.; Siegle, S.; Kaskel, S. *Microporous Mesoporous Mater.* **2009**, *120*, 325.
(404) Ehrenmann, J.; Henninger, S. K.; Janiak, C. *Eur. J. Inorg. Chem.* **2011**, 471.
(405) Lin, X.; Blake, A. J.; Wilson, C.; Sun, X. Z.; Champness, N. R.; George, M.; Hubberstey, P.; Mokoya, R.; Schröder, M. *J. Am. Chem. Soc.* **2006**, *128*, 10745.
(406) Pan, L.; Parker, B.; Huang, X.; Olson, D. H.; Lee, J. Y.; Li, J. *J. Am. Chem. Soc.* **2006**, *128*, 4180.
(407) Lee, J. Y.; Olson, D. H.; Pan, L.; Emge, T. J.; Li, J. *Adv. Funct. Mater.* **2007**, *17*, 1255.
(408) Chen, Y. F.; Lee, J. Y.; Babarao, R.; Li, J.; Jiang, J. W. *J. Phys. Chem. C* **2010**, *114*, 6602.
(409) Wu, T.; Shen, L.; Luebbers, M.; Hu, C.; Chen, Q.; Ni, Z.; Masel, R. I. *Chem. Commun.* **2010**, *46*, 6120.
(410) Nguyen, J. G.; Cohen, S. M. *J. Am. Chem. Soc.* **2010**, *132*, 4560.

(411) Ma, D.; Li, Y.; Li, Z. *Chem. Commun.* 2011, *47*, 7377.
(412) Brandani, F.; Ruthven, D. M. *Ind. Eng. Chem. Res.* **2004**, *43*, 8339.
(413) Castillo, J. M.; Vlugt, T. J. H.; Calero, S. *J. Phys. Chem. C* **2008**, *112*, 15934.
(414) Grajciar, L.; Bludský, O.; Nachtigall, P. *J. Phys. Chem. Lett.* **2010**, *1*, 3354.
(415) Liu, J.; Benin, A. I.; Furtado, A. M.; Jakubczak, P.; Willis, R. R.; LeVan, M. D. *Langmuir* **2011**, *27*, 11451.
(416) Higman, C.; van der Burgt, M. *Gasification*; Elsevier: New York, 2003.
(417) Sircar, S.; Golden, T. C. *Sep. Sci. Technol.* **2000**, *35*, 667.
(418) Damle, A. *Hydrogen Fuel: Production, Transport and Storage*; CRC Press: Boca Raton, FL, 2004.
(419) *Hydrogen and Syngas Production and Purification Technologies*; Sircar, S., Golden, T. C., Liu, K., Song, C., Subramani, V., Eds.; Wiley-AIChE: Hoboken, NJ, 2010, p 414.
(420) U.S. Department of Energy, National Energy Technology Laboratory: http://www.netl.doe.gov/technologies/carbon_seq/corerd/pre-combustion.html#sorbents, 2011.
(421) Cormos, C.-C.; Starr, F.; Tzimas, E.; Oeteves, S. *Int. J. Hydrogen Energy* **2008**, *33*, 1286.
(422) Plasynski, S. I.; Litynski, J. T.; McIlvried, H. G.; Srivastava, R. D. *Crit. Rev. Plant Sci.* **2009**, *28*, 123.
(423) Figueroa, J. D.; Fout, T.; Plasynski, S.; McIlvried, H.; Srivastava, R. D. *Int. J. Greenhouse Gas Control* **2008**, *2*, 9.
(424) U.S. Department of Energy, National Energy Technology Laboratory: http://www.netl.doe.gov/technologies/carbon_seq/corerd/pre-combustion.html, 2011.
(425) http://www.duke-energy.com/about-us/igcc.asp.
(426) Damen, K.; Gnutek, R.; Kaptein, J.; Nannan, N. R.; Oyarzun, B.; Trapp, C.; Colonna, P.; van Dijk, E.; Gross, J.; Bardow, A. *Energy Procedia* **2011**, *4*, 1214.
(427) Agarwal, A.; Biegler, L. T.; Zitney, S. E. *Ind. Eng. Chem. Res.* **2010**, *49*, 5066.
(428) Wei, W.; Kulkarni, P.; Liu, K. *Hydrogen and Syngas Production and Purification Technologies*; Wiley-AIChE: Hoboken, NJ, 2010.
(429) U.S. Energy Information Administration: Existing Capacity by Energy Source: www.eia.doe.gov/cneaf/electricity/epa/ epat1p2.html (accessed October 24, 2010).
(430) Grande, C. A.; Lopes, F. V. S.; Ribiero, A. M.; Louriero, J. M.; Rodrigues, A. E. *Sep. Sci. Technol.* **2008**, *43*, 1338.
(431) Lopes, F. V. S.; Grande, C. A.; Ribiero, A. M.; Vilar, V. J. P.; Louriero, J. M.; Rodrigues, A. E. *J. Chem. Eng. Data* **2010**, *55*, 184.
(432) Kumar, R. *Ind. Eng. Chem. Res.* **1994**, *33*, 1600.
(433) Ho, M. T.; Alinson, G. W.; Wiley, D. *Ind. Eng. Chem. Res.* **2008**, *47*, 4883.
(434) Krishna, R.; Long, J. R. *J. Phys. Chem. C* 2011, *115*, 12941.
(435) Loulergue, L.; Schilt, A.; Spahni, R.; Masson-Delmotte, V.; Blunier, T.; Lemiuex, B.; Barnola, J.-M.; Raynaud, D.; Stocker, T. F.; Chappellaz, J. *Nature* **2008**, *453*, 383.
(436) Hamon, L.; Serre, C.; Devic, T.; Loiseau, T.; Millange, F.; Férey, G.; De Weireld, G. *J. Am. Chem. Soc.* **2009**, *131*, 8775.
(437) Petit, C.; Mendoza, B.; Bandosz, T. J. *ChemPhysChem* **2010**, *11*, 3678.
(438) Scholes, C. A.; Smith, K. H.; Kentish, S. E.; Stevens, G. W. *Int. J. Greenhouse Gas Control* **2010**, *4*, 739.
(439) Zornoza, B.; Martinez-Joaristi, A.; Serra-Crespo, P.; Tellez, C.; Coronas, J.; Gascon, J.; Kapteijn, F. *Chem. Commun.* **2011**, *47*, 9522.
(440) Chmelik, C.; Heinke, L.; Valiullin, R.; Kärger, J. *Chem. Eng. Technol.* **2010**, *82*, 779.
(441) Skoulidas, A. I.; Sholl, D. S. *J. Phys. Chem. B* **2005**, *109*, 15760.
(442) Salles, F.; Jobic, H.; Devic, T.; Llewellyn, P. L.; Serre, C.; Férey, G.; Maurin, G. *ACS Nano* **2010**, *4*, 143.
(443) Gallo, M.; Mitnik-Glossman, D. *J. Phys. Chem. C* **2009**, *113*, 6634.
(444) Liu, J.; Johnson, J. K. *J. Low Temp. Phys.* **2009**, *157*, 268.
(445) Keskin, S. *J. Phys. Chem. C* **2010**, *114*, 13047.
(446) Chae, H. K.; Siberio-Pérez, D. Y.; Kim, J.; Go, Y. B.; Eddaoudi, M.; Matzger, A. J.; O'Keeffe, M.; Yaghi, O. M. *Nature* **2004**, *427*, 523.
(447) Sumida, K.; Hill, M. R.; Horike, S.; Dailly, A.; Long, J. R. *J. Am. Chem. Soc.* **2009**, *131*, 15120.
(448) Choi, H. J.; Dincă, M.; Long, J. R. *J. Am. Chem. Soc.* **2008**, *130*, 7848.
(449) Jiang, J. *AIChE J.* **2009**, *55*, 2422.
(450) Babarao, R.; Eddaoudi, M.; Jiang, J. W. *Langmuir* **2010**, *26*, 11196.
(451) Babarao, R.; Jiang, J. W. *Ind. Eng. Chem. Res.* **2011**, *50*, 62.
(452) Van Tassel, P. R.; Davis, H. T.; McCormick, A. V. *Langmuir* **1994**, *10*, 1257.
(453) Babarao, R.; Jiang, J. W. *J. Am. Chem. Soc.* **2009**, *131*, 11417.
(454) Yang, Q.; Xu, Q.; Liu, B.; Zhong, C. *Chin. J. Chem. Eng.* **2009**, *17*, 781.
(455) Kather, A.; Scheffknect, G. *Naturwissenschaften* **2009**, *96*, 993.
(456) Kakaras, E.; Kounamakos, A.; Doukelis, A.; Giannakopoulos, D.; Vorrias, I. *Fuel* **2007**, *86*, 2144.
(457) Rezvani, H.; Huang, Y.; McIlveen-Wright, D.; Hewitt, N.; Wang, Y. *Fuel* **2007**, *86*, 2134.
(458) Greenwood, N. N.; Earnshaw, A. *Chemistry of the Elements*, 2nd ed.; Butterworth Heinemann: Burlington, MA, 2002.
(459) Nandi, S. P.; Walker, P. L., Jr. *Sep. Sci. Technol.* **1976**, *11*, 441.
(460) Feig, A. L.; Lippard, S. J. *Chem. Rev.* **1994**, *94*, 759.
(461) Kitajima, A.; Morooka, Y. *Chem. Rev.* **1994**, *94*, 737.
(462) Magnus, K. A.; Tonthat, H.; Carpenter, J. E. *Chem. Rev.* **1994**, *94*, 727.
(463) Que, L.; Dong, Y. *Acc. Chem. Res.* **1996**, *29*, 190.
(464) Sono, M.; Roach, M. P.; Coulter, E. D.; Dawson, J. H. *Chem. Rev.* **1996**, *96*, 2841.
(465) Karlin, K. D.; Kanderli, S.; Zuberbuhler, A. D. *Acc. Chem. Res.* **1997**, *30*, 139.
(466) Kovaleva, E. G.; Neibegall, M. B.; Chakrabarty, S.; Lipscomb, J. D. *Acc. Chem. Res.* **2007**, *40*, 475.
(467) Chufan, E. E.; Puiu, S. C.; Karlin, K. D. *Acc. Chem. Res.* **2007**, *40*, 563.
(468) Rolff, M.; Schottenheim, J.; Decker, H.; Tuczek, F. *Chem. Soc. Rev.* **2011**, *40*, 4077.
(469) Ma, S.; Yuan, D.; Chang, J.-S.; Zhou, H.-C. *Inorg. Chem.* **2009**, *48*, 5398.
(470) Zhong, R.-Q.; Zou, R.-Q.; Du, M.; Yamada, T.; Maruta, G.; Takeda, S.; Li, J.; Xu, Q. *CrystEngComm* **2010**, *12*, 677.
(471) Chang, Z.; Zhang, D.-S.; Hu, T.-L.; Bu, X.-H. *Cryst. Growth Des.* **2011**, *11*, 2050.
(472) Collman, J. P.; Del, G.; Guadio, J.; La Mar, G. N.; Balch, A. L. *J. Am. Chem. Soc.* **1977**, *99*, 5486.
(473) Baldwin, J. E.; Cameron, J. H.; Crossley, M. J.; Dagley, I. J.; Hall, S. R.; Klose, T. *J. Chem. Soc., Dalton Trans.* **1984**, *48*, 1739.
(474) Sheldon, R. A.; van Santen, R. A. *Catalytic Oxidation: Principles and Applications*; World Scientific: Singapore, 1995.
(475) Dubois, G.; Tripier, T.; Brandès, S. P.; Denat, F.; Guilard, R. *J. Mater. Chem.* **2002**, *12*, 2255.
(476) Bloch, E. D.; Murray, L. J.; Queen, W. L.; Chavan, S.; Maximoff, S. N.; Bigi, J. P.; Krishna, R.; Peterson, V. K.; Grandjean, F.; Long, G. J.; Smit, B.; Bordiga, S.; Brown, C. M.; Long, J. R. *J. Am. Chem. Soc.* **2011**, *133*, 14814.
(477) Babcock, H. D.; Herzberg, L. *Astrophys. J.* **1948**, *108*, 167.
(478) Wong-Foy, A. G.; Matzger, A. J.; Yaghi, O. M. *J. Am. Chem. Soc.* **2006**, *128*, 3494.
(479) Wu, C.-D.; Hu, A.; Zhang, L.; Lin, W. *J. Am. Chem. Soc.* **2005**, *127*, 8940.
(480) Seo, J. S.; Whang, D.; Lee, H.; Jun, S. I.; Oh, J.; Jeon, Y. J.; Kim, K. *Nature* **2000**, *404*, 982.
(481) Chen, B.; Wang, L.; Xiao, Y.; Fronczek, F. R.; Xue, M.; Cui, Y.; Qian, G. *Angew. Chem., Int. Ed.* **2009**, *48*, 500.
(482) Zhou, X.; Xu, Z.; Zeller, M.; Hunter, A. D. *Chem. Commun.* **2009**, 539.

(483) Shultz, A. M.; Sarjeant, A. A.; Farha, O. K.; Hupp, J. T.; Nguyen, S. *J. Am. Chem. Soc.* **2011**, *133*, 13252.
(484) Merkel, T. C.; Lin, H.; Wei, X.; Baker, R. *J. Membr. Sci.* **2010**, *359*, 126.
(485) Gascon, J.; Kapteijn, F. *Angew. Chem., Int. Ed.* **2010**, 49.
(486) Zacher, D.; Shekhah, O.; Woll, C.; Fischer, R. A. *Chem. Soc. Rev.* **2009**, *38*, 1418.
(487) Shekhah, O.; Liu, J.; Fischer, R. A.; Woll, C. *Chem. Soc. Rev.* **2011**, *40*, 1081.
(488) Scherb, C.; Schodel, A.; Bein, T. *Angew. Chem., Int. Ed.* **2008**, *47*, 5777.
(489) Horcajada, P.; Serre, C.; Grosso, D.; Boissiere, C.; Perruchas, S.; Sanchez, C.; Férey, G. *Adv. Mater.* **2009**, *21*, 1931.
(490) Demessence, A.; Horcajada, P.; Serre, C.; Boissiere, C.; Grosso, D.; Sanchez, C.; Férey, G. *Chem. Commun.* **2009**, 7149.
(491) Yoo, Y.; Jeong, H.-K. *Chem. Commun.* **2008**, 2441.
(492) Liu, Y.; Ng, Z.; Khan, E. A.; Jeong, H.-K.; Ching, C.-B.; Lai, Z. *Microporous Mesoporous Mater.* **2009**, *118*, 296.
(493) Yoo, Y.; Lai, Z.; Jeong, H.-K. *Microporous Mesoporous Mater.* **2009**, *123*, 100.
(494) Guo, H.; Zhu, G.; Hewitt, I. J.; Qiu, S. *J. Am. Chem. Soc.* **2009**, *131*, 1646.
(495) Ranjan, R.; Tsapatsis, M. *Chem. Mater.* **2009**, *21*, 4920.
(496) Bux, H.; Liang, F.; Li, Y.; Cravillon, J.; Wiebcke, M.; Caro, J. *J. Am. Chem. Soc.* **2009**, *131*, 16000.
(497) Bux, H.; Chmelik, C.; van Baten, J. M.; Krishna, R.; Caro, J. *Adv. Mater.* **2010**, *22*, 4741.
(498) Bux, H.; Feldhoff, A.; Cravillon, J.; Wiebcke, M.; Li, Y.-S.; Caro, J. *Chem. Mater.* **2011**, *23*, 2262.
(499) Li, Y.-S.; Bux, H.; Feldhoff, A.; Li, G.-L.; Yang, W.-S.; Caro, J. *Adv. Mater.* **2010**, *22*, 3322.
(500) Li, Y.-S.; Liang, F.-Y.; Bux, H.; Feldhoff, A.; Yang, W.-S.; Caro, J. *Angew. Chem., Int. Ed.* **2010**, *49*, 548.
(501) Li, Y.; Liang, F.; Bux, H.; Yang, W.; Caro, J. *J. Membr. Sci.* **2010**, *354*, 48.
(502) Huang, A.; Bux, H.; Steinbach, F.; Caro, J. *Angew. Chem., Int. Ed.* **2010**, *49*, 4958.
(503) Huang, A.; Dou, W.; Caro, J. *J. Am. Chem. Soc.* **2010**, *132*, 15562.
(504) Venna, S. R.; Carreon, M. A. *J. Am. Chem. Soc.* **2010**, *132*, 76.
(505) McCarthy, M. C.; Varela-Guerrero, V.; Barnett, G. V.; Jeong, H.-K. *Langmuir* **2010**, *26*, 14636.
(506) Yao, J.; Dong, D.; Li, D.; He, L.; Xu, G.; Wang, H. *Chem. Commun.* **2011**, *47*, 2559.
(507) Snyder, M. A.; Tsapatsis, M. *Angew. Chem., Int. Ed.* **2007**, *46*, 7560.
(508) Choi, J.; Jeong, H.-K.; Snyder, M. A.; Stoeger, J. A.; Masel, R. I.; Tsapatsis, M. *Science* **2009**, *325*, 590.
(509) Lai, Z.; Bonilla, G.; Diaz, I.; Nery, J. G.; Sujaoti, K.; Amat, M. A.; Kokkoli, E.; Terasaki, O.; Thompson, R. W.; Tsapatsis, M.; Vlachos, D. G. *Science* **2003**, *300*, 456.
(510) Takamizawa, S.; Takasaki, Y.; Miyake, R. *J. Am. Chem. Soc.* **2010**, *132*, 2862.
(511) Krishna, R.; van Baten, J. M. *J. Membr. Sci.* **2011**, *377*, 249.
(512) Aguado, S.; Nicolas, C.-H.; Moizan-Basle, V.; Nieto, C.; Amrouche, H.; Bats, N.; Audebrand, N.; Farrusseng, D. *New J. Chem.* **2011**, *35*, 41.
(513) Won, J.; Seo, J. S.; Kim, J. H.; Kim, H. S.; Kang, Y. S.; Kim, S. J.; Kim, Y.; Jegal, J. *Adv. Mater.* **2005**, *17*, 80.
(514) Car, A.; Stropnik, C.; Peinemann, K.-V. *Desalination* **2006**, *200*, 424.
(515) Zhang, Y.; Musselman, I. H.; Ferraris, J. P.; Balkus, K. J. J. *J. Membr. Sci.* **2008**, *313*, 170.
(516) Perez, E. V.; Balkus, K. J. J.; Ferraris, J. P.; Musselman, I. H. *J. Membr. Sci.* **2009**, *328*, 165.
(517) Adams, R.; Carson, C.; Ward, J.; Tannenbaum, R.; Koros, W. *Microporous Mesoporous Mater.* **2010**, *131*, 13.
(518) Diaz, K.; Garrido, L.; Lopez-Gonzalez, M.; del Castillo, L. F.; Riande, E. *Macromolecules* **2009**, *43*, 316.
(519) Ordoñez, M. J. C.; Balkus, K. J. J.; Ferraris, J. P.; Musselman, I. H. *J. Membr. Sci.* **2010**, *361*, 28.
(520) Bae, T.-H.; Lee, J. S.; Qiu, W.; Koros, W. J.; Jones, C. W.; Nair, S. *Angew. Chem., Int. Ed.* **2010**, *49*, 9863.
(521) Basu, S.; Cano-Odena, A.; Vankelecom, I. F. J. *J. Membr. Sci.* **2010**, *362*, 478.
(522) Hu, J.; Cai, H.; Ren, H.; Wei, Y.; Xu, Z.; Liu, H.; Hu, Y. *Ind. Eng. Chem. Res.* **2010**, *49*, 12605.
(523) Keskin, S.; Sholl, D. S. *Energy Environ. Sci.* **2010**, *3*, 343.
(524) Robeson, L. M. *J. Membr. Sci.* **2008**, *320*, 390.